

AD-A091 689

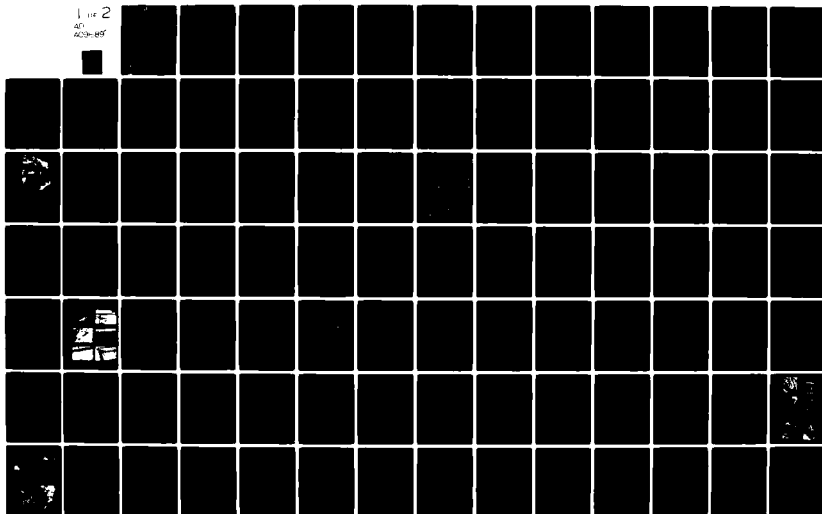
HEBREW UNIV JERUSALEM (ISRAEL) INST OF EARTH SCIENCES
ARID ZONE GEOSYSTEMS.(U)
SEP 80 A P SCHICK

F/6 8/8

UNCLASSIFIED

DA-ERO-78-6-111
NL

1 of 2
40
403-105



AD A091689

C FILE COPY

LEVEL II - 12

W
A

ARID ZONE GEOSYSTEMS

A RESEARCH REPORT

EDITED BY

ASHER P. SCHICK

DTIC
ELECTE
NOV 7 1980
C



PHYSICAL GEOGRAPHY
INSTITUTE OF EARTH SCIENCES
THE HEBREW UNIVERSITY OF JERUSALEM

1980

DISTRIBUTION STATEMENT A

Approved for public release.
Distribution Unlimited

80 11 07 062

UNCLASSIFIED

2369A-EN

SECURITY CLASSIFICATION OF THIS PAGE (When Data Entered)

REPORT DOCUMENTATION PAGE		READ INSTRUCTIONS BEFORE COMPLETING FORM
1. REPORT NUMBER	2. GOVT ACCESSION NO. AD-A091689	3. RECIPIENT'S CATALOG NUMBER
4. TITLE (and Subtitle) (6) Arid Zone Geosystems.	5. TYPE OF REPORT & PERIOD COVERED (9) Final Technical Report. Aug 78 - Jan 80	6. PERFORMING ORG. REPORT NUMBER
7. AUTHOR(s) (10) Asher P. Schick	8. CONTRACT OR GRANT NUMBER(s) (15) ✓ DAERO-78-G-111	9. PROGRAM ELEMENT, PROJECT, TASK AREA & WORK UNIT NUMBERS (16) IT161102BH57-01
10. PERFORMING ORGANIZATION NAME AND ADDRESS Department of Geography The Hebrew University of Jerusalem Jerusalem, Israel	11. CONTROLLING OFFICE NAME AND ADDRESS (11) USARDSG-UK Box 65 FPO New York NY 09510	12. REPORT DATE (17) Sep 80
13. MONITORING AGENCY NAME & ADDRESS (if different from Controlling Office) (12) 168	14. SECURITY CLASS. (of this report) None	15a. DECLASSIFICATION/DOWNGRADING SCHEDULE
16. DISTRIBUTION STATEMENT (of this Report) Approved for public release; Distribution unlimited		
17. DISTRIBUTION STATEMENT (of the abstract entered in Block 20, if different from Report)		
18. SUPPLEMENTARY NOTES		
19. KEY WORDS (Continue on reverse side if necessary and identify by block number) arid zones; modelling; geomorphology; hydrology; sediment		
20. ABSTRACT (Continue on reverse side if necessary and identify by block number) Report presents the second comprehensive collection and analysis of geosystem-oriented environmental data based on the Nahal Yael Research Watershed, located in the Negev Desert just north of Eilat, Israel. Report reflects transition from direct measurements of basic rainfall, streamflow, sediment transport, and other data to an environmental modelling approach which integrates these data on a dynamic process basis.		

DD FORM 1 JAN 73 1473

EDITION OF 1 NOV 65 IS OBSOLETE

UNCLASSIFIED

SECURITY CLASSIFICATION OF THIS PAGE (When Data Entered)

4/12/83

6/16

UNCLASSIFIED

SECURITY CLASSIFICATION OF THIS PAGE(When Data Entered)

20. ABSTRACT (continued)

Two aspects presented in detail are (i) the development of an areal framework designed for future use in a deterministic distributed process model (Ch. 8), and (ii) the functional correlation of infiltration parameters with terrain properties, based on field experiments supplemented by geomorphic terrain evaluation (Ch. 9).

Other topics treated more briefly include: the instrumental record of the research watershed; description of the earth dam constructed for the purpose of future calibration of the available hydrologic and sediment data; development of a quantitative relationship between event rainfall energy and watershed sediment yield; the bedload transport problem in arid, flashy streams; results of the application of simplified lumped hydrologic modelling procedures to the Nahal Yael data; a seismic refraction survey of the Nahal Yael alluvial formation; and the development of a method to evaluate small-unit terrain characteristics for the future input into the Nahal Yael Arid Zone Geosystem Model.

Accession For	
NTIS	<input checked="checked" type="checkbox"/>
DTIC	<input type="checkbox"/>
Unannounced	<input type="checkbox"/>
Justification	
By	
Distribution/	
Availability Codes	
Dist	Avail and/or Special

UNCLASSIFIED

SECURITY CLASSIFICATION OF THIS PAGE(When Data Entered)

ARID ZONE GEOSYSTEMS *

Asher P. Schick

Division of Physical Geography
Institute of Earth Sciences
The Hebrew University of Jerusalem

September 1980

U.S. Army Research & Standardization Group (Europe)
Final Report, August 1978 - January 1980
DA-JA - Grant Number DAERO-78-G-111

APPROVED FOR PUBLIC RELEASE
DISTRIBUTION UNLIMITED

*Partially supported also by the Water Commission, Ministry of Agriculture, Government of Israel; the Melamid Foundation; and the Central Research Fund of the Hebrew University. Reproduction in whole or in part is permitted for any purpose of the United States Government.

THE FINDINGS IN THIS REPORT ARE NOT TO
BE CONSTRUED AS AN OFFICIAL DEPARTMENT
OF THE ARMY POSITION, UNLESS SO DESIGNATED BY OTHER AUTHORIZED DOCUMENTS

PRECEDING PAGE BLANK-NOT FILMED

C O N T E N T S

COLLABORATORS, 1978 - 80	9
ACKNOWLEDGMENTS	10
PROJECT PUBLICATIONS	12
1 INTRODUCTION	14
2 BASIC DATA	17
3 THE NAHAL Yael DAM	24
4 THE RELATIONSHIP BETWEEN RAINFALL AND EROSION IN NAHAL Yael	31
by Judith Lekach and Asher P. Schick	
5 PHYSIOGRAPHIC CHARACTERISTICS OF AREAL UNITS	34
by Oded Salmon, Eyal TaubenhauS and Asher P. Schick	
6 BEDLOAD TRANSPORT AND STREAM POWER - EXAMPLES FROM DESERT FLOODS	38
by Judith Lekach and Asher P. Schick	
7 GEOPHYSICAL SURVEY OF NAHAL Yael CHANNEL BED	50
by Asher P. Schick	
8 INFILTRATION TESTS	55
by Oded Salmon and Asher P. Schick	
9 THE AREAL FRAMEWORK OF THE NAHAL Yael MODEL	116
by Gabriel Sharon and Asher P. Schick	
10 RESULTS OF THE APPLICATION OF A SIMPLIFIED VERSION OF THE STANFORD WATERSHED MODEL TO NAHAL Yael WATERSHED 05	165
by Harriet Feldman	

COLLABORATORS

(1978 - 1980)

Schick, Asher P.	Coordinator, geomorphologist
Sharon, David	Climatologist
Shanan, Leslie	Consulting hydrologist
Porath, Asher	Consulting instrumentation engineer
Lekach, Judith	Senior research assistant
Nachmanovitch, Adina	Senior research and administrative assistant
Salmon, Oded	Research assistant (1978-80)
Zaken, Menashe	Laboratory of Geomorphology
Becker, Asaf	Observer and technical assistant (1979-80)
Enzel, Yehuda	Observer and technical assistant (1978-80)
Feldman, Harriet	Research assistant
Finkelstein, Sari	Research assistant (1979)
Gattegno, David	Technical assistant (1978-79)
Lieberman, Gil	Observer and technical assistant (1978-80)
Porath, Asaf	Observer and technical assistant (1978-79)
Sharon, Gabriel	Research assistant (1979)
Tal, Eran	Technical assistant (1979)
Taubenhaus, Eyal	Photogrammetric technician (1979)
ten Brink, Uri	Technical assistant (1978)

ACKNOWLEDGMENTS

Without the devotion of many of the collaborators listed on the previous page to tasks which were often frustrating, dull, thankless, distant from home, obstructive with regard to study assignments or teaching duties, and nearly always very hot and very dry, this report would not have been written.

Numerous other persons and institutions have been helpful in many ways, and it would be near-impossible to mention them all. By singling out a few, apologies are offered to the many who are not mentioned by name.

My colleague David Sharon has assumed responsibility for the project during my study trip to Australia (November 1979 - April 1980). He has contributed immeasurably throughout the years by lending an ear to problems - sometimes intractable, and to ideas - often wild, and by being a mainstay of level-headed advice.

Leslie Shanan was always a mine of experience as far as desert and water go.

Many other Hebrew University colleagues - in the Physical Geography section of the Institute of Earth Sciences as well as in the Department of Geography, have helped in various ways.

The Nahal Yael dam would not have been built without the help and interest of the Division of Soil Conservation and Drainage of the Israel Ministry of Agriculture (especially E. Henkin, Y. Wolf and S. Rudin), of the Jewish National Fund (especially Mr. Shamir), and of the Melamid Foundation (especially Professor Alexander Melamid). Nor would the dam be nearly as valuable as it is without the contribution of the Israel Water Commission's Hydrological Service (especially D. Kornic and S. Pollak).

Avihu Nelson of Eilat willingly went out of his way to assist with any field problem encountered. The help accorded, on various occasions, by the Hebrew University Oceanographic Station in Eilat, the Society for the Protection of Nature in Eilat, and the head office and Eilat personnel of the Israel Meteorological Service, is also gratefully acknowledged.

This report was finalized while the undersigned spent a research period of six months as a Minerva scholar at the Technical University of North Rhineland-Westphalia in Aachen; its chair of Physical Geography (Prof. F. Ahnert) offered the free use of its secretarial and editorial facilities. Mrs. Zemler typed the manuscript and the Institute of Geography drafting staff (Mr. Boug  and associates) produced most of the final figures.

Finally, I am grateful to the former and present research liaison officers at the U.S. Army European Research Office - Hoyt Lemons and Warren Grabau - for their unwavering interest and support.

Asher P. Schick

PROJECT PUBLICATIONS, 1977 -1979

- Schick, 1977, A tentative sediment budget for an extremely arid watershed in the Southern Negev. In "Geomorphology in Arid Regions" (D.O. Doehring, ed.), Publications in Geomorphology, State University of New York, Binghamton, N.Y., 139-163.
- Schick, 1977, Study of sediment generation, transport and deposition in semi-arid zones. Hydrological Sciences Bulletin 12: 535-542.
- Schick, 1977, The shaping of the landscape in the extreme desert: how much? when? how? (Hebrew). Abstract, Annual Meeting, Israel Geographical Society, Beer Sheba, 2p.
- Schick & Lekach, 1977, Concentration of suspended sediment and erosion mechanism in small watersheds in the rocky desert (Hebrew). Abstract, Annual Meeting, Israel Geographical Society, Beer Sheba, 3p.
- Schick, 1978, Field experiments in arid fluvial environments: considerations for research design. Zeitschrift für Geomorphologie, Supplementband 29: 22-28.
- Schick, A.P., D. Magid, 1978, Terraces in arid stream valleys - a probability model. Catena, 5: 237-250.
- Schick, 1978, The modelling of hydrologic and geomorphic processes in a watershed (Hebrew). Abstract, Annual Meeting, Israel Geographical Society, Bar-Ilan University, Ramat Gan.
- Bull, W.B., A.P. Schick, 1979, Impact of climatic change on an arid watershed: Nahal Yael, Southern Israel. Quaternary Research, 11: 153-171.

Schick, 1979, Fluvial processes and man in arid environments - applications to planning. GeoJournal, 3: 353-360.

Inbar, M., A.P. Schick, 1979, Bedload transport associated with high stream power, Jordan River, Israel. Proceedings, National Academy of Science, USA, 76(6): 2515-2517.

Shanan, L., A.P. Schick, 1979, The hydrology of the Negev desert highlands. International Symposium on the Hydrology of Low-Precipitation Areas, Canberra, December 1979. Programme & Late Papers, p. C21-C33. (To be published in Bulletin, Hydrological Sciences).

1. INTRODUCTION

Station 02 - the main streamflow gauging station of the Nahal Yael watershed - has recorded eight flows during the 14 runoff events that occurred in the catchment since the inception of the program in 1965. The six remaining flows were not large enough to traverse the mid-basin alluvial channel reach, into which they infiltrated. The last of these eight "throughflows" took place as a result of event 12, on 20-21 February 1975. Since then, for a period of five-and-a-half years, not a drop of floodwater has wetted the weir of station 02.

This example is one of many that could be presented for the extreme variability in time of phenomena which control the mechanics of arid zone geosystems. We have for Nahal Yael a data bank which, however, valuable and unique, parallels - from several points of view - a record of one or two years' duration only in a non-arid watershed. This has been expected, of course, at the time the program originated 15 years ago, but the extremity of the behavior could not have been fully appreciated. It is clear now that a period of a few decades is the minimum period of observation for supplying a reasonable measurement record of cumulatively dominant terrain processes in the extreme desert.

Given this situation, the other approach possible for understanding quantitatively the mechanics of hydro-geomorphic watershed response on an event-to-event scale is a strictly deterministic process approach. This can be accomplished only on the basis of responses of small unit areas during short time intervals, with results, subsequently appropriately integrated over time

and space, meaningfully compared with data measured on the watershed scale.

The report herewith presented reflects the transition of the emphasis of the Nahal Yael Research Project from the direct measurement approach of the late sixties and early seventies, to the deterministic modeling approach of recent years, which we hope to develop in the early eighties. As in the earlier major report (Schick & Sharon, 1974), we elected also in the present report to include certain studies in detail, while others are treated only in summary form. In this sense the central parts of this report are chapter 8, which presents an areal framework for the development of a geosystem-oriented, distributed, deterministic model, and chapter 9, which summarizes an innovative series of field experiments designed to functionally correlate infiltration parameters with terrain properties.

The "instrumental" part of the work is summarized in chapter 2 and 3. As shown in chapter 2 the last few years were lean ones in terms of major flood events. This fact, however, gave us the opportunity to complete the design, construction, and instrumentation of the Nahal Yael dam, over a period of more than a year, without the loss of either data or construction equipment and material. The dam, described in chapter 3, is expected to impound total flow volumes and total sediment yields for all events up to a near-catastrophic magnitude, and thus will considerably enhance the credibility of the water and sediment data recorded since 1965.

Work more oriented toward modelling the watershed processes is summarized in chapter 4, which presents a relationship between rainfall energy and watershed sediment yield, and in chapter 6, which discusses the bed-

load transport problem in arid streams. The results of an attempt at conventional, simplified lumped modelling for runoff is summarized in chapter 10. Chapter 7 is a brief report on a geophysical survey conducted along the main alluvial reach of the Nahal Yael watershed in order to obtain depth to bedrock, and through it, an estimate of its water storage capacity and flood abstraction potential. Finally, chapter 5 presents the initial results of our search for a method to quantitatively represent such small-unit terrain characteristics which affect the parameters of the Nahal Yael arid zone geosystem model.

Contrary to many other modelling studies, which depend heavily on sophisticated mathematical-hydraulic exercises with but little organic input of real-world conditions and processes, the study reported here is essentially field-based. Although an effort is continuously made to work with general principles and universally applicable techniques (such as, for example, the areal framework and unit terrain characterization), the opportunity of constant intercourse with a real-life, operating, and process-oriented instrumented watershed while developing the model is regarded by us as a definite advantage. We hope to be able to continue this dual task in future.

2. BASIC DATA

The Nahal Yael watershed instrumental network continued to function along the lines indicated in the previous report (Schick & Sharon, 1974), with the following changes:

Rainfall: Four recorders are now regarded as satisfactorily representative of the catchment rainfall, as concluded on the basis of the elaborate network maintained for a number of years in the past. Rainfall values applicable to the small upstream Nahal Yael catchments 04 and 05 are adequately represented by averaging one hilltop and one valley station.

Instrument 30 had to be moved a few meters uphill, as it stood originally too close to the rock-cut central part of the reservoir overflow channel (see chapter 3 below).

Considerable use was made of information available from radar screens with regard to alerts for probable events and decisions as to organizing flood survey teams.

Runoff: Station 01 at the foot of the Nahal Yael alluvial fan near Nahal Roded confluence was discontinued with the beginning of the construction of the dam. Its instrument was moved to the upstream side of the dam and installed as a reservoir water level gauge (see chapter 3 below).

The hydraulic controls associated with the gauging stations of the Nahal Yael watershed have gradually silted up to an unacceptable degree during their decade of operation. On several occasions in the past, sediment from the immediate vicinity of the connecting intake

pipes was cleared, but the continued piling up of sediment in the larger area behind the weirs posed a severe problem. Plans for the removal of this sediment and the restoration of the original stilling basin properties were complicated by the inaccessibility of all four sites for vehicles or for any other mechanical equipment too heavy to carry up the dam and the rock waterfall by hand.

In July-August 1978 the sediment clearing was accomplished by a group of four student-assistants. About 50 cubic meters of sediment were excavated by shoveling according to predetermined specifications, hauled by wheelbarrow to the weir and dumped down the downstream side of the control. Thereby the gauging stations have been restored to their original level of accuracy at least for the few coming events.

Sediment: Automatic suspended samplers 71 and 72, previously located on or downstream of the dam site, have been discontinued. The middle and lower bedload traps have also been dismantled.

In line with our increased interest in the small upstream watersheds due to their importance for evaluating watershed processes, two new automatic suspended sediment samplers (Nos. 78 and 79) were installed in 1979 in tributaries of watershed 04.

Narration of events: Since event 12, which occurred in February 1975, a period of "non-flows" set in. This was nearly broken early in 1977, when on one occasion runoff threshold was closely approached, but not actually reached.

On 7 February 1978 simultaneous reports were received from several voluntary informers and through the radio of a storm which hit Eilat and yielded 14 mm of rainfall. On the assumption that such a considerable amount of

rainfall (nearly one half of the mean annual amount) is bound to have some regional influence, and therefore also affect Nahal Yael 3 km away, a flood survey team of six was quickly organized. The team left Jerusalem within a few hours of the event, but upon reaching the watershed was disappointed to find that, due to a particularly sharp rainfall gradient which existed between Eilat and Nahal Yael, only 3 mm fell in the latter. This amount was insufficient to generate any flow except on a few rocky slopes.

Event 13 finally arrived on 11 December 1978. It began with a few intermittent rains of low intensity (0.05 mm/min and less). Gradually the rains became stronger, but the peak intensities for the 3-hour rain duration reached only medium-low values: 0.33 mm/min for station 24; 0.27 mm/min for station 30. These values obtain for periods of 2-3 minutes only; hence the total storm rainfall of 11.0 mm (a mean value between one hilltop gauge and one valley gauge) fell in an exceptionally temperate and inerosive manner.

The response of the watershed to this kind of rainfall is of particular interest. Despite the large rainfall amount, which in all earlier events did not fail to yield at least some flow at the downstream stations (03, 02), only the upstream stations recorded a flow.

The main data are listed in Table 2.1.

The peak discharges are very low. All of the considerable volume of water percolated into the alluvial reaches downstream of station 04, as well as in the short alluvial reach upstream of station 03. The capacity of the alluvial fill to absorb the floodwaters must have been close to the absolute maximum, as nearly four full years have elapsed since the previous flow. Thus this event also provides important information as to the storage volume of the alluvial fill.

Fortunately event 13 occurred during the presence in the watershed of the team doing rainfall-infiltration-runoff experiments (see chapter 9 below). This team managed to organize itself and perform several useful observations and measurements during the event, as well as to make sure that all instruments functioned properly. Only the vacuum-type liquid sampler did not yield data, because its intake level was above the stream water level during the entire flow. Originally a very low and protracted flood wave such as in event 13 was not anticipated, but steps have since been taken to lower the intake.

From manual water samples collected by the team the following suspended sediment concentration values were obtained:

Slope runoff in the vicinity of stn 02	1500 ppm
Channel flow, peak stage	1500
" " , immed. post-peak	600
" " , 40 min. after peak	100

A "near-event" occurred on 7 February 1979, and was caused by a low-intensity rainfall of 5.4 mm (station 33) spread over a period of nearly 3 hours; 4.7 mm fell evenly during 40 minutes. As on 7 February 1978 - exactly one year earlier - only some rocky slopes generated surface runoff, and channel alluvium quickly absorbed all incoming flow.

Event 14 came 2 days later, on Friday, 9 February. A small team was working in the watershed on routine maintenance assignments. Arriving just in time for the effective part of the rainstorm, useful work during the flow could be accomplished.

The mean total rainfall over the watershed for event 14 was 6.9 mm. Intensities were low, but the rainfall amount was sufficient to generate a flow in the upper part of

the watershed. Undoubtedly the partial saturation of the colluvial and alluvial deposits by the rainfall two days earlier contributed to the flow. At stations 05 and 04 the flow was very low, but it lasted for about $1 \frac{1}{2}$ hours; its farthest downstream extension was only 200 meters below 04. Evidently the storage of the main alluvial reach was still in a state of nearly total depletion, due to the lack of any large scale replenishment during the preceding period of four years (since event 12 - February 1975).

The hydrologic data for event 14 are listed in Table 2.1.

The presence of a team in the watershed at the time of the flow enabled the detailed sampling of the floodwaters for sediment content. As in a previous event, station 05 was selected for the purpose. Manual sampling of the total load was made at $2 \frac{1}{2}$ -minute intervals, starting with the peak flow. In addition, data are available from the vacuum-operated sampler, whose level had been appropriately lowered following event 13, as well as one sample from Hayim-type instrument 77.

Preliminary results indicate that, for total load, concentration jumped from 310 ppm at the time of peak flow to 1750 ppm 3 minutes thereafter. Concentration remained over 1000 ppm for another 10 minutes, and fell gradually to 110 ppm in the flow recession. The vacuum-type samples (fine suspended material only) had concentrations between 730 and 260 ppm.

A detailed grain-size analysis of all samples is currently underway.

Late May and the first half of June 1979, had numerous cloudy days in the project area. Situations of near-rain developed several times. Accordingly, it was decided to prolong the recording season through the end of July. However, by mid-late June, weather returned to the normal summer heat and dryness, and no rain fell until

Table 2.1: Events 13 and 14, Nahal Yael Watershed -
Hydrologic Data

	<u>Stn 05</u>	<u>Stn 04</u>	
<u>Event 13 - 11 Dec 1978</u>			
Peak discharge	0.038	0.02	m ³ /s
Rainfall	11.0	11.0	%
Rainfall volume	550	1240	m ³
Runoff volume	53	110	m ³
Runoff-rainfall ratio	9.6	9	%
<u>Event 14 - 9 Feb 1979</u>			
Peak discharge	0.029	0.029	m ³ /s
Rainfall	6.9	6.9	mm
Rainfall volume	345	770	m ³
Runoff volume	31	30	m ³
Runoff-rainfall ratio	9	4	%

the closing date of this report.

Contrary to 1978, when 50% of the instruments were kept in operation in the watershed (in rotation, to facilitate summer maintenance), it was decided in 1979 to dismantle the entire system for the three summer months. A few years earlier, it was decided to continue one half of the basic instrumentation throughout the summer on a rotating basis, in order to take care of a possible, though quite unlikely, occurrence of a summer cloudburst of the 1926 type. This resulted in some mechanical problems in certain instruments, probably due to excessive heat, which had generated ambient temperature levels inside the instrument housings which were beyond the tolerance of certain parts. This caused considerable problems, which will be hopefully prevented in future.

Contrary to the very rainy character of the 1979/80 water year in the entire country, including the northern and even central Negev, no runoff event occurred in Nahal Yael during the entire year. Even the destructive floods of the southern Sinai, which caused so much damage in and around Ophira (Sharm-esh-Sheikh) left the Nahal Yael stream channels dry.

3. THE NAHAL Yael DAM

A tentative water and sediment budget for the 0.5 km² Nahal Yael watershed 02 has been prepared on the basis of detailed observations of rainfall, streamflow, sediment transport and deposition, and of quantitative changes in geomorphic features (Schick, 1977). For the ten year period considered, (1965/66 to 1974/75), the mean annual rainfall was 31.6 mm. 99 per cent of the geomorphic work was accomplished during five days by seven discrete events.

Sediment in suspension, computed from data obtained from automatic sampling program, accounted for a mean annual yield of 127 tons. Bed load yield was estimated on the basis of (1) distance of transport determined from traceable particles, (2) determination of the area and depth of the scour layer for the in-channel bed and for the gravel bars, and (3) a comparison of grain sizes on the bed and bars with sediment in transport as sampled by liquid samplers and bed load traps. A mean annual yield of 66 tons was found. The dissolved load was only about one per cent of the total load. The resulting mean annual sediment yield of 388 tons/km² considerably exceeded the accepted norm for arid environments. It also exceeded by a factor of 3 the estimated sediment yield, corrected for drainage area, for the 3,100 km² watershed of Wadi Watir, located in a similar environment in Eastern Sinai.

While the internal sediment delivery ratios of the Nahal Yael drainage system as found were reasonably consistent, the aggradation rates, as measured directly on the alluvial fan over a period of six years, were only

one fifth of what they should be on the basis of the sediment transport computations. The main reasons for this large difference seem to be an insufficient understanding of the transport mechanism during violent desert floods, exchanges between suspended and bed load transport modes, and the importance of transient alluvial storage and its intense localization. But inadequacies of the sampling and measurement network may also be responsible for the discrepancy, at least in part.

The idea to construct a 100% trap efficiency structure for water and sediment within the Nahal Yael project is not new. Actually watershed 03 has been kept "free" for this purpose since the detailed instrumentation network was installed at the beginning of the 1967/68 water year. The need for calibrating the measurements during transport of water and sediment in relation to uncontroversial data of total flow volume and total sediment load became much more pressing in the light of the results of the ten year budget.

But watershed 03 did not seem any longer to be a suitable candidate for calibration by damming: it had only one gauging station with little variety in its predominantly bedrock channel (the alluvial reach is limited to the lowest 70 meters); its suspended sediment record is dull, no bedload data (traps or traced particles) were available, and the network of channel cross sections was practically non-existent. Above all, watershed 03 was too small a tributary (drainage area 0.13 km^2) for reasonable generalizations of the anticipated results.

Therefore the choice turned toward damming the entire Nahal Yael watershed, approximately at the apex of the alluvial fan. The decision to do so was not taken lightly. The construction meant the termination of gauging station 01 at the foot of the alluvial fan near confluence to Nahal Roded, as well as of the automatic sediment samp-

lers 71 and 72 and of the lower and middle bedload traps. Moreover, it meant the discontinuation of the topographic sections which monitored the changes on the alluvial fan from flood to flood.

However, the prospect of obtaining an independent check on the runoff and sediment data obtained from the various station in the middle and upper part of the watershed outweighed the reservations mentioned above. Monitoring the water flow - total volume in the reservoir as well as the inflow (and overflow) discharge - would considerable improve the rating curves of the gauging stations. Accurate volumetric determinations of the sediment volume which accumulates in the reservoir during discrete events would lend much confidence to the sediment discharge figures which were up to now based mostly on floodwater samples abstracted during the rise of the flow.

Additional benefits of such a venture would be: I) observation on and accumulation of experience with regard to the construction operational aspects of small, simple and inexpensive earth dams in an extremely arid environment; and II) evaluation of longer-term environmental effects, caused by the expected increased percolation in the reservoir bed, with subsequent vegetation response (mainly acacia trees) and the concomitant increase of faunal activity (mainly gazelles) - all factors which could result in changing the spot into a pleasant rest site for hikers and motorists.

Detailed plans were accordingly drawn in 1977 for the construction of a 7 meter high earth dam, with an impounding capacity of about $8,500 \text{ m}^3$. A flood volume of such a magnitude is caused by an event frequency of one in 15 to 20 years. The amount of gravel and sand involved in such a structure was estimated at $6,000 \text{ m}^3$, to be derived locally from the present and Pleistocene fans immediately downstream the dam site. The plans also called

for the reduction of the dam permeability, conditioned by the coarse-grained character of the material on site, by suitable methods such as a plastic coating. A concrete spillway with an appropriate hydraulic control were designed for the right-hand valley side near rainfall recorder 30; in such a way the potentially dangerous overflow would be kept away from the earth embankment.

Because of financial constraints, the project as described above had to be subsequently redesigned on a more modest scale. The structure as actually built used only $3,000 \text{ m}^3$ of earth. It has an overall height of 5.5 meters, a maximum depth of impoundment of 5 m, and a water/sediment capacity of somewhat over $3,000 \text{ m}^3$. The material was local sand and gravel, with large boulders forming the base of the downstream embankment slope. Construction started in December 1977 and was completed in summer 1978. (Photographs 1-3). Ancillary work completed a few months thereafter included:

I) A concrete-lined overflow channel with a prefabricated metal crump weir were constructed and installed on the right-hand valley side over a bedrock sill several meters away from the end of the embankment.

II) Two independent water level recorders, to monitor the impounded water level and the depth of overflow. One is a conventional float-operated Ott recorder and the other is a pneumatic type Rimco (Australia) recorder.

III) The reservoir bottom was completely graded, in order to facilitate post-flood accurate surveys of water and sediment. Several marker plates, made of sheet metal, were installed. These should facilitate augering and sampling after the expected silting. The plates were coated with a layer of sediment particles, to keep their hydraulic roughness similar to that of the "natural"

bottom. Approximately 25 benchmark referenced cross-sections were accurately surveyed across the expected lake area.

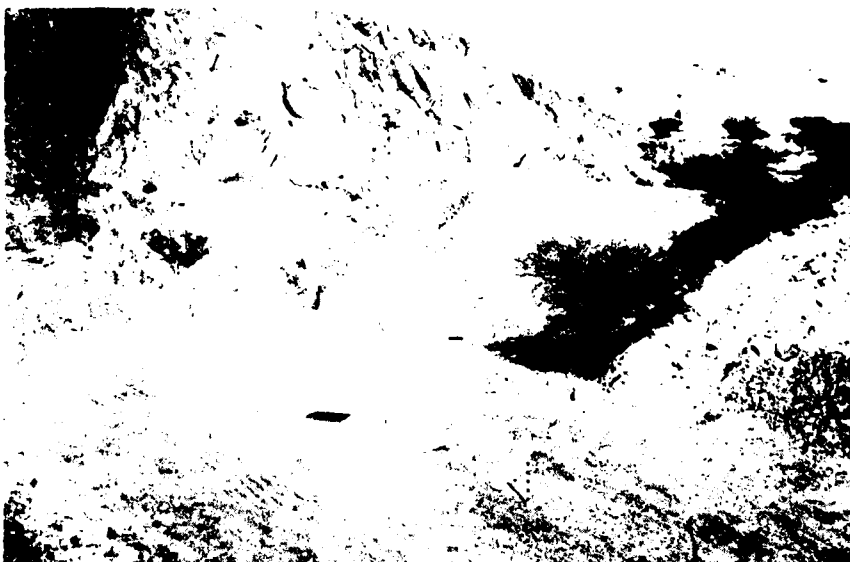
IV) The presence of the earthmoving equipment on the site was utilized for an exploratory excavation, 2.5m deep, at the apex of the active alluvial fan. The exposed section of alluvium is being studied in relation to a similar section in the Pleistocene fan, also freshly exposed during the construction. The purpose of this study is to evaluate the spectrum of hydrologic events in each of the fans, with a bearing on extreme events recorded and on climatically effected changes.

V) The steep downstream side of the overflow channel has been protected with combined stone-concrete masonry work, to prevent erosion of the toe of the embankment by a major overflow. The dam was designed in such a way as to lose water by controlled seepage through the embankment. Although the rate of seepage is as yet unknown, it is expected to be slow enough so that the interpretation of the inflow rate into the lake and the eventual outflow rate through the overflow channel will not be seriously jeopardized. For future flows which will fill the reservoir, the seepage losses are expected to gradually decline.

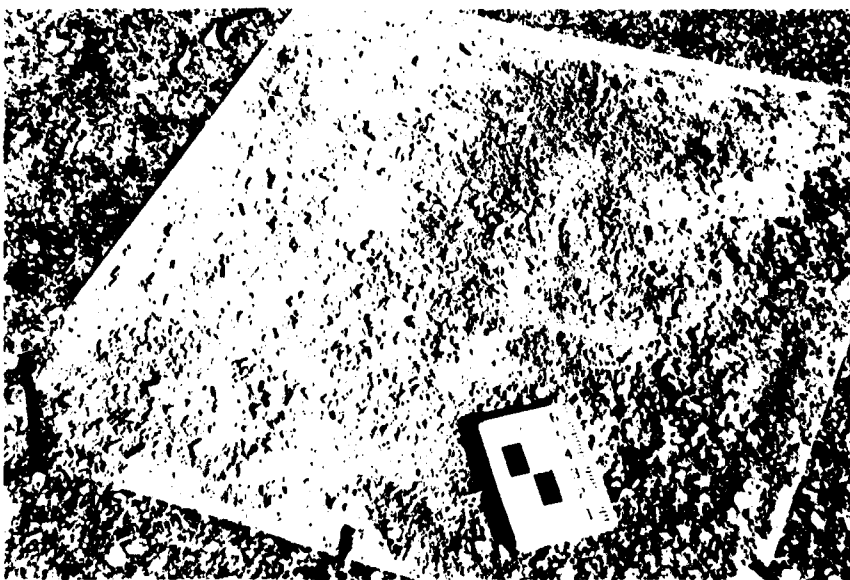
During the first two water years after the completion of the dam (1978/79 and 1979/80) not a single drop of water passed through Nahal Yael station 02 to enter the reservoir. During the thirteen previous years a flood which would have flowed into the reservoir occurred eight times. In fact, no flow was recorded at station 02 (at the top of the dry waterfall immediately upstream of the reservoir) since event 12 (20/21 February 1975), i.e. during the last five and a half years.



1 The Nahal Yael dam site before construction



2 The reservoir bottom and the completed dam



3 A reservoir sedimentation reference plate

It is hoped that the dam will yield important information for research as well as of an applied nature.

4. THE RELATIONSHIP BETWEEN RAINFALL AND EROSION IN NAHAL Yael

by Judith Lekach and Asher P. Schick

In order to better understand some of the factors which underlie the fluvial erosion process of the extreme desert, as represented by the by now numerous data obtained from the network of multiple stage automatic suspended sediment samplers (Schick & Sharon, 1974, and subsequent data), several preliminary analyses of the Nahal Yael record were undertaken.

A fairly large number of two-variable and error regressions between various assumed causative factors (mostly rainfall derivatives) and the erosion data - represented by the mean vertical suspended sediment concentration - were conducted. For small non-alluvial watersheds such as 03, 04, and 05 at Nahal Yael, the best fit was consistently obtained between a rainstorm derivative defined as effective rainfall energy calculated for 3-minute time intervals, and the mean vertical suspended sediment concentration. The linear regressions yielded correlation coefficients between 0.94 and 0.83. Then the goodness of fit was further improved by varying: I) the initial rainfall loss prior to the initiation of runoff, and II) the infiltration rate during the period of effective rainfall (assumed to be constant). By best-fit procedures, the initial loss was found to be a function of drainage area, as follows:

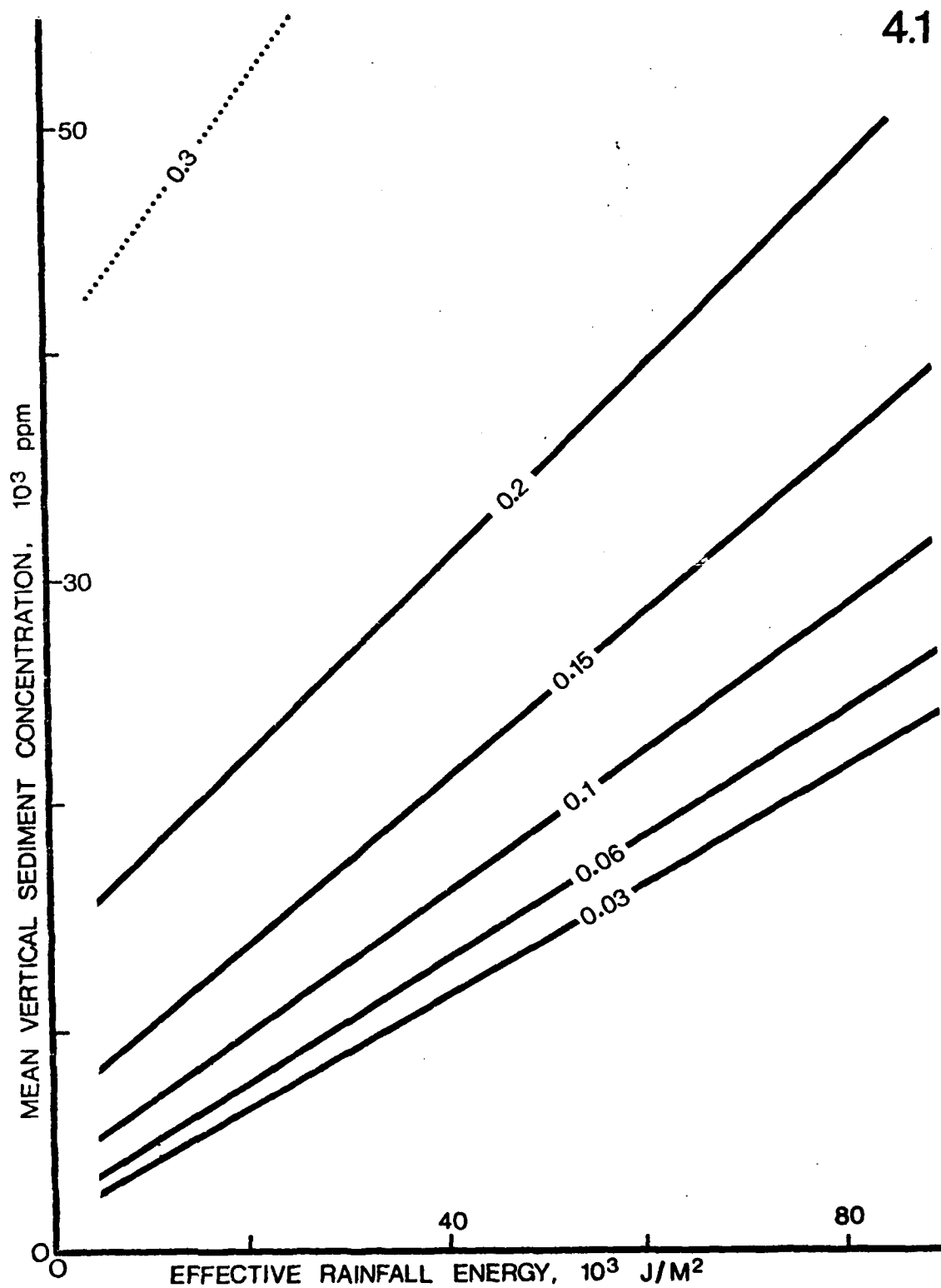


Fig. 4.1: Fluvial suspended sediment content and rainfall energy for floods in extremely arid small, non-alluvial watersheds, based on Nahal Yael watersheds 03, 04, and 05. The lines inside the diagram represent drainage area in square kilometers.

watershed 05 - 4 mm

watersheds 04 & 03 - 5.5 mm

The procedure further indicated a preferred constant infiltration rate of 0.5 mm/3 min. Both findings corroborate, independently, the general range of the conclusions concerning runoff generation summarized in Schick (1970), and are also in general agreement with results of infiltration tests summarized in this report (see chapter 9 below).

The resulting erosion rate model is summarized in figure 4.1, which correlates the effective rainfall intensity of the event with the mean vertical suspended sediment concentration, for various watershed sizes. A similar, though not identical, relationship was found satisfactory for erosion values derived from small ($2m^2$) plots (Pearce 1976), indicating the validity of the Hortonian overland flow model in preference to the partial area contribution model. The fact that physiographically fully developed watersheds in the 0.05-0.5 km^2 size range behave identically, further supports the Hortonian overland flow interpretation over the saturation overland flow concept in arid terrain.

The relationship shown on fig. 4.1 breaks down when data from watersheds which include a sizeable portion of continuous channel alluvium are used. Under these conditions, which are practically universal for desert watersheds whose area exceeds 0.3 km^2 , an additional factor must be introduced.

5. PHYSIOGRAPHIC CHARACTERISTICS OF AREAL UNITS

by Oded Salmon, Eyal Taubenhaus and Asher P. Schick

5.1. Selected elements

In order to obtain a "feel" for data collection, handling, and relevance for the purposes of developing a deterministic and distributed hydrologic and geomorphic model for Nahal Yael, six areal elements in watershed 05 were selected for detailed field study. This work was carried out at a time when our idea was to develop the model on the basis of a triangular grid. In such a framework, each areal element is an equilateral triangle, side 21.65 m, height 18.75 m, and unit area very close to 200 m^2 (actually 202.975 m^2).

This triangular grid was subsequently abandoned as the basis for the model in favor of a rectangular grid. The information assembled, however, continues to be of importance as a basis for correlations between field truths and information derived manually or automatically by means of remote sensing methods.

Each of the six sites was first located on an aerial photograph by using criteria of terrain representativity. Then each triangle was sited in the field. The corners were staked and the sides marked and bounded by colored plastic tape. Each triangle was photographed in totality from behind of each of its three apices. Several terrain closeups were also taken.

A level survey determined the relative elevation of the three apices and of the centermass point of the triangle. This procedure was aimed specifically at getting a measure of "internal relief" - a factor of potential relevance to the approximation of several physiographic controls for the model, as well as one possible objective yardstick for a further subsequent sub-division of certain areal elements until a desired degree of homogeneity is achieved (see chapter 8).

A field sketch of each triangle was made, showing the distribution of colluvium and of rock (defining different types), and topographic irregularities such as scarplets, joints, rills, hollows, etc. Information on colluvium character and particle size was also noted.

In addition, the following measurements or semi-quantitative estimates were recorded for each triangle:

- (1) percent bedrock and percent colluvium;
- (2) depth of colluvium;
- (3) density of colluvium (qualitative estimate in three classes);
- (4) roughness of colluvium surface (four classes);
- (5) median size of colluvium particles;
- (6) concentration potential of runoff (five classes) judged mainly by connectivity of bedrock patches;
- (7) "internal relief", defined as the difference in elevation between the actual height of the centermass point and the mean value of the heights of the three apices.

In most parameters significant differences among triangles was obtained. The prospects of obtaining most of values from remote sensing procedures seem good. As a first step, a relationship will be established between

5.1

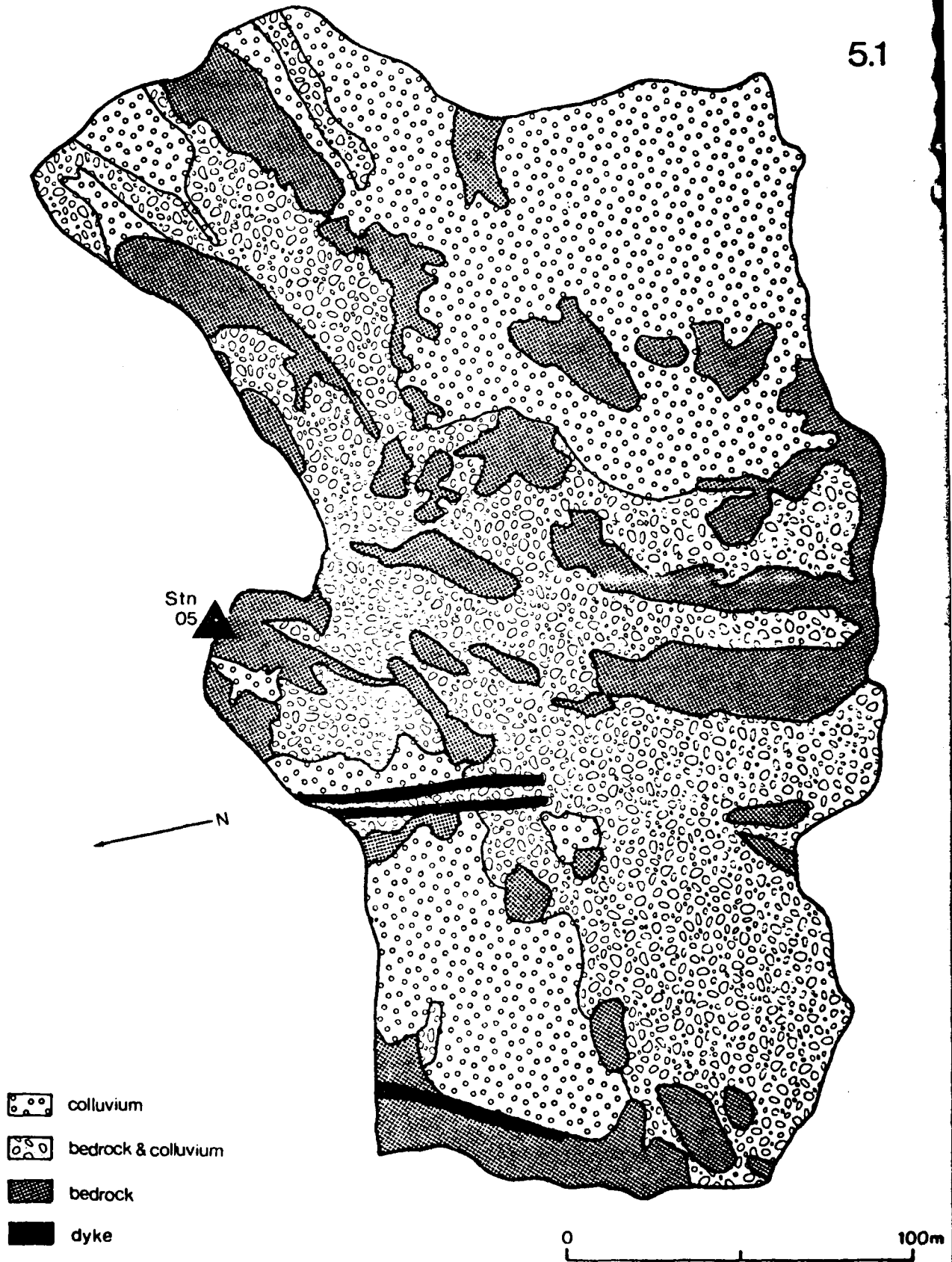


Fig. 5.1: Terrain lithology, Nahal Yael watershed 05. Based on aerial photograph interpretation with limited ground control. Map has not been corrected for photo distortion.

the detailed site characterization and the mapping off aerial photographs of bedrock/colluvium areas (paragraph 5.2 below).

5.2 Bedrock/ colluvium airphotomap, watershed 05

Figure 5.1. shows the distribution, in Nahal Yael watershed 05, of bedrock, colluvium, and colluvium/bedrock combination. Major dyke rocks are also shown.

The "colluvium/bedrock combination" represents an inter-fingering of areas of the two lithologies too fine to differentiate at the scale employed. In many cases it represents intermittent and/or thin patches of colluvium which overlies bedrock which crops out at fairly close intervals beneath the colluvium.

The distribution was mapped on the basis of aerial photography interpretation, with only a limited amount of ground control.

A rough approximation of the areal extent of the three main formations is:

bedrock	30 per cent
colluvium	10 " "
colluvium/bedrock	60 " "

The colluvium/bedrock combination is estimated to comprise, areally, two-thirds colluvium and one-third bedrock. Substituting these figures, we find that roughly one half of watershed 05 is covered by a colluvial veneer; the other half is bare rock.

The areal distribution (fig. 5.1) will be used in future, together with the geological map, the detailed triangles study, and additional work, to define numerically each unit area for physical characteristics such as infiltration and roughness.

6. BEDLOAD TRANSPORT AND STREAM POWER EXAMPLES FROM DESERT FLOODS

by Judith Lekach and Asher P. Schick

6.1 Bedload transport and stream power for two floods, Nahal Yael watershed 05.

Events 12A (20 February 1975) and 14 (9 February 1979) occurred in Nahal Yael, fortuitously, during field periods of the study team, whose presence on site facilitated the collection of usually unobtainable manually sampled and time-discharge controlled sediment data.

Both flows were really of a relatively small magnitude, peak discharges between 0.04 and 0.12 m³/s. But given the extreme paucity of such data, even these flows should provide an important insight into the factors and mechanisms of sediment transport in small extremely arid watersheds.

Event 12A was rather untypical: 38.4 mm of low-intensity rain (mean between valley station 30 and ridge station 26) fell over a period of 9 $\frac{1}{2}$ hours, and generated during its latter half an extended hydrograph with several low peaks. During the flow APS collected manually 25 samples of the total load at the foot of a bedrock riffle immediately upstream of gauging station 05. Most of the samples were taken from the first flood-wave and from its recession, but a few were also taken at certain intervals from the subsequent floodwaves.

Table 6.1: Bedload transport rate for event 14 (9 Feb 1979), Nahal Yael watershed 05;
slope = 0.044

Sample number	Sediment discharge (kg/s)	Percent bedload (%)	Bedload transport rate (kg/s)	Unit bld. transport rate (kg/m.s)	Water discharge (m ³ /s)	Unit stream power (kg/m.s)	Median bedload size (mm)
1	0.018	56	0.010	0.020	0.027	1.81	0.32
2	0.037	30	0.011	0.022	0.028	1.88	0.174
3	0.05	54	0.027	0.054	0.029	1.96	1.06
4	0.04	60	0.024	0.048	0.027	1.81	0.82
5	0.027	68	0.018	0.037	0.022	1.43	0.82
6	0.025	87	0.022	0.044	0.016	1.06	0.84
7	0.007	76	0.005	0.011	0.011	0.75	0.60
8	0.003	47	0.0014	0.003	0.009	0.57	0.167

6.1

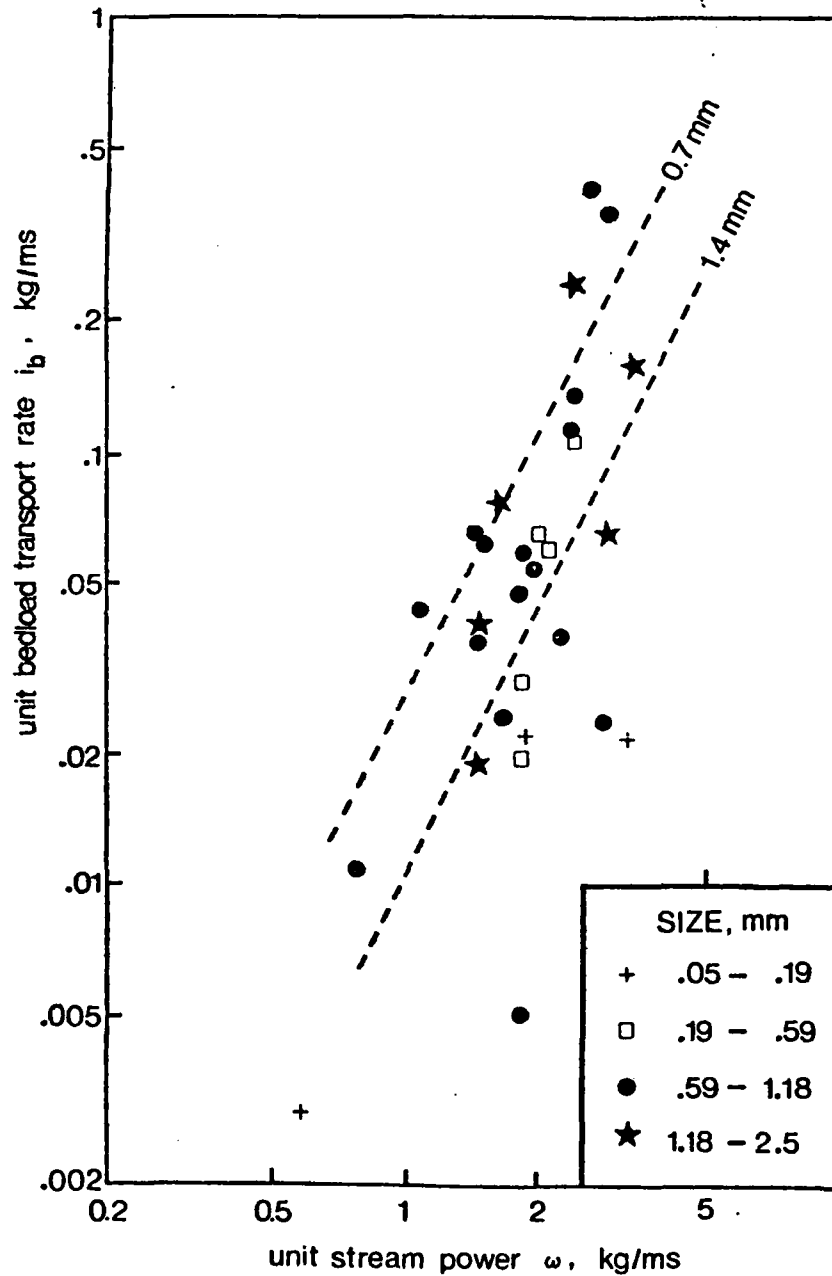


Fig. 6.1: Bedload transport and stream power, Nahal Yael watershed 05. Based on events 12A (20 Feb 1975) and 14 (9 Feb 1979). Figures inside graph indicate median grain size of the bedload (> 0.063 mm) only.

Event 14 was a small flood, very typical of desert conditions: a short high-intensity rain yield a steep flow rise with a slower decline, uncomplicated by any additional rainfall.

Sediment concentration peaked simultaneously with discharge in event 12A, and was slightly later than peak discharge in event 14. There is some suggestion of a secondary peak in concentration down the recession of event 12A, but this needs further corroboration.

The samples of both floods were subjected to a particle size analysis. For the following analysis only the bedload fraction, defined here as larger in size than 0.063mm, is considered. The median size of the bedload fraction is determined, and the associated unit bedload transport rate and unit stream power are computed. The unit power needed for initial motion proved to be negligible, and is disregarded. Table 6.1 shows the detailed data for event 14.

The data for both events align well on the standard i_b versus ω graph, and seem to parallel, more or less, data for other streams (see 6.2 below). A comprehensive treatment of the bedload transport rate in Nahal Yael must incorporate data on larger particles such as available from bedload traps and tracing experiments.

6.2. Bedload transport and stream power for an extreme event, Wadi Mikeimin, Sinai

6.2.1 Abstract

A reconstruction of a low-frequency high-magnitude flood event, which occurred in 1971 in Wadi Mikeimin in the arid SE Sinai Mts., enabled the evaluation of bedload transport rates in relation to flow characteristics. Unit transport rates between 20 and 100 kg/m.s (at least one order of magnitude higher than nearly all data previously reported), accord with data on other rivers. The proportionality of bedload transport rate to unit stream power in excess of

that necessary for initial motion, raised to the power of $3/2$, has been validated for these very high transport rates which approach debris flows in character.

6.2.2. Introduction

Direct measurement of the transport of coarse bedload in heavily laden desert floods is practically impossible to accomplish. In certain fortuitous cases, in which the total load is found as a deposit and measurable, and enough data are available to reconstruct the stream-flow and evaluate its characteristics, indirect estimates of bedload transport are possible. The value of these estimates is two-fold: They may offer additional experimental validation of the proportionality between bedload transport rate and the $3/2$ power of excess unit stream power (1,2); and they extend the body of data beyond the range presently available from direct measurements (3, 4). Such estimates for an exceptional event in the Jordan and Meshushim rivers, northern Israel, yielded compatible data of bedload transport rate and stream power one order of magnitude higher than previously known (5). The exceptional event of January 1971 in Wadi Mikeimin, southeastern Sinai, which caused large quantities of bedload to be transported and deposited them in entirety as a new alluvial fan at the watershed outlet, enables another controlled estimate of the same type.

6.2.3. The Watershed

Wadi Mikeimin is an uninhabited tributary of Wadi Watir, which drains 3100 km^2 of extremely arid mountainous country towards the large alluvial fan of Neviot (Noueiba) on the shore of the Gulf of Aqaba. The 12.9 km^2 watershed is entirely composed of precambrian basement

rocks with tertiary volcanic intrusions, crossed by numerous NNW-SSE runoff faults. The mean annual rainfall is estimated at 30-40 mm and is highly erratic. Due to a relief difference of 600 m in the 5 km long watershed, slopes are rocky and steep but covered in part by coarse grained colluvium. Average stream channel gradients of Wadi Mikeimin and of its main tributaries are between 5 and 10 per cent. Most of the valley network is alluvium-covered, braided between rocky banks, and its low bars are composed of particles mean size between 29 and 53 mm. Large boulders of diameter up to 1500 mm are also present.

6.2.4 Mikeimin Flood

In January 1971 the sudden appearance of an alluvial barrier at the mouth of Wadi Mikeimin was reported. Being located at the western margins of the Ein Fortagha springs area, the barrier caused the emergence of an up to 400 m long "finger" lake on its upstream side.

The barrier proved to be an alluvial fan deposited by a highly localized and short-lived flood event in Wadi Mikeimin. Detailed field work both before and after the complete erosion of the fan by the November 1972 flood in Wadi Watir (7) enabled a reconstruction of the water and sediment characteristics of the Mikeimin event (8).

6.2.5 Methods

The analysis involved in the reconstruction of the event proceeded along the following stages: (a) high water marks at 8 judiciously selected stations in the watershed enabled the evaluation of peak discharges for the event; (b) comparison with other flood events which occurred over the last 15 years in Nahal Yael and in Eastern Sinai (9, 10), evaluated in the light of various studies on rain characteristics (11) enabled the construction of probable hypothetical hydrographs.

Table 6.2. Summary reconstructed data of river hydraulics and bedload transport, Wadi Mikeimin, Sinai

Station	M, main channel	tributary D	tributary 1
Discharge range $Q, m^3/s$	5 - 68	5 - 80	2 - 47
Width w, m	18.8	28.5	40
Slope $s, m/m$	0.087	0.085	0.075
Depth d, m	0.4	0.36	0.20
Unit stream power ^a $\omega, kg/m.s$	169	127	46
Bedload size ^b D_{50}, mm	31 ^c	16 ^d	8 ^d
Bedload yield tons ^e	10,000 ^f	8,000 ^g	3,400 ^g
Duration ^h min	60	50	35
Unit transport rate ^k $i_b, kg/m.s$	92	58	25
Unit power ¹ at initial motion $\omega_0, kg/m.s$	0.37-3.6	0.15-1.5	0.05-0.52
Excess unit power ^m $\omega - \omega_0, kg/m.s$	165	125.5	46
Ratio of flow depth to median bldd size $Y/D_{50}, m/m$	12.9	22.5	25
Unit transport rate ⁿ	45	62	21

- ^a $\omega = Qs/w$; mean value for discharge range.
- ^b Estimated median diameter of particles (b axis).
- ^c Based on measurements along the truncated face of the Mikeimin alluvial fan.
- ^d Based on Leopold (13) counts at the station.
- ^e Immersed weight, metric tons.
- ^f Estimated from deposit.
- ^g Estimated by the Einstein (12) procedure, compared with the deposit.
- ^h Estimated from reconstructed hydrographs.
- ^k Based on this research.
- ^l Estimated by multiplying the Shields critical shear stress by the reconstructed mean velocity; range reflects two different variants of the computation.
- ^m Using highest value of estimated ω_0 .
- ⁿ Computed by the Bagnold (2, equation 4) procedure.

(c) the Einstein bedload computation procedure (12) was applied to three of the cross sections, in relation to the computed hydrographs and bed material size. The bulk size distribution of the alluvial fan deposit was also taken into account. (d) Comparison between the total bedload yield as computed with the actual bedload volume as deposited in the Mikeimin alluvial fan enabled the validation of the components of the procedure: i.e., because of the agreement between the computed and observed bedload volumes, the data on which the bedload computation is based (bedload transport rate, hydrographs) are assumed to be reasonably correct.

6.2.6 Results and Discussion

Unit transport rates in the range of 20-100 kg/m.s are indicated (Table 6.2) as a mean value for a 30-60 min long flow event in a small arid watershed with very steep stream channels. These rates derive from the Bagnold (2) procedure. The data suggest that the proportionality of bedload transport rate to unit stream power in excess of that necessary for initial motion, raised to the power of $3/2$, is valid also for short-lived violent torrents which approach debris flows in character.

The data for Wadi Mikeimin agree well with those for Elbow River (14) (fig. 6.2); both rivers transport bedload of similar median size.

The Mikeimin data also agree well, despite their very special characteristics, with data from other rivers representing widely varying conditions (2,3,4,5,15). Subject to the morphological distribution between rivers whose bed material grain size approximates the size of the transported bedload and those whose effective bed surface roughness size is significantly larger (2), and provided bedload material is available in unlimited supply, these new data provide further encouragement in the search for

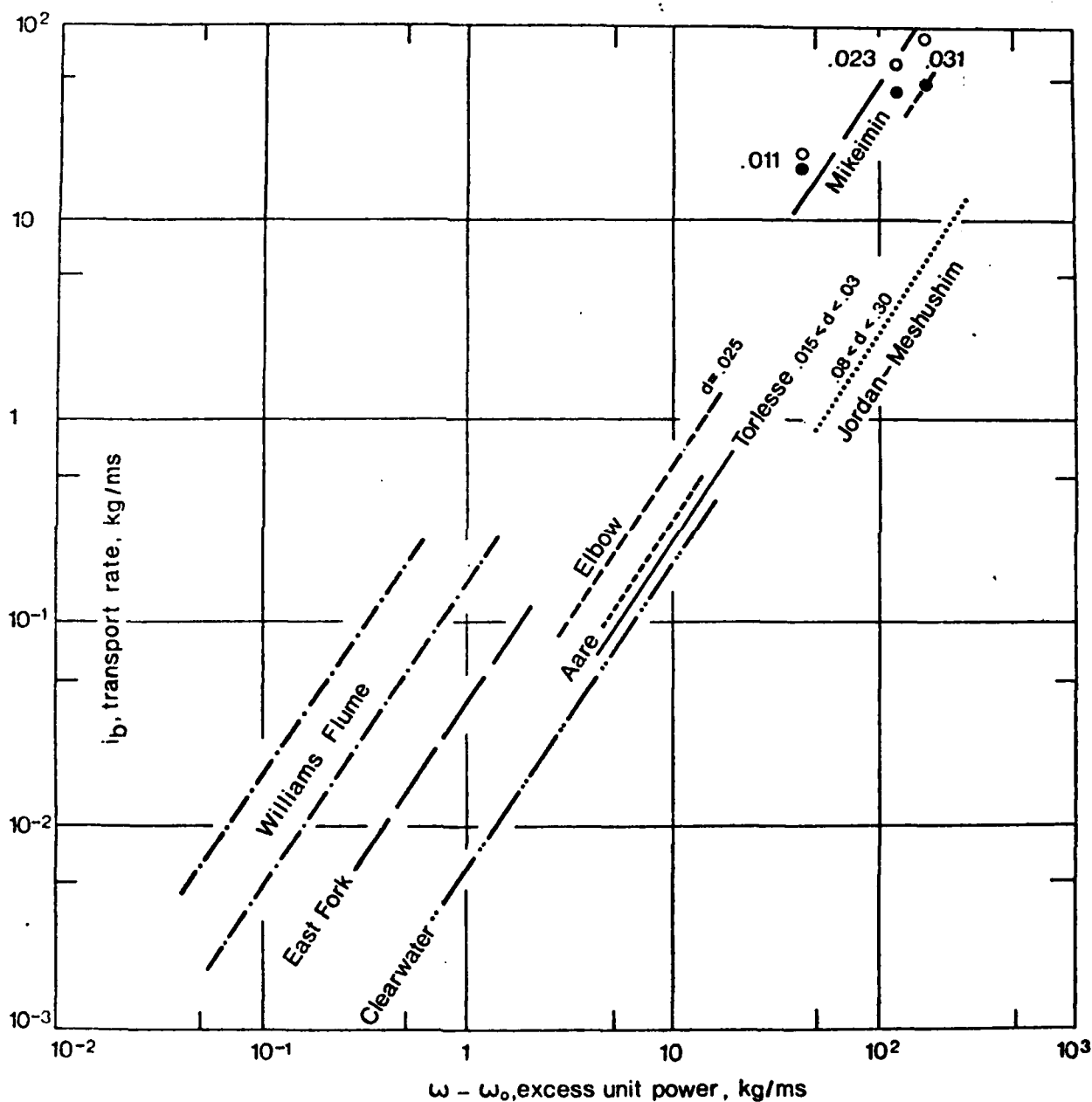


Fig. 6.2: Bedload transport as a function of excess stream power, in relation to data from Wadi Mikeimin, Eastern Sinai. Bedload transport rate is by immersed weight. Figures inside graph indicate representative median grain size in meters.

a satisfactory universal method for predicting bedload transport rates of rivers on the simple basis of excess power, size and depth alone.

6.2.7 References

- Bagnold, R.A. (1977) Water Resour. Res. 13, 303-312
- Bagnold, R.A. (inpress)
- Leopold, L.B. & Emmett, W.W. (1976) Proc. Natl. Acad. Sci. USA 73, 1000-1004
- Leopold, L.B. & Emmett, W.W. (1977) Proc. Natl. Acad. Sci. USA 74, 2644-2648
- Inbar, M. & Schick, A.P. (1979) Proc. Natl. Acad. Sci. USA 76, 2515-2517
- Floods in Eastern Sinai, Report No. 3 (1972) (mimeogr.).
Dept. Geog., Hebrew University, Jerusalem (hebrew)
- Lekach, J. (1974) The January 1971 event in Wadi Mikeimin and its geomorphic significance. M.Sc. thesis,
Dept. Geog. Hebrew University, Jerusalem (Hebrew) (meogr.)
- Schick, A.P. (1970) Intl. Assoc. Sci. Hydr., Publ. 96, 478-493
- Schick, A.P. (1974) Z. f. Geomorph. Suppl. Bd. 21, 88-105
- Sharon, D. (1972) J. Hydr. 17, 161-175
- Colby, B.R. & Hubbell, D.W. (1961) Simplified methods for computing total sediment discharge with the modified Einstein procedure, U.S. Geological Survey Water Supply Paper 1593 (GPO, Washington, DC)
- Leopold, L.B. (1970) Water Resour. Res. 6, 1357-1366

Hollingshead, A.B. (1971) J. Hydraulics Div., Proc. Am.
Soc. Civ. Eng., HYII (no. 8521), 97, 1817-1834

Mutzner, C. (1939) Amt für Wasserwirtschaft, Mitt. Nr.33
(Bern, Switzerland)

7. GEOPHYSICAL SURVEY OF NAHAL Yael CHANNEL BED

by Asher P. Schick

In sequence to a few seismic soundings carried out by Bull and Schick four years ago, a more systematic survey, consisting of about forty seismic soundings, was carried out by means of a portable refraction instrument.

The objective of the survey was to obtain a reasonably accurate quantitative estimate of the potential water storage in the alluvium beneath the channel bed, so that this factor can be evaluated, together with other water losses, which affect the generation of floods within the watershed.

Since the main alluvial body of the channel system of the catchment above the waterfall (station 02) lies in the one kilometer long main channel between stations 02 and 04, the sounding activity was confined to this reach.

Excepting the central part of the alluvial fan beyond the mountain front, where bedrock depths in excess of 8 meters were indicated, all data within the alluvial channel range between 0.5 and 2.0 meters. In general, for the main alluvial reach between the beginning of continuous alluvial fill (station 02) and the waterfall (station 04), the following picture emerges (Table 7.1): for the upper and lower sub-reaches, a fill of around 0.6 to 1.2 meters is indicated, while for the middle sub-reach the figure is more like 1.5 meters. This is in line with the fact that the alluvial terraces in the middle and middle-upper sub-reaches are also considerably higher above the present channel bed than those at the two ends of the main alluvial reach. This similarity of behavior between the highest and deepest flow profiles is remarkable in that it suggests a unified geomorphic mechanism for periods of cut and of fill, such as proposed, for example, by the

superflood theory.

Three years ago Bull and Schick dug a few pits in an attempt to obtain a correlation between their seismic soundings and the actual section exposed. In one of those pits, near 470, bedrock was not encountered even at the depth of 3.30 meters; at this point the pit had to be abandoned, as it was completely silted up by event 12 which occurred on the next morning. Because of the fact that in the present survey no sounding showed a depth more than 2 meters, it could well be that the pit dug by Bull and Schick was at a chance and unrepresentative site. But it could also mean that very close to concave bends undercutting an alluvial terrace - as was the case with that pit - deeper fills are present. Usually it is impossible to align a proper sounding line at such sites because of topographic difficulties.

The dominant width of the "probable" flood channel varies systematically from about 3.5 m at station 400 (60 meters downstream of station 04), to about 24.5 m at station 485 (70 meters upstream of station 02) (see fig. 9, curve 2, in Schick 1977). Using these figures in conjunction with the data of table 10.1, we arrive at the following volumetric estimate of the sub-channel alluvial fill of Nahal Yael above the waterfall:

	Length (m)	Width (m)	Depth (m)	Volume (m ³)
Upper part, 400-430	300	7.4	1.12	2,486
Middle part, 430-477	470	18.4	1.21	10,464
Lower part, 477-490	130	23	1.04	<u>3,110</u>
Total, 400-490				16,060

Clearly this figure of total, sub-channel level alluvial fill volume of the Nahal Yael watershed is only somewhat more accurate than an order of magnitude. In its computation we have neglected a number of factors, such

Table 7.1: Summary of seismic soundings, Nahal Yael
alluvial channel

Distance marker* 10 ¹ m	Depth to bedrock** m	Remarks
510-508	13, 9, 8.0?	on alluvial fan in damned area
505-502	1.76	
	-----	Station 02
488	0.8 0.55	
486	1.8 1.1	
480	0.9 1.1	
	-----	Station 03
474	0.6 0.8	
472	1.1	
470	1.0	
468	0.7	
464	1.95	
462	1.3	
458	1.6?	
454	1.0	
450	1.05	
446	1.0	
442	0.8	
440	1.3?	
438	1.8	
436	1.1	
434	1.3	
432	1.6	
	-----	Station 75
428	1.4	
	0.9?	on terrace (conglomerate layer?)
422	0.7	
420	1.1	
418	1.0	

Table 7.1 (cont.)

416	1.4					
414	1.2					
410	0.6	1.7	1.8	1.2	1.0	
398						upstream end of alluvial channel; Station 04

* Distance alongside main channel of Nahal Yael, in tens of meters. Note that upper divide is not zero. System originates at a point located between the dam and station 02, labelled 500 in order to avoid negative values.

** Result rounded off to nearest decimeter. Due to the similarity of sound velocity through alluvium and through intensely weathered granite and schist, the depth values may include a bottom layer of weathered bedrock 1-2 decimeters thick.

as the usual curved shape of a fluvially formed cross section instead of a rectangular form, or the disregard of lateral effluence during floods at alluvial banks. Incidentally, these two factors may quantitatively offset one another.

Assuming that the volume of alluvial channel fill of 16000 m^3 is correct, and assuming further a mean porosity of 25-30 per cent of the alluvial material, we arrive at a total potential water storage of $4000\text{-}5000 \text{ m}^3$. This represents equivalent watershed rainfall of 8 - 10 mm - a reasonable figure in agreement with the available runoff data.

The question whether the entire sub-channel alluvial body must indeed be saturated before runoff occurs at station 02 cannot as yet be conclusively answered. Other factors as yet unknown are the amount of shallow groundwater stored near the alluvium-bedrock contact (preferably in pools, perhaps at the foot of sub-alluvial waterfalls?), as well as the rate of depletion of this storage with increasing time interval between successive runoff events.

8. INFILTRATION TESTS

by Oded Salmon and Asher P. Schick

8.1 Introduction

The work reported here deals with the determination of approximate quantitative values of infiltration rates for several lithologies in an extremely arid environment. These values were arrived at by means of infiltration trials which utilized simulated rainfall on very small plots, supplemented by comparisons with other data whenever available.

The impetus for the work was two-fold. First, the infiltration data are of prime importance for understanding the mechanism of surface runoff in deserts. Inasmuch as the Nahal Yael watershed is composed of magmatic rocks like much of the major deserts of the world, it seemed reasonable to make the field study within this watershed, in which runoff data available for the past 15 years offer a means of verifying the results.

Second, actual infiltration data are needed as an input to the Nahal Yael runoff and sediment model which is currently being developed (see chapter 9). This model is based on very small unit areas, and it is necessary to understand and quantify the infiltration process on a similar level of detail.

The physiography of the Nahal Yael watershed has been described in detail in several sources. The lithologic composition is of immediate relevance to the infiltra-

tion tests reported here, and will be briefly summarized. Most of the catchment is underlain by metamorphic rocks, mainly schist, amphibolite, and some gneiss (Shimron, 1974). The lower part of the catchment is composed of granite of the Elat type. All rocks are crossed by two fairly dense systems of dykes. Occasional colluvium on the slopes, which are mostly very steep (up to roughly 40°), merges into alluvium on terraces above the larger channels. The first and second order channel beds are almost exclusively bedrock. Only in some lower reaches does the channel bed widen to more than 10 meters and is completely underlain by alluvium. Such channels as well as the few "soil" pockets carry the only vegetation present in the region - low shrubs. Acacias grow only in the lower part of the main channel.

The infiltration trials were conducted over a time span of nearly two years. In total, 19 plots were constructed, and 24 infiltration trials were accomplished over 8 field periods.

The first stages of the field work were afflicted by difficulties in making the plot borders watertight. Only after we included in the procedure a routine check by applying colored water to the border strips, could impermeability be verified and the result considered trustworthy. Sometimes, though, plots that seemed watertight prior to the start of rainmaking, developed leaks during the test or towards its end, probably because of a difference between dry and wet hydraulic conductivity of joints.

Although it is possible to obtain an adequate description of runoff development and infiltration rate for certain of the plots which developed border leaks, we have tabulated and used only the data for those tests which proceeded faultlessly and are thus completely

trustworthy. The only item of information utilized from all tests was the total amount of water needed for the initiation of runoff, for rocks other than amphibolite. This variable is not affected by the faults mentioned.

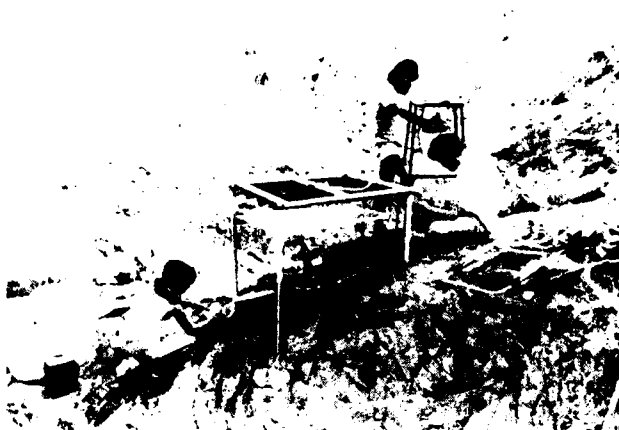
8.2 The infiltration tests

8.2.1 Rain simulation

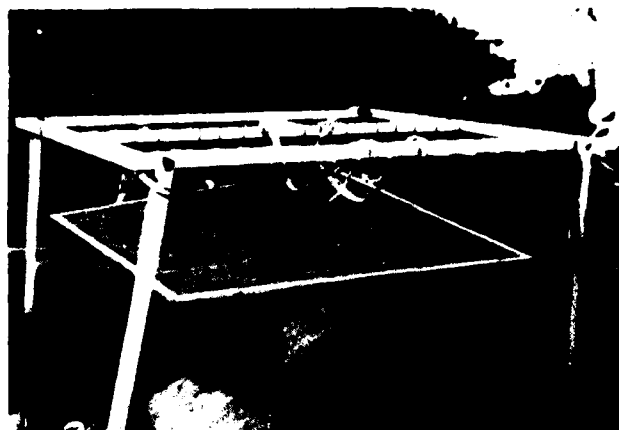
The rainmaking device (photographs 1-6) consists of a drop generator, area 0.8m^2 , which applies simulated rain to a bordered micro-plot, area 0.25m^2 . The drop generator consists of a rectangular aluminum frame along whose width a rubber tube winds back and forth. Syringe needles (type $20 \times 1\frac{1}{2}$ G) are stuck into the tube so that their sharp end is inside and the wide end points downwards. These needles form the drops, with the intensity controlled by water pressure in the tube. A constantly moving netting installed below the needles distributes the drops over some area. Constant pressure is ensured by a constant head tank (with a float) which supplies the drop generator, and is supplied in turn from a tank located at a higher elevation.

The device is levelled by means of four adjustable legs. The plot is delimited by low fences made of putty (on bedrock) or sheet metal (on colluvium), and has a funnel at its lower end which facilitates the collection of runoff into containers. Starting with the time of runoff initiation, the containers are exchanged every minute, so that mean infiltration rates for 60-second time intervals can be obtained.

As already mentioned, border effectiveness and possible leaks around the outlet funnel are checked by the application of colored water.



1 The rainfall simulator



2 Plot covered to prevent wetting during calibration of intensity



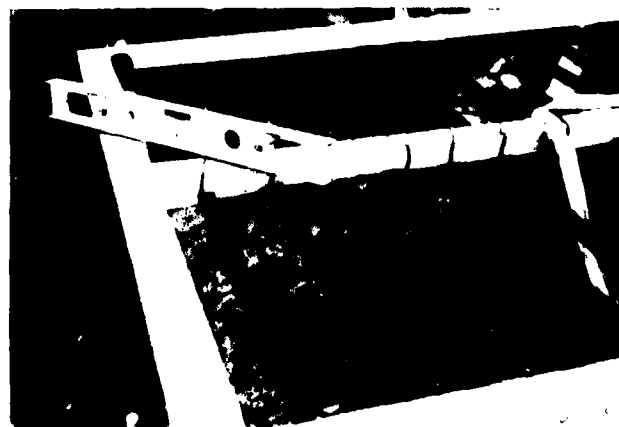
3 Plot outlet funnel during runoff measurement



4 First stage of drop formation



5 A drop is detached; size: 5 mm



6 The orifices are spaced 7 cm apart

Some technical data:

Size of drops:	about 5mm
Spacing between needles:	7x7 cm
Size of device:	100x93 cm
Size of plot:	50x50 cm

The last two measures are horizontal.

The rain distribution was tested in a closed space over an area of 10 cm^2 , with the following results:

Test No.	Rainage No.	Cumulative rainfall, mm
1	1	3
	2	2 1/2
2	1	2
	2	1 1/2
3	1	3
	2	3 1/2
	3	4

The distribution in the open is assumed to be better because of wind effect.

Rainfall intensity was determined by measuring the water collected in a measuring tray, size 0.5m^2 , i.e. identical to that of the plot. Three measurements, one minute long each, were carried out; two were made prior to the exposure of the plot to rain, and the third was made at the end of the infiltration trial.

The advantages of the rainfall simulator are:

1) mobility: the device enables tests in areas unsuita-

ble for vehicular transport. It can be operated by two persons (though three are better) and is carried from site to site by the operators.

II) water economy: water is the heaviest component of the simulator. At distances of 2km from the vehicle, the motto "conserve every drop" acquires a very special significance! The device uses 10-15 liters to prepare it for a set of tests (this can be done near the vehicle) and then 20-30 liters for each infiltration test; the exact amount depends on the time needed to achieve the terminal infiltration rate and on possible faults in the device or in the plot during the test.

III) selectivity of rain intensity: the device performs accurately in the intensity range of 15-120mm/hr, and maintains a uniform intensity (the deviations are 1-3%) with a reasonable drop distribution. Switching to different size needles should enable the simulation of rain of any desired intensity.

IV) versatility: the device can be used in the laboratory as well as in the field. It is adaptable to a slope range of 0-100%.

V) The device is simple and inexpensive to construct.

Some disadvantages of the rainfall simulator are connected with the drop generator: the drops are not ideally distributed, they are larger than those of natural rain, and their fall velocity is smaller. The first two factors can be disregarded for rainmaking on rocky surfaces, but the third one may indeed be a problem.

Other disadvantages concern the plots: the waterproofing in jointed rocks and in coarse colluvium poses considerable problems, especially on steep slopes. In the putty-fenced plots the border strip is appreciably disturbed: the inner part of the fence, mean width 0.75 cm, produces an area of

$$0.75 \times 200 = 150\text{cm}^2$$

i.e. approximately 6% of the plot area of 2500cm^2 .

For reasons we cannot explain, it is not possible to use the device, over two days, for more than ten tests. Thereafter the simulator begins to perform erratically, and the intensity varies within a single test.

Another limitation of the device is its requirement of distilled or filtered water, to avoid the clogging of the syringe needles.

8.2.2 Test results

The results of 13 infiltration tests conducted on eight plots are listed in Tables 8.1 to 8.11. The location of these plots is shown on fig. 8.1.

8.2.3 The correction of the measured infiltration rates

In the tests the plot infiltration rate was calculated by subtracting the runoff collected in the outlet funnel from the plot rainfall, over successive periods of one minute duration. The value of this infiltration rate was corrected according to the following criteria:

1) For sloping plots the splash balance is not zero because the drop generator is horizontal, i.e. at the lower end the drops fall from a higher elevation. Consequently the loss of water to the plot by the down-splash component of the bottom inner border strip is larger than the gain to the plot by the downsplash component of a top outer border strip of identical width. The width of the rained-on outer margins of the plot is about 20cm.

An estimate of the loss of water to the plot caused by the above factor, based on data on the number of drops and their fall velocity, yielded the following correc-

8.1

- ② rainfall recorder
- ▼ stream gauging station
- 7 infiltration test site

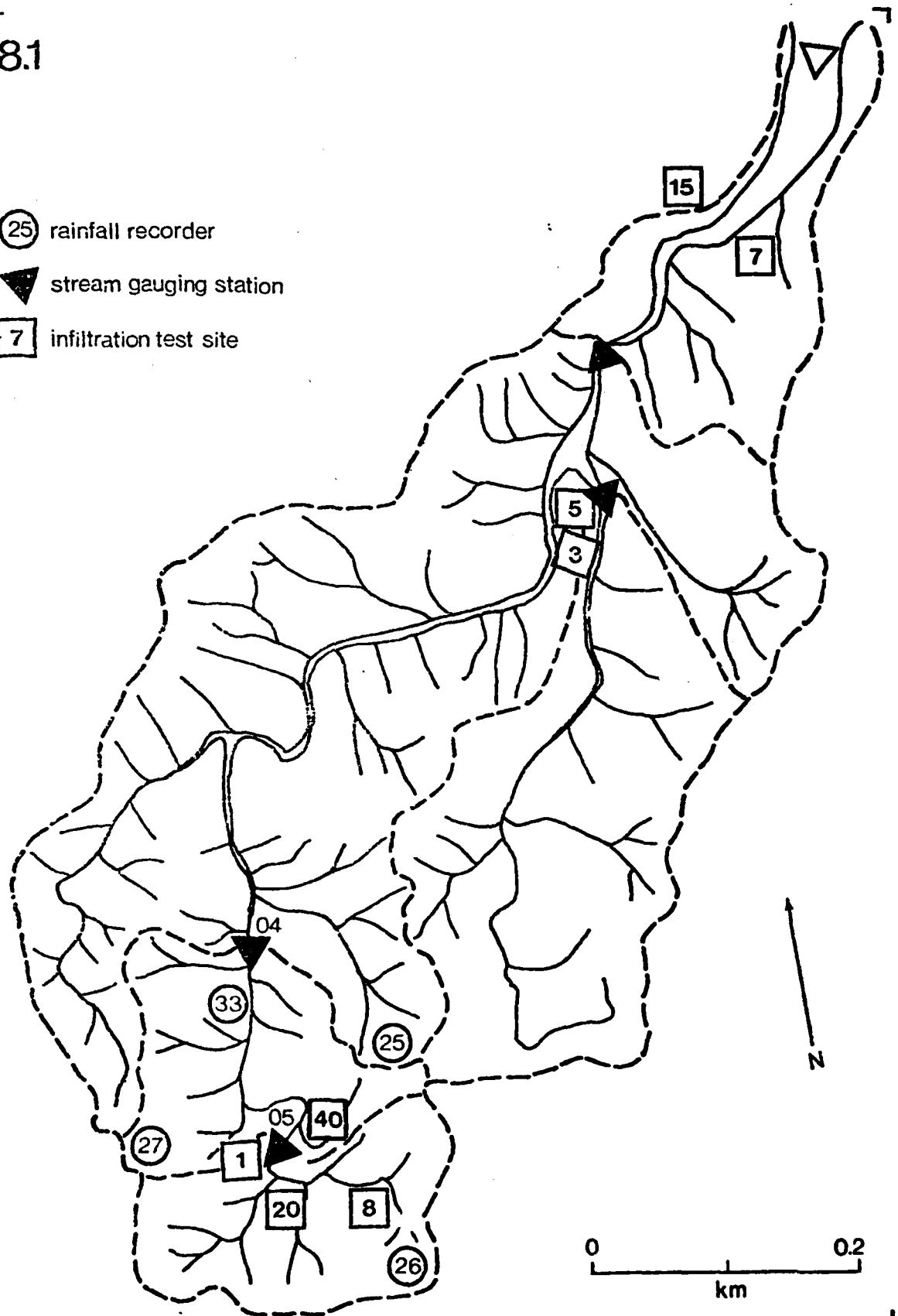


Fig. 8.1: Nahal Yael infiltration test sites and relevant instrumentation.

Table 8.1. : Infiltration test at site No. 7

Photograph No. 11

Figure No. 8.2

Lithology: granite, medium grain,
unjointed

Date of test: 10.9.78

Slope: 2°

Rain int.: 36 mm/hr
41 "

Area of plot, horizontal: 2480 cm²

Runoff begins after: 0 min 58 sec

Time min	Runoff		Inf. rate mm/hr	Comments
	cm ³	%		
1				
2	93	55.1	18.2	rain 36 mm/hr
3	137		7.6	"
4	148		5.0	"
5	157	93.1	2.8	rain 41 mm/hr
6	154		3.5	
7	166		0.62	
8	165		0.87	
9	167		0.38	
10	166	98.4	0.62	
11				
12				
13				
14				
15				
16				
17				
18				
19				
20				

Terminal conditions

Stable infiltration rate:

Rainfall-runoff ratio:

0.62 mm/hr

98.4 per cent

Table 8.2. : Infiltration test at site No.15

Photograph No. 9

Figure No. 8.3

Lithology: granite, coarse-grained,
sparsely jointed

Date of test: 8. 1.79

Slope: 34 °

Rain int.: 31.4 mm/hr
32.2 "

Area of plot, horizontal: 2355 cm²

Temp:water: 20 °C

Runoff begins after: . 1 min 12 sec

Time min	Runoff		Inf. rate mm/hr	Comments
	cm ³	%		
1				
2	90	73.1	10.5	rain 31.4 mm/hr
3	95		7.1	"
4	110		3.6	"
5	114	89.7	3.2	rain 32.2 mm/hr
6	116		2.8	"
7				"
8				"
9				"
10				"
11	116	91.3	2.8	"
12	116		2.8	"
13				
14				
15				
16				
17				
18				
19				
20				

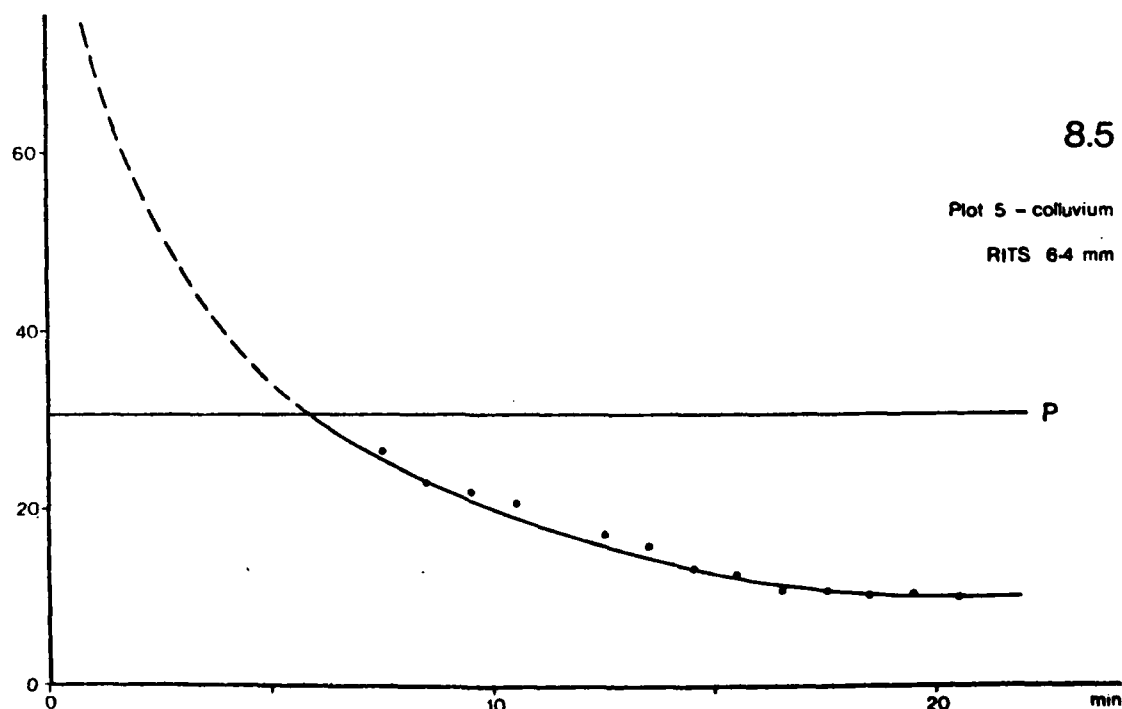
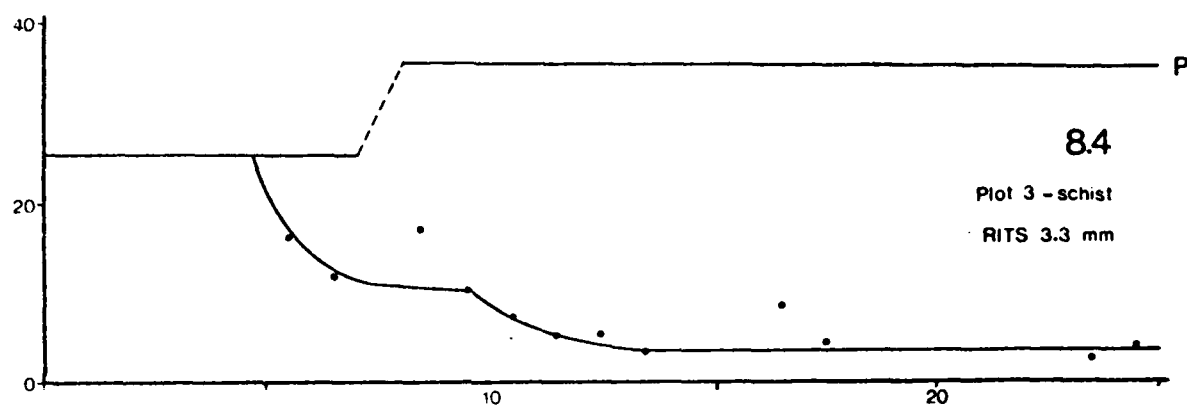
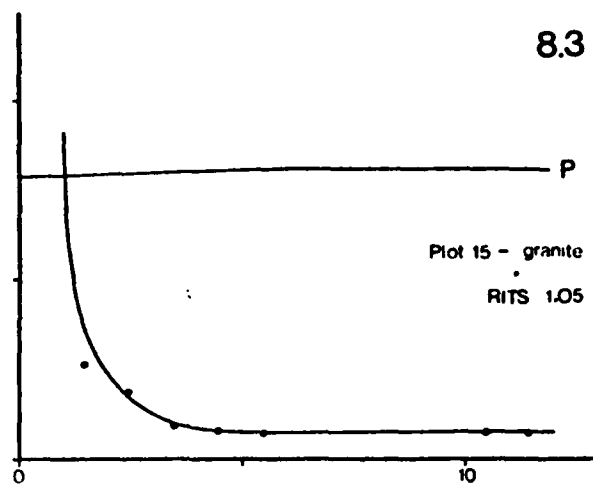
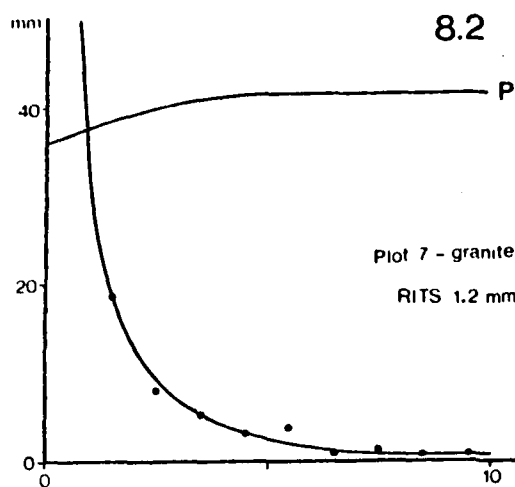
Terminal conditions

Stable infiltration rate:

Rainfall-runoff ratio:

2.8 mm/hr

91.3 per cent



Figs. 8.2 - 8.5: Nahal Yael infiltration tests - granite, schist, colluvium. P = precipitation; RITS = Rainfall amount Infiltrated Till Stability achieved.

Table 8.3 : Infiltration test at site No.3

Photograph No.10

Figure No. 8.4

Lithology: schist, densely jointed;
joints perpendicular to slope

Date of test: 8. 1.79

Slope: 33°

Rain int.: 25.2 mm/hr
 35.5 "

Area of plot, horizontal: 2316 cm²

Temp:water: 20°C

Runoff begins after: 3 min 05 sec

Time min	Runoff		Inf. rate mm/hr	Comments
	cm ³	%		
1				
2				
3				
4				
5	38		30.0	rain 25.2 mm/hr
6	33	34.0	16.6	
7	42		14.2	
8				intensity increased
9	71		17.1	rain 35.5 mm/hr
10	95	69.3	10.9	"
11	108		7.5	"
12	117		5.2	"
13	116	84.6	5.4	"
14	124		3.4	"
15				no data
16				no data
17	104		8.6	rain 35.5 mm/hr
18	120		4.4	"
19				no data
20				no data
21				no data
22				no data
23				no data
24	126	91.9	2.8	rain 35.5 mm/hr
25	119	86.9	4.6	"

Terminal conditions

Stable infiltration rate:

Rainfall-runoff ratio:

3.8 mm/hr

89 per cent

Table 8.4 : Infiltration test at site No. 1

Photograph No. 7

Lithology: Colluvium in an area of
amphibolite and dykes; stone cover
85%; angular stones, size 5-10 mm,
some up to 40 mm

Date of test: 11. 8.78

Slope: 11°

Rain int.: 51.6 mm/hr

Area of plot, horizontal: cm²

Runoff begins after: 3 min 20 sec*

Time min	Runoff		Inf. rate mm/hr	Comments
	cm ³	%		
1				
2				
3	172		10.3	
4	150		15.6	
5	148		16.1	
6	148		16.1	
7	172		10.3	
8				
9				
10				
11				
12				
13				
14				
15				
16				
17				
18				
19				
20				

Terminal conditions

Stable infiltration rate:

Rainfall-runoff ratio:

13.6 mm/hr

73.6 per cent

* plot was dry at onset of rain

Table 8.5 : Infiltration test at site No. 5

Photograph No. 8

Figure No. 8.5

Lithology: colluvium in an area of
schist and dykes; stone cover 95%;
angular stones, size 10-40 mm

Date of test: 9. 1.79
 Slope: 9°
 Rain int.: 30.7 mm/hr

Area of plot, horizontal: 2354 cm²
 Runoff begins after: 5 min 40 sec

Temp: water:

Time min	Runoff		Inf. rate mm/hr	Comments
	cm ³	%		
1				no data
2				
3				
4				
5				
6				
7	6			
8	16	13.2	26.7	
9	30		23.2	
10	34		22.2	
11	40		20.7	
12				
13	54	42.6	17.1	
14	58		16.1	
15	67		13.7	
16	71		12.7	
17	79	65.2	10.7	
18	78		11.0	
19	79		10.7	
20	78		11.0	
21	82	67.7	10.0	

Terminal conditions

Stable infiltration rate:

Rainfall-runoff ratio:

10.5 mm/hr

65 per cent

Table 8.6 : Infiltration test at site No. 8

Photograph No.12

Figure No. 8.6

Lithology: amphibolite; dense
joints

Date of test: 12. 8.78

Slope: 20°

Rain int.: 56.4 mm/hr
55.2 "
54.0 "

Area of plot, horizontal: 2022 cm²

Runoff begins after: 0 min 50 sec

Time min	Runoff		Inf. rate mm/hr	Comments
	cm ³	%		
1				
2	107		24.6	rain 56.4 mm/hr
3	139	68.4	17.6	"
4	145		13.3	"
5	147		11.6	rain 55.2 mm/hr
6	152		10.1	"
7	152	81.7	10.1	"
8	155		8.1	rain 54.0 mm/hr
9	131		15.1	"
10	159	87.3	6.8	"
11				
12				
13				
14				
15				
16				
17				
18				
19				
20				

Terminal conditions

It is doubtful whether stability has indeed been reached

Table 8.7 : Infiltration test at site No.20

Photograph No. 13

Figure No. 8.7

Lithology: amphibolite; medium

Date of test: 9. 4.79

dense jointing

Slope: 18°

Rain int.: 40.8 mm/hr

Area of plot, horizontal: 2665 cm²

Temp: water: 26°C

Runoff begins after: 1 min 45 sec

air : 23°C

soil : 31°C

Time min	Runoff		Inf. rate mm/hr	Corrected inf. rate * mm/hr
	cm ³	%		
1				
2 1/2	44	24.3	30.84	33.4
3	90		20.48	22.1
4	97		18.91	20.1
5	102	56.3	17.78	18.6
6	102		17.78	18.6
7	113		15.30	15.7
8	125		12.60	12.5
9	114	62.9	15.0	15.2
10	119		13.95	14.0
11	112		15.53	15.7
12	122	67.4	13.28	13.2
13	118		14.18	14.2
14	121	66.8	13.5	13.5
15				
16				
17				
18				
19				
20				

Terminal conditions

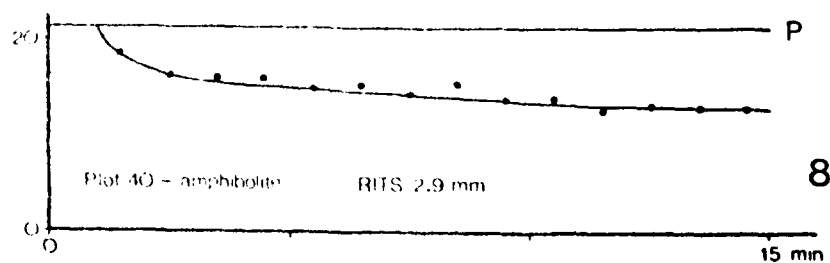
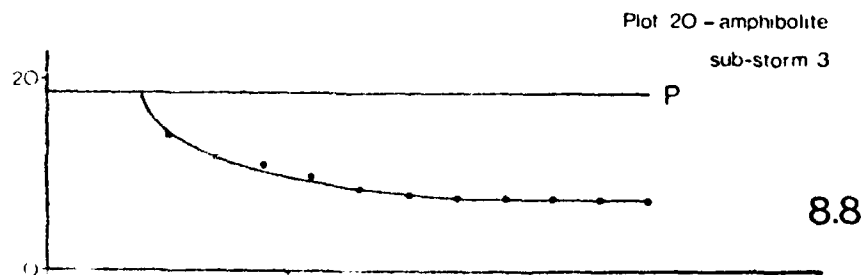
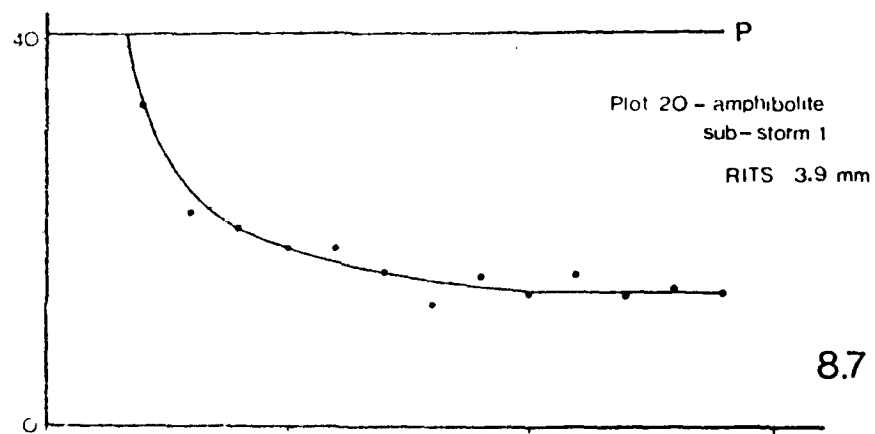
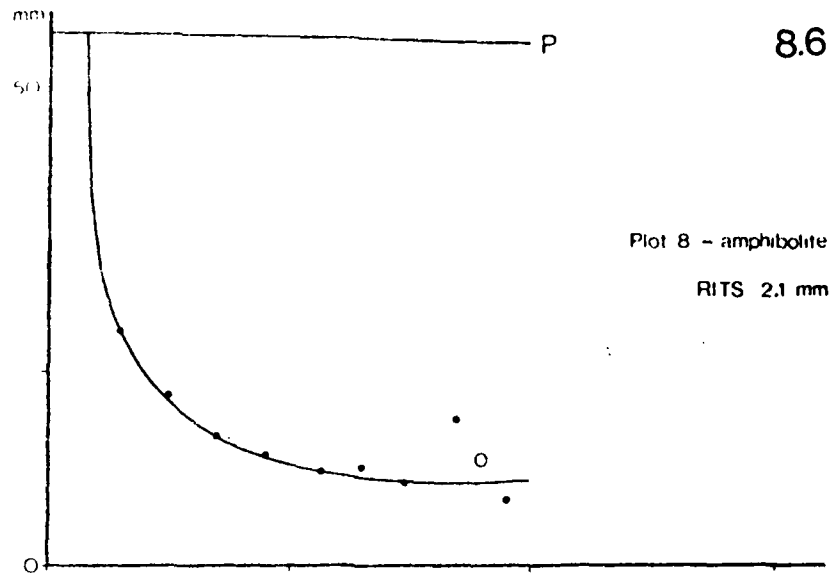
Stable infiltration rate:

Rainfall-runoff ratio:

13.5 mm/hr

66.8 per cent

*see text



Figs. 8.6-8.9: Nahal Yael infiltration tests
P = precipitation; RITS = Rainfall amount Infiltrated Till Stability achieved.

Table 8.8 : Infiltration test*at site No.20

Photograph No.13

Lithology: as in table 8.7

Date of test: 9. 4.79

Slope: 18°

Rain int.: 19.9 mm/hr

Area of plot, horizontal: 2665 cm²

Temp:water: 29 °C

Runoff begins after: 2 min 30 sec

air : 28 °C

soil*: 24 °C

Time min	Runoff		Inf. rate mm/hr	Corrected inf. rate mm/hr
	cm ³	%		
1				
2				
3	25	28.4	14.2	15.5
4	44		9.9	10.8
5	58		6.7	7.3
6	64		5.4	5.9
7	64		5.4	5.9
8	64	72.7	5.4	5.9
9	62		5.8	6.4
10	66		4.9	5.4
11				
12				
13				
14				
15				
16				
17				
18				
19				
20				

Terminal conditions

Stable infiltration rate:

Rainfall-runoff ratio:

5.9 mm/hr

72.7 per cent

* this is a repeat test conducted 3 hours after the first test (table 8.7). Note the difference in temperature between wet and dry soil. The reason for the low terminal rate is not clear.

Table 8.9 : Infiltration test^{*} at site No. 20

Photograph No. 13

Figure No. 8.8

Lithology: as in table 8.7

Date of test: 10. 4.79

Slope: 18°

Rain int.: 18.7 mm/hr

Area of plot, horizontal: 2665 cm²

Temp: water: 21°C

air : 20°C

Runoff begins after: 2 min 00 sec

soil*: 17°C

Time min	Runoff		Inf. rate mm/hr	Corrected inf. rate mm/hr
	cm ³	%		
1				
2				
3	25	30	13.0	14.1
4	34		11.1	11.9
5	38		10.1	10.9
6	43		9.0	9.7
7	48	57	9.9	10.5
8	50		7.4	8.0
9	52		7.0	7.5
10	52	62	7.0	7.5
11	52		7.0	7.5
12	52		7.0	7.5
13	54	65	6.5	7.0
14				
15				
16				
17				
18				
19				
20				

Terminal conditions

Stable infiltration rate:

Rainfall-runoff ratio:

7.5 mm/hr

62 per cent

* this is a repeat test conducted 22 hours after the first test (table 8.7) and 19 hours after the second test (table 8.8). Note the difference in temperature between dry and wet soil.

Table 8.10 : Infiltration test*at site No.20

Photograph No.13

Lithology: as in table 8.7

Date of test: 10. 4.79

Slope: 18°

Rain int.: 42 mm/hr

Area of plot, horizontal: 2665 cm²

Temp:water: 23°C

air : 22°C

Runoff begins after: 0 min 25 sec

Time min	Runoff		Inf. rate mm/hr	Corrected inf. rate mm/hr
	cm ³	%		
1	132	70.9	12.2	13.3
2	142		9.9	10.7
3	144		9.5	10.1
4	145	77.9	9.2	9.6
5	148		8.6	8.6
6	148	79.5	8.6	8.6
7	144		9.5	10.1
8				
9				
10				
11				
12				
13				
14				
15				
16				
17				
18				
19				
20				

Terminal conditions

Stable infiltration rate:

Rainfall-runoff ratio:

8.6 mm/hr

79.5 per cent

* this is another repeat test, performed one hour after the previous one (table 8.9).

Table 8.11 : Infiltration test at site No.40

Photograph No.14

Figure No. 8.9

Lithology: amphibolite, medium jointing. Rain deliberately stopped twice during test.

Date of test: 19. 9.79

Rain int.: 21.6 mm/hr
19.4 "
26.4 "

Area of plot, horizontal: 2550 cm²
Runoff begins after: 0 min 55 sec

Temp: water: 23.5 °C
air : 23 °C
soil : 25 °C

Time min	Runoff		Infiltration rate		Rain int. mm/hr
	cm ³	%	direct mm/hr	corrected mm/hr	
1					
2	16	17.5	17.9	18.6	21.6
3	24		15.9	16.5	21.6
4	26		15.5	16.1	21.6
5	26	28.5	15.5	16.1	21.6
6	28		15.0	15.5	21.6
7	26		15.5	16.1	21.6
8	31		14.3	14.8	21.6
9	28		15.0	15.5	21.6
10	33	36.2	13.8	14.2	21.6
11	33		13.8	14.2	21.6
12	39		12.4	12.7	21.6
13	36	39.5	13.1	13.5	21.6
14					
15					
16	36		13.1	13.5	21.6
17	37	40.5	13.3	13.7	21.6
18					0.0
19					
20					
21					
22					
23					
24					
25					
26					
27					
28					
29					
30					

continued on following page

Table 8.11 : Infiltration test at site No.40 (cont.)

Time min	Runoff		Infiltration rate		
	cm ³	%	direct mm/hr	corrected mm/hr	
31					0.0
32					"
33					
34	82		9.9	10.5	19.4
35	47	56	8.5	8.9	"
36	51		7.5	7.9	"
37	50		7.8	8.1	"
38					
39	50	60	7.8	8.1	"
40					0.0
41					
42					
43					
44					
45					
46					
47					
48					
49	76	68	8.4	9.1	26.4
50	72		9.4	10.2	"
51	76		8.4	9.1	"
52	76		8.4	9.1	"
53	79	70.5	7.7	8.4	"

Terminal conditions

Stable infiltration rate: Rainfall-runoff ratio:

Stage 1:	13.5	mm/hr	39.5	per cent
Stage 2:	8.1	"	60	" "
Stage 3:	9.1	"	68	" "

tion coefficients: For plots sloping $30-35^{\circ}$, deduct 5% from incoming rainfall; for plots sloping $15-20^{\circ}$, deduct 2% from incoming rainfall; for plots of lesser slope, no correction is warranted.

II) Disturbance of margins: great care was exercised to construct the micro-fence bordering the plots in such a way that the horizontal area of its inward sloping side becomes as small as possible. The fence walls were slightly bent inward so as to "cover" the putty strip at its base. However, in certain plots the putty strip reached the substantial width of up to 1 cm mean value, totalling 200 cm^2 per plot or roughly 8 per cent of its area.

Since the putty strip produces 100% runoff, the water amount contributed by it was deducted from the total collected at the outlet funnel, and the plot area was also reduced by subtracting the area of the putty strip. This correction was applied to the two amphibolite plots (No.20 and No.40), in which it was expected to exercise a considerable influence on the result. However, the difference proved to be slight. Consequently, this factor was neglected for all other plots.

III) The infiltration tests were conducted over different seasons, consequently different temperature values for the simulated rainwater as well as for the air and the soil should be considered. Although the effect of temperature on infiltration has been well documented for some cases (Shanan 1975; and others), the complete relationship is far from clear and may be variable from one soil type to another. We decided, arbitrarily, to apply a conservative correction: in order to standardize the test results for infiltration of cold rain water in winter, we have reduced the terminal infiltration rates of tests carried out in winter with the artifi-

cially warmer water by 10 per cent; for all other tests the reduction was fixed at 20 per cent.

Table 8.12, the data summary sheet of all infiltration tests, lists also the values as corrected by the above procedures.

8.2.4 Infiltration into joints

In highly jointed areas the tests described above did not yield accurate results because it was impossible to adequately waterproof the joints located under the plot boundaries.

Two sets of experiments were carried out in order to evaluate the infiltration rate into joints:

I) The application of simulated rainfall on an unbounded, jointed surface and the subsequent determination of the time of runoff initiation and of the infiltration rate into the joints. The latter figure was approximated by dividing the depth of wetting by the duration.

II) The application of water to an intersection of joints at a rate exceeding the infiltration rate, for a relatively long duration, and the approximation of the infiltration rate as above.

Infiltration test on an unbounded surface: The surface selected for this test is composed of schists with wide joints filled with fine-grained material. The total rainfall amounted to 3.3 mm and was applied by the same device used in the tests described earlier. The results were:

Table 8.12: Infiltration trials at Nahal Yael - data summary sheet

Plot No.	Trial No.	L i t h o l o g y	Rainfall intensity (mm/hr)	Stable infiltration rate (mm/hr)			Time needed to achieve stable infiltration rate (min)	Water amount infiltrated until rate stabilized (mm)		Water input before initiation of runoff (mm)
				measured	corrected for winter	corrected for winter and standard intensity ^a		measured	corrected for winter	
7		Granite, medium-grain, unjointed	41	0.62	0.50	0.40	7	1.2	0.96	0.58
15		Granite, coarse-grain, sparsely jointed	32.1	2.8	2.5	2.2	6	1.05	0.94	0.61
3		Schist, densely jointed, joints perpendicular to slope	35.5	3.8	3.4	2.9	14	3.3	2.9	1.26
3		Amphibolite, medium dense joints	54.0	8.1	6.5	4.5	9	2.6	1.44	0.78
40	1	Amphibolite, medium sparse joints	21.6	13.5	10.8	10.4	11	2.9	2.3	0.33
	2	" " " "	19.4	7.8	6.5	6.5				
	3	" " " "	26.4	9.1	7.3	6.6				
20	1	Amphibolite, medium dense joints	40.8	13.5	10.8	8.7	10	3.9	3.1	1.19
	2	" " " "	19.9	5.9	4.7	4.3				
	3	" " " "	18.7	7.6	5.9	6.0				
	4	" " " "	2.0	8.6	6.9	5.9				
1		Colluvium, stone cover 85%	51.6	13.6	10.9	8.8	15	7.6	6.08	3.2 ^{**}
5		Colluvium, stone cover 95%	30.7	10.5	5.5	8.7	17	6.4	5.7	2.9

^a of 20 mm/hr of rainfall ^{**} based on an earlier test

Time (min)	Rain intensity (mm/hr)	Observation on runoff	Comments
0 - 4	31	Runoff starts after a few seconds	
4 - 7	0	Water continues to stand in depressions formed by the joints	rain stopped
7 - 14	12	Runoff	

Ten minutes after the termination of rain, the depth of wetting in most points was observed to be 1-2 cm; in the wide joints - 4.5 cm. Horizontal joints, i.e. those partitioning pseudostrata, at a depth of 2-3 cm were all dry. This means that no lateral flow in depth occurred.

The mean depth of wetting was determined to be roughly 3 cm per 25 min (till the time of exposure), i.e. 1.2 mm/min (72 mm/hr). But since the water occupies only 50% of the joint volume*, the actual rate is only 0.6 mm/min (36 mm/hr). Areally the joints occupy about 20 per cent; therefore the rate of infiltration into the joints is only one fifth. Accepting that the rock itself absorbs only negligible amounts of water (Lavee 1973), we arrive at an infiltration rate of 7 mm/hr.

* During vertical movement within joints under such wet conditions, the "soil" within the crack can be assumed to be supersaturated; the "soil" texture is a silty sand, with a one cm thick vesicular layer at the top, and a compact or platy (parallel to the crack surfaces) structure.

Joints intersection test No.1 (same lithology - schists with wide joints): these rain simulation tests were designed solely to observe the rate of advance of the wetting front in the joints. The rain intensity exceeded by far the infiltration rate into the joints, and considerable runoff occurred. The surface depressions were filled to capacity and created a certain hydraulic head, probably no different from the conditions during natural rain, as observed during the test on an unbounded surface described earlier.

Rain equivalent to 0.140 liters was applied over a period of 3 minutes to an area size 8x20 cm. The depth of the wetting front was determined when the water disappeared from the micro-depressions, i.e. 5 minutes after the termination of the rainfall, to be 2 cm (average value). Considering that the reading was made 8 minutes after the beginning of the rainfall, this indicates a mean rate of advance for the wetting front of 2.5 mm/min. Based on the consideration detailed earlier, the infiltration rate indicated for the joints surface area is 1.25 mm/min, or 75 mm/hr.

Joints intersection test No.2 (a densely jointed dyke rock surface): As a result of a 5 minute long application of 0.400 liters of simulated rain, water flowed in two microchannels conditioned by joints at their bottom. Ten minutes after the onset of rainfall the wetting front was found to have advanced to a depth of 2 cm, on average, i.e. a rate of 120 mm/hr. This means, as above, a water equivalent of 60 mm/hr for the joint surface area.

Joints intersection test No.3 (same site as No.2): This test was carried out at a T-intersection of 3 wide joints (width 1-3.5 mm). Water was applied at a relatively very high discharge - 7.3 liters over 20 minutes -

from a tap. Three minutes after the termination of the water input, i.e. 23 minutes after its beginning, the following data were observed:

In the joints above which the water flowed, the depth of the wetting front ranged from 3-4 cm (minimum) to 12 cm (maximum); mean value 8 cm. Therefore, the water equivalent infiltration rate is, roughly, 45 mm/hr (minimum), 150 mm/hr (maximum), and 100 mm/hr (mean value).

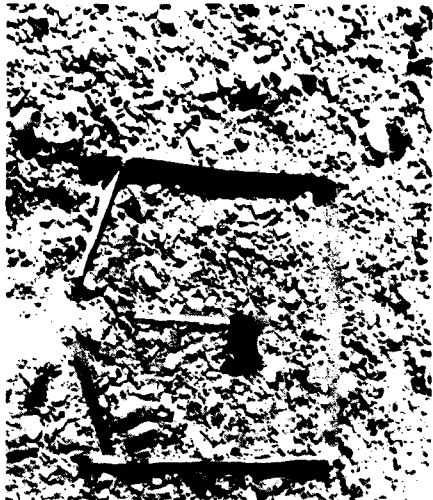
Summary of tests:

The mean water equivalent infiltration rate of all the tests described above is 67 mm/hr. If the last test, in which exceptionally large amounts of water were applied, is ignored, the value becomes 55 mm/hr. We conclude that the infiltration rate of 60 mm/hr represents well the behavior of joints.

Remembering the negligible absorption of water during rainstorms by rocks such as granite, schist, and quartz porphyry (Lavee 1973), the dominant factor which controls infiltration in a rocky area is the number of joints per unit area and their width; or, the proportion of joint surface area in the entire area considered. The schist site tested is very highly jointed (photograph 15), and its joints occupy 20 per cent of its area. However, at a depth of 1 cm and beyond the aggregate joint surface area diminishes to between 5 and 10 per cent. Thus the infiltration rate of such an area in its entirety is only 3-6 mm/hr. In normally jointed terrain (table 8.13), the cracks at depths of 1 cm and lower occupy only 2-3% of the total surface area, and the areal infiltration rate is only 1-1.5 mm/hr. However, some of the slope terrain, in particular of granitic lithology, is crossed by very wide joints which produce a veritable microtopography of

Table 8.13: Summary of infiltration tests at joints

Rock type	Number of jointing directions	Approx. width of joints (mm)	Proportion of joint area (%)	Comments
Dyke rock	2	0.5	2.25	8-10 joints over 40 cm
Schist	1 *	0.5	3	* cleavage; 12 joints over 20 cm
Schist	1 **	0.5	2	** perpendicular to cleavage; 8 joints over 20 cm
Granite	1	1	1.5	6 joints over 40 cm
Granite	2	2	2	3 and 5 joints, respectively, over 40 cm each



7 Plot 1: colluvium



8 Plot 5: colluvium



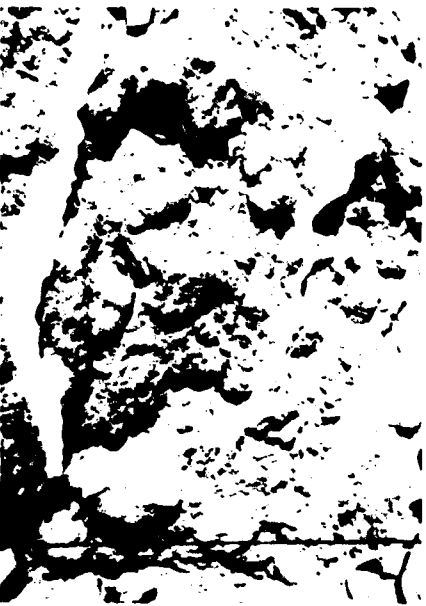
9 Plot 15: granite



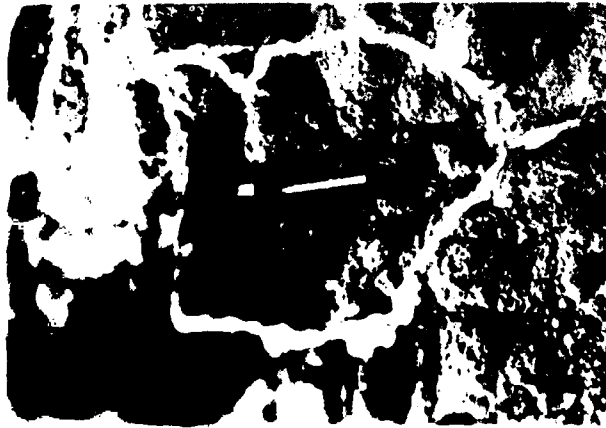
10 Plot 3: schist



11 Plot 7: granite



12 Plot 8: amphibolite



13 Plot 20: amphibolite

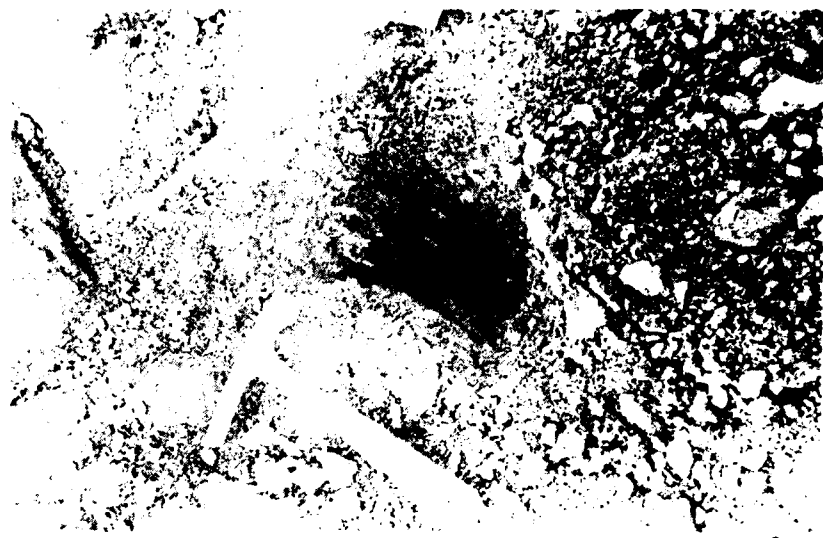


14 Plot 40: amphibolite

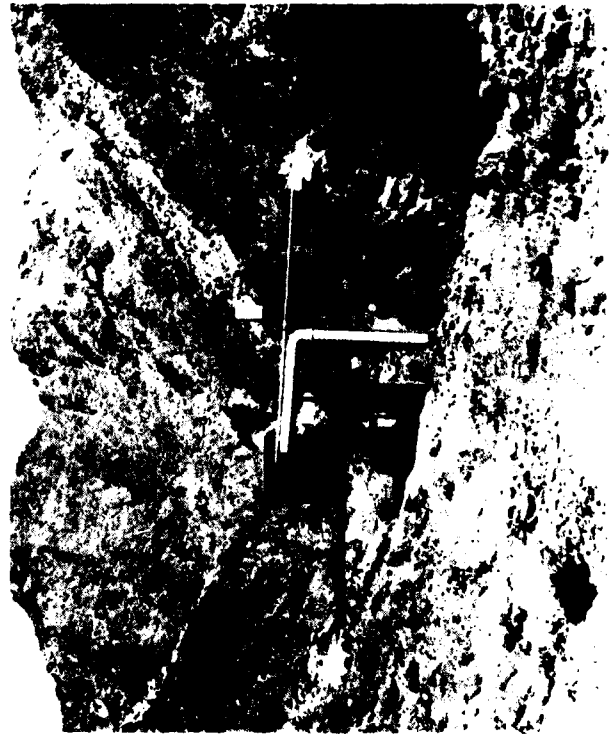


15 Unbounded plot: densely jointed schist

16



Pit in weathered amphibolite
near plot 40



17

Upper part of Nahal Yael watershed;
station 05 in foreground

rills and depressions; these must cause a considerable increase in the infiltration capacity of the entire slope.

Evaluation: In the tests, the relation between infiltration into the joint and the width of the joint is not treated, though some influence can be expected. Likewise, the effect of rain intensity is disregarded, but this factor appears to be of no consequence, as any rainfall amount which generates runoff produces also storage depression which covers the joints with water.

Observations during the tests suggested that infiltration proceeds very rapidly into the top centimeter characterised by the vesicular structure, and slows down considerably below that depth, when the wetting front reaches denser (platy or massive) material. Therefore the infiltration rate, after a few millimeters of initial rainfall, is probably even lower than the mean values as stated above. Observations in cuts in magmatic, volcanic, and metamorphic rocks disclose that most joints virtually disappear at a depth of several decimeters; at most they become so thin that no fill material is present and hence no water can pass through them.

In conclusion, after being wetted by a continuous rain of several hours' duration, or by a series of several shorter rainstorms, the joints become saturated over their entire depth, at which time the infiltration rate of rocky jointed terrain becomes nearly equal to that of rocky unjointed terrain.

The infiltration rates, as determined by the above tests, are lower by a factor of 2-3 than the infiltration rate obtained in a plot test of a similar terrain (plot No.3, table 8.3.). The discrepancy can be explained by the relatively low level of accuracy inherent in the type of

tests used for the joints. However, as indicated by the plot tests and independently substantiated by the "joint" tests, the infiltration rate in rocky jointed terrain is much lower than might be expected from the visual surface impression of widely gaping cracks with but little fill material.

8.3 Infiltration rates in various lithologies

Granite: Granitic slopes constitute only the lower part of Nahal Yael, and are, therefore, of little importance as runoff contributors to the watershed. Granite is, however, very widespread in the Sinai as well as in other deserts elsewhere.

The granite at Nahal Yael is composed of feldspars, quartz, and biotite, and is medium to coarse (0.5 - 3 mm). Some slopes are smooth, others are jointed with a fairly sharp microrelief.

Out of four tests carried out on granite, two (plot No.7, table 8.1 and plot No.15, table 8.2) proved dependable. Plot 7 represents medium, unjointed, resistant and smooth granitic terrain. Plot 15 represents coarse-grained granite, somewhat jointed and slightly crumbly with a very rough surface. Averaging the results of the two plots, we conclude that 0.6 mm of rainfall are necessary for the infiltration of runoff; the stable infiltration rate, standardized to a 20 mm/hr winter rainfall, is 1.3 mm/hr.

It seems that the infiltration rate obtained for plot 15 is not the terminal one, the reason being that in depth the rock becomes harder and less weathered.

Data for four natural rainfall events, measured on a steep, coarse grained, thinly jointed granitic site near the Santa Katherina monastery in the Sinai (A. Yair, personal communication) suggest that, for a rainfall

intensity of 8 mm/hr, the mean infiltration rate is on the order of 2 mm/hr. For the event of 11 December 1978 in Nahal Yael, a little runoff began to flow on the smooth granite slopes already at the intensity of 2.2 mm/hr (after an initial wetting of 3 mm); however, no flow was observed on jointed slopes at the same time. Only when the rainfall intensity increased to 4.35 mm/hr, considerable runoff resulted on both types of slopes.

In conclusion, granitic slopes generate runoff quickly; the infiltration rate is low and the runoff high. For a shower whose intensity exceeds the infiltration rate, the granite absorbs 1-1.25 mm of water over 5-6 minutes prior to reaching the stable infiltration rate; this value is suggested for use in short rainstorms (lasting from some minutes to a few tens of minutes). For larger storms the rate probably decreases.

The terminal infiltration rate, for a medium-intensity rain (10-20 mm/hr) is, approximately:

Unjointed granite	1 mm/hr
Thinly jointed granite	1.5-2 mm/hr
Medium to densely-jointed granite	2.5-3.5 mm/hr

Schist: Most of the Nahal Yael catchment is schist. The schist is pelitic, highly foliated, and is composed mainly of biotite, muscovite, plagioclase, and quartz (Shimron, 1974). "Dip" slope schists produce smooth surfaces, sometimes jointed downslope, and generate runoff rapidly; their terminal infiltration rate is low. Slopes with schist cleavage planes which are inclined opposite to the slope produce very rough and densely jointed terrain surfaces, characterised by a very high depression storage as well as a high infiltration capacity.

The second type is represented by plot 3 (table 8.3).

The trials indicate that runoff begins only after the fall of 1.26 mm of rain, and that the terminal infiltration rate (standardized as above) is 2.9 mm/hr.

Tests conducted on a "dip"-slope schist site failed due to our inability to waterproof the wide joints under the plot boundaries. Our qualitative impression was that the terminal infiltration rate of these slopes was much lower, perhaps 1-1.5 mm/hr.

Amphibolite: In the simulated rainfall experiments special attention was devoted to the infiltration capacity of the amphibolite, because most of watershed 05 is underlain by it, as well as because it is so different from the other rocks investigated. The amphibolite of Nahal Yael is a massive rock of a fairly low metamorphism stage. It is very similar to gabbro and sometimes difficult to distinguish from it. Its mineralogic composition is actinolite, and hornblende-plagioclase-biotite (Shimron, 1974). Texture is coarse, with crystals from 0.5 to 3 mm in size. The amphibolite weathers more readily than granite, schist, or quartz-porphyry; it occurs in two terrain types:

- I) continuous, relatively soft rock surfaces, with a high degree of roughness and with joints which cause depressed strips. This facies is found on the slopes.
- II) resistant and topographically conspicuous, jointed, rocky knolls, located on numerous summit areas.

The "soft" facies is dominant and, by percentage of area cover, the "resistant" facies is nearly negligible. The massive appearance of the rock surfaces conveys the impression that the amphibolite is similar to the granite in infiltration rate and runoff generation; however, this impression is wrong.

It is clear from the substantial number of tests carried out in amphibolite terrain (plot 8, Table 8.6; plot 20,

table 8.7-8.10; plot 40, table 8.11; and additional, undependable plots) that this rock type reacts in a manner intermediate between rock and colluvium. Its infiltration capacity is much higher than that of granite or dyke rocks, and is also considerably higher than that of very jointed schist.

The three plots indicate, as an average, that runoff on amphibolite develops only after 0.7-0.8 mm of rainfall, and that the terminal infiltration rate (standardized for a 20 mm/hr winter rainfall) is between 5 and 6 mm/hr.

After each test on amphibolite, a 25 cm deep pit was dug just outside each plot (photograph 16). In all three pits the material was weathered rock in the form of coarse sand mixed with some finer material; the largest particles, size 1-4 mm, were composed of individual crystals or small rock chips. This "sand" was found, in all 3 cases, to be completely saturated right down to the bottom of the pit. This "sand" possesses a very high hydraulic conductivity, and it seems that the infiltration rate is controlled by the less permeable top layer and by the unweathered rock in depth.

Dykes: Two perpendicular systems of dykes criss-cross the entire area of Nahal Yael in a variable density. They are composed of different rock types, the most important being quartz-porphyry.

The dyke rock is very densely jointed and sometimes even completely shattered. For this reason no dependable results could be obtained in all four tests conducted, as water leaked under the plot boundaries.

On the basis of these rainfall simulation test and the "point" tests described above, we assume that a relatively small initial amount of water (roughly 0.5 mm) is needed to satisfy depression and joint storage; thereafter

a low infiltration of 1-2 mm/hr applies.

Colluvium: Extensive areas in the Nahal Yael catchment, in particular in its upper part, are covered by a colluvial veneer. This colluvium is composed of fine sand with a large amount of stones size 20 to 80 mm. Between 80 and 100 per cent of its surface is covered by angular stones size 10-50 mm. Observations following the runoff event of 9 February 1979 disclosed that during natural rain a thin crust forms on that part of the surface not covered by stones. Hence it is possible that the simulated rain, which obviously does not permit such a crust to form, exaggerates the natural infiltration rates.

In the tests, runoff was initiated after 3 mm infiltrated. The standardized mean terminal infiltration rate was about 9 mm/hr.

Klein (1972) collected runoff from natural rain over colluvial plots in Nahal Yael, but his series, which consisted of very small, low-intensity events with considerable interference from contributing dykes as well as instrumental surfaces, cannot be used for comparison with the present data.

The present results, however, agree well with those of Lavee (1973), who applied simulated rainfall to 6 talus slopes in eastern Sinai, three of which (Nos. 1,2,3) were schist and granite. Each slope was subjected to three spells of simulated rain totalling 20 mm over 40 minutes. The mean terminal infiltration rate for the last two spells on the three above slopes was 12.8 mm/hr. If standardized in the sense of the present report, this figure becomes 10.1 mm/hr, and is comparable to the results obtained for plots 1 (table 8.4) and 5 (table 8.5). The difference of 1.5 mm might be explained by the coarser material in the Sinai taluses.

For Lavee's third rain spell alone, the rate is 9.4 mm/hr (= 9.1 mm/hr standardized).

The agreement between the two sets of data is surprising, because Lavee simulated his rainfall over large plots (area about 100m^2), and he stresses large difference in infiltration rate within the plot (rills vs. ridges), while in the present work very small (0.25m^2) homogeneous micro-plots were used.

8.4 Factors which affect the infiltration rate

8.4.1 Rainfall and time needed to achieve terminal infiltration rates

The following discussion and conclusions are based on Table 8.12.

Rainfall amount: As shown by the two tests conducted on granite, about 1 mm of rainfall is needed to reach the terminal infiltration rate. However, in evaluating the effect of joints, a general value of 1.5-2 mm seems more representative, because the two plots tested had below average jointing.

The measured value for schist - 2.9 mm - seems, on the other hand, to be on the high side, as the tested plot was excessively jointed. A reasonable representative value for schist slopes with outcropping cleavage planes would be 2-2.5 mm, and less for slopes with concordant schistosity.

The mean value for the amphibolite plots, 2.3 mm, being the average of 3 plots, seemed to be representative.

Dependable trials for colluvial slopes are available at only one plot, but evaluation of trials on plot that leaked suggest that a value of 6 ± 1.5 mm is a reasonable estimate.

These results are of considerable importance for the

prediction of runoff. Whenever the pre-rain is fairly intense, i.e. approaching the infiltration rate, then the downward movement of water proceeds almost under saturated conditions. If, during such a pre-rain, the infiltration rainfall amount suffices for achieving a stable infiltration rate, then only very small additional amounts (tenths of mm?) during a very short time interval (tens of seconds?) are needed to achieve the terminal infiltration rate.

Time: The time needed to achieve a stable infiltration rate, for various rainfall intensities, is 7 minutes in granite, 10-12 minutes in schist and amphibolite, and 15-20 minutes in colluvium. However, the tests on two of the amphibolite plots (plot 20, table 8.10, and plot 40, table 8.11) indicate that, during a rain duration of 15 minutes, a stable infiltration rate is indeed achieved, but it is not the terminal rate. Although this could be caused by inadequacies in the graphic approximation by the asymptote in relation to the sensitivity of the measured data, a physical reason should also be considered. It is possible that the wetting front reaches, as the rain proceeds, some different horizon of lower hydraulic conductivity or somewhat different moisture content. Similar changes in the "terminal" infiltration rate have also been observed by Morin et al. (1976) and Yair and Lavee (1976).

We will assume that the infiltration rate of amphibolite becomes terminal if the pre-rain lasted at least 30 minutes and, of course, fell in a sufficient amount. For all other terrain types the rates and times will be taken as stated above.

8.4.2 Infiltration rate as a function of rainfall intensity

Contrary to a decrease in terminal infiltration rate

with increased rainfall intensity, presumably because of crusting on exposed soils (Moldenhauer, 1960; Morin et al., 1976; Vaston, 1965), some of the data of this study suggest a positive linear relationship between these two variables (plots 20 and 40; tables 8.10, 8.11).

The magnitude of this factor can be illustrated by the following example: on amphibolite, if a terminal infiltration rate of 7.25 mm/hr applies for a rainfall intensity of 12 mm/hr, then doubling the intensity to 24 mm/hr would increase the terminal infiltration rate to 8.2 mm/hr. As a first approximation, a linear relationship might be developed.

A possible explanation hypothesizes lateral changes within one plot of infiltrating properties, similar to those assumed by Shanan (1975) to be areally normally distributed.

As the data base available from this study for the evaluation of this factor is too small, it is not further discussed here. It was, however, taken into account when deriving the relevant terminal infiltration rates for several examples (see section 8.5 below).

8.5 Runoff computed on the basis of this study

8.5.1 Methods

The factors which affect runoff are the infiltration rate during the runoff-producing rain spell and the intensity of this rain. Also important are rainfall amount (and intensity) prior to the effective rain spell, and initial moisture.

Each rainstorm (= event) analysed was timewise divided as follows:

1) Initial wetting rain: those parts of the event pre-

ceding rains II) and III);

II) Pre-rain: a relatively intense rain which immediately precedes rain III);

III) Effective rain: the part of the event which generates runoff;

IV) Post-rain: that part of the event which immediately follows rain III).

Whenever the effective rain fell on dry terrain, the time of runoff initiation was calculated by dividing the amount of water needed to achieve a stable infiltration rate by the rain intensity, using the data obtained from the infiltration tests. Effective rain preceded by low-intensity rainfall presents some difficulty, as in all our experiments the simulated rain applied was much more intense than the terminal infiltration rate. The procedure adopted was, in cases where stages I) and II) were both present, to calculate the time of runoff initiation from rain II) as above, and to "postpone" its time of initiation by 10 to 30 seconds. In cases of an intermission in the rain between stages I) and II), the calculation was done as if the ground were dry, and the time of runoff "initiation" was "postponed" by an arbitrary length of time.

The terminal infiltration rate was calculated by using the results of the simulated rainfall tests, corrected in relation to effective rain intensity as illustrated in section 8.4.2.

The relatively short interval between the time of runoff initiation and the achievement of stable infiltration - about 8 to 15 minutes - exerts a confining influence on the form of the infiltration curve. Although it is impossible to compute the infiltration curves, using the Horton formula, on the basis of the three variables alone (time of runoff initiation; infiltration rate at

that time; terminal infiltration rate), the curves as drawn after these data and in accordance with the general form obtained during the tests, actually leave a margin of error of no more than ± 0.1 mm. The infiltration rates as used for these evaluations are summarized in table 8.14. The influence of the post-rain was neglected at this stage, and will be discussed later.

Whenever the pre-rain or the post-rain were intense enough to yield runoff on non-amphibolite rocks, we included in the calculations one half of the excess volume of these spells, on the assumption that such a condition decreases the losses during the effective rain spell.

The discharge data for watershed 05 have been measured over the last 13 years. Because of minimal routing losses due its small size and rocky channels, the data for this watershed provide an opportunity of comparison with runoff as computed on the basis of the infiltration data and detailed in the previous sections.

A special geomorphic mapping project was undertaken to provide the detailed terrain information required for the development of a deterministic, hydro-geomorphic dynamic model (see chapter 5 of this report). This information can be adapted for use in our comparative calculation, as follows:

	A	R	E	A
	hectares		per cent	
Watershed 05, total	5.0		100	
Colluvium, contiguous areas	1.0		20	
Colluvium + rocky surfaces (areal ratio 2 to 1)	3.0		60	
Rocky surfaces, contiguous	1.0		20	

Table 8.14: Infiltration values for various slope terrains used for calculating excess rainfall

	Amphibolite	Other rocks	Colluvium	
Stable infiltration rate standardized to a rainfall of 20 mm/hr	5.66	1.83	8.75	mm/hr
Duration of rainfall until achievement of stable infiltration rate	30*	9	16	min
water amount infiltrated until infiltration rate stabilized, standardized to winter conditions	3.1	1.6	5.9	mm
Water amount infiltrated until initiation of runoff	0.76	0.6**	3.05	mm
Evaluated as an average of plots no.	8,20,40	7,15,3***	1,5	

* estimated on the basis of the follow-up rains in plots 20 and 40.

** average of eight plots, of which only three have been reported here.

*** a finer distinction could be obtained by using the available data for individual rock-terrain types (see section 8.2 above); however, a similar value would have been obtained for most rock-terrain associations which include components of some moderately cleaved schist, some gneiss-granite and some jointed quartz - porphyry dyke material.

Disaggregating the "mixed" area and differentiating the rock types, we get:

	A	R	E	A
	hectares		per cent	
Colluvium	2.5		50	
Amphibolite	1.75		35	
Other rocks	0.75		15	

This is only a gross estimate for a number of reasons: the areal measurements were not very accurate and the rock characteristics vary also within the lithologic units. In particular, the depth and composition of the colluvium vary. Also, the spatial distribution of the lithologic units is disregarded, though this factor probably exercises a decisive influence on runoff generation.

8.5.2 The event of 25 March 1971

The event of 25 March 1971 is taken below as a computational example. This runoff event was generated by a uniform, high-intensity rainfall which followed immediately a fairly intense pre-rain. It produced a good approximation of the unit hydrograph of the catchment.

Rainfall data:

Time from begin of event (min)	Rain stage	Amount (mm)	Duration (min)	Intensity (mm/hr)
0 - 15	pre-rain	1	15	0 - 30
15 - 18	effective rain	3.25	3	66
18 - 31	post rain	0.5	17	1.8

The intensity of the pre-rain rose gradually.

Runoff from amphibolite: According to our results, runoff from amphibolite is initiated after 0.6 mm infiltra-

F/G 8/8

DA-ERO-78-G-111

NL

 2×2 40
409r-89r

END
DATE
FILMED
12 80
DTIC

te into the ground (this amount includes depression storage). The duration until a terminal infiltration rate is achieved: 10 minutes. In the event discussed the runoff-producing rain had an intensity of 66 mm/hr. Prior to it already 1 mm of rainfall had infiltrated, and the last part of this pre-rain was already intense. Thus it is realistic to assume immediate runoff as soon as the effective rain sets in, at a rate controlled by the stable infiltration rate for a 15 minute rain duration, corrected for the intensity of 66 mm/hr. This rate comes out to be 10.9 mm/hr.

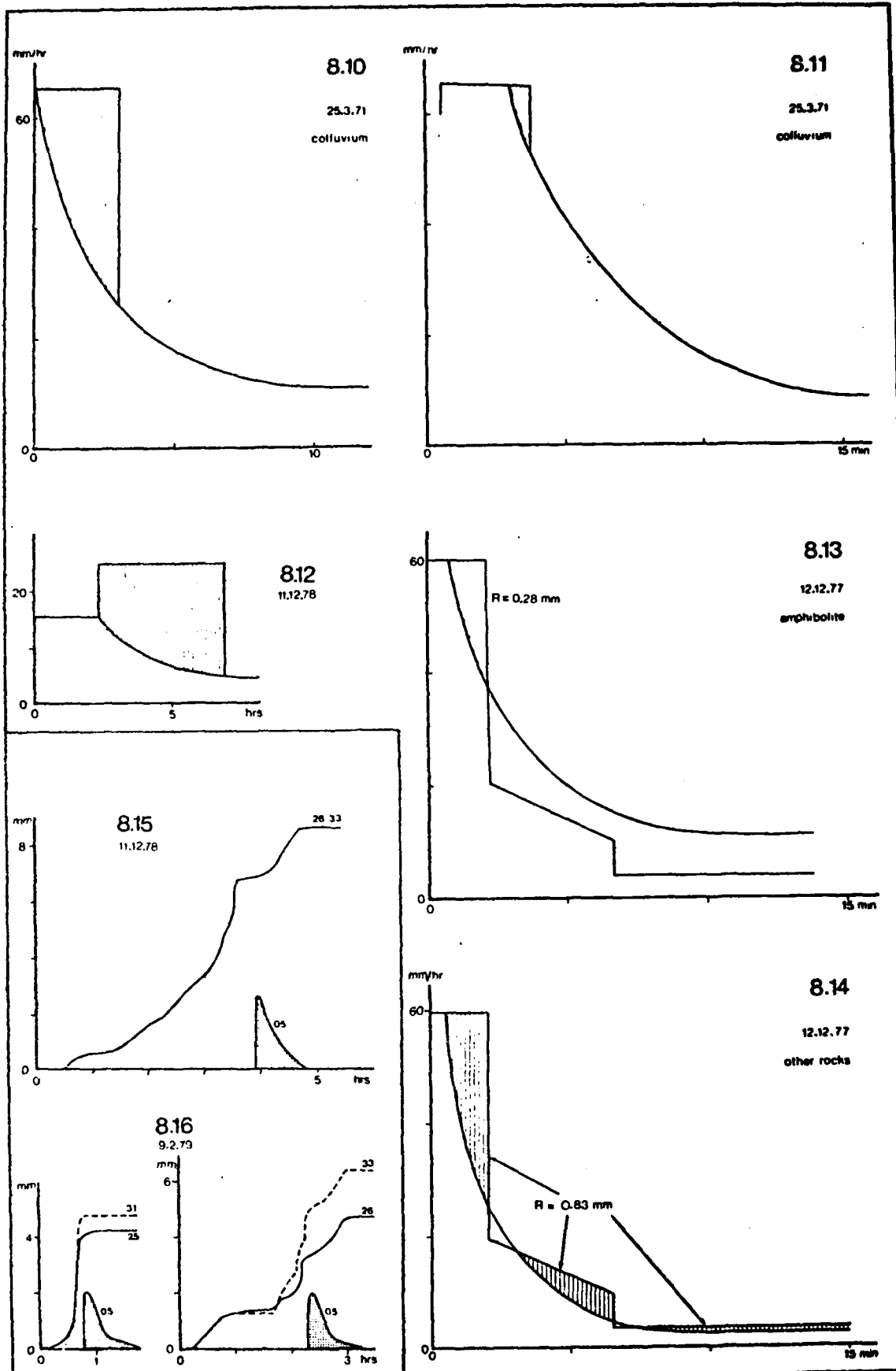
From these three data - initial losses 0.6 mm; time to stability 10 min; stable infiltration rate 10.9 mm/hr - a continuous infiltration curve for the event is constructed (fig. 8.10). Although the curvature of the graph could be evaluated from the Horton equation, we preferred to draw the curve in accordance with the mean curvature obtained from the field data.

Measurement of the shaded area on fig. 8.10 results, by the usual procedure, in the runoff volume. In the present case this value is found to be 1.25 mm; multiplied by the amphibolite area of 1.75 ha, we get an excess rainfall volume of 22m³.

Note that in fig. 8.10 the infiltration curve has been shifted 40 seconds to the left, to account for the effect of the pre-rain which must have caused the immediate generation of runoff with the onset of the effective rain.

Runoff from other rocks: The infiltration curve used is based on the results from three plots - two on granite and one on schist. Although the non-amphibolite rock assemblage in watershed 05 is not identical to this composition, it is sufficiently close to warrant this generalization.

Initiation of runoff after the infiltration of 0.6 mm;



Figs. 8.10 - 8.14: Nahal Yael watershed 05: infiltration and excess rainfall R , events of 25.3.71, 12.12.77, and 11.12.78.

Figs. 8.15 - 8.16: Nahal Yael watershed 05: hyetograph (rain gauges 25, 26, 31 and/or 33, and scaled hydrograph, events of 11.12.78 & 9.2.79.

Time to infiltration stability - 9 min;

Stable infiltration rate - 3.25 mm/hr.

These data yield an excess rainfall of 3.0 mm over the partial area of 0.75 ha, i.e. 22.5m^3 excess rainfall volume.

The total rainfall excess from the rocky surfaces of watershed 05 was, for this event, 44.5m^3 .

Runoff from colluvium: The basic data which govern runoff from colluvium were determined to be:

I) At rain intensity of 60 mm/hr, runoff will start after 3 minutes;

II) The terminal infiltration rate is 9 mm/hr. Figure 8.11 shows that the excess rainfall is only 0.1 mm or, over 2.5 ha, 2.5m^3 .

In comparison, Klein's (1972) colluvial plot 102 yielded, for the same event, at least 0.75 mm. Extended to the 2.5 ha of colluvium in watershed 05, this is equivalent to 18m^3 , at least. The reason for the discrepancy cannot be determined with certainty.

Runoff volume from entire watershed: Totalling the contributions of the lithologic units, we get a watershed rainfall excess of 47m^3 , or - using Klein's (1972) data - of 62.5m^3 . The hydrograph at station 05 yielded a runoff volume of 37.5m^3 . Thus, the transmission losses were about 10m^3 , or, if we accept Klein's (1972) data, 25m^3 or more.

8.5.3 The event of 11 December 1978

This event consisted of a low flow at stations 05 and 04. O.S. was present in Nahal Yael at the time of the event.

Rainfall: The rainfall data for the event were are detailed in table 8.15. The intensity of the so-called

Table 8.15: Rainfall data, event of 11 December 1978

Time from beginning of event (hr:min)	Type (phase) of rain	Amount (mm)	Duration (min)	Intensity (mm/hr)	Cumul. amount (mm)
					0
0:00	pre-rain A	4.5		2.2	4.5
2:20	pre-rain B	1.8	19.5	5.5	6.3
2:40	medium	0.6	2.25	15.9	6.9
2:42	intense	2.3	4.5	30.6	7.6
2:47	post-rain	0.7	35	1.3	8.3

wetting rain, which lasted over two hours, is only an average value, representing an actually variable intensity. Likewise, the intensity of the post-rain is also an average value.

Beginning of runoff: Because of the relatively intense pre-rain (B), slope runoff was initiated immediately with the onset of the effective rainfall, and it stopped right at the end of the effective rainfall period.

The terminal infiltration rates for a rain lasting several hours and corrected to an intensity of 30 mm/hr are:

for amphibolite	6.5 mm/hr;
for other rocks	2.1 mm/hr.

As pre-rain B was fairly intense, and the entire pre-rainfall totalled 6.3 mm, the terminal rate applies, approximately, to all rock types from the onset of the medium-effective rain.

Excess rainfall, amphibolite: $2.15 \text{ mm} \times 1.75 \text{ ha} = 37.6 \text{ m}^3$;

Excess rainfall, other rocks: $2.6 \text{ mm} \times 0.75 \text{ ha} = 16 \text{ m}^3$.

Total excess rainfall on non-colluvial surfaces: 54 m^3 .

The estimation of the infiltration rate into the colluvium is especially difficult, because it cannot be assigned the terminal rate from the onset of the effective rain stage. No data are available to enable the assessment of the effect of the pre-rains on the infiltration rate. In practice, however, several reasonable assumptions which bridge this gap of information yield quantitatively similar results. We assumed, arbitrarily that the medium-effective rain spell is needed to initiate runoff, and thereafter, only one half of the duration needed in fig. 8.11 is necessary to achieve stability; i.e. 5 minutes. The resulting curve (fig. 8.12) yields an excess rainfall of 1.2 mm, equivalent for the colluvial area of 2.5 ha to 30 m^3 .

In case a crust on the colluvium begins to develop, due to the relatively long rainfall duration, this excess rainfall might become larger.

The non-amphibolitic rocks yielded some runoff during the pre-rain stages. The added excess rainfall from this sources is estimated to be 3.5m^3 .

Totalling the excess rainfall, we get 88m^3 , in relation to the runoff volume of 51m^3 measured at the gauging station of watershed 05; i.e. the transmission losses were 33m^3 .

Expressed in a different way, the excess rainfall for this event constitutes 61% of the runoff-producing rain, but the watershed yield is only 35%.

8.5.4 The event of 9 February 1979

Rainfall: The rainfall data listed in table 8.16 are mean values for rain recorders 26 and 33. A rainless interval of one hour followed the initial wetting phase.

Evaluation: The pre-rain did not yield any appreciable runoff. In order to reach stable infiltration rate, 2.3 mm of water must infiltrate into the amphibolite as saturated flow (Table 8.14). The intensity of the pre-rain exceeded slightly that stable rate. This means that infiltration proceeded as unsaturated flow at the beginning of the pre-rain phase, and approached saturation conditions towards its end. Therefore it is permissible to assign terminal infiltration rates to the amphibolite terrains (as well as to the other rocky surfaces) as of the onset of the effective rain, or very shortly thereafter.

The stable infiltration rate for amphibolite was determined to have been 5.2 mm/hr, and for the other rocky surfaces - 1.6 mm/hr. A correction to an intensity of 16 mm/hr was taken into account in the deviation of these

Table 8.16: Rainfall data, event of 9 February 1979.

Time from beginning of event (hr:min)	Type (phase) of rain	Amount (mm)	Duration (min)	Intensity (mm/hr)	Cumul. amount (mm)
					0
0:00 - 0:40	initial wetting	1.6	40	2.4	
					1.6
1:40 - 2:05	pre-rain	2.9	23	7.8	
					4.5
2:05 - 2:11	effective	1.6	6	16	
					6.1
2:11 - 2:25	post-rain	0.4	15	1.8	
					6.5
2:25 - 2:33	post-rain	0.5	8	3.5	
					7.0

values. The resulting excess rainfall for the non-colluvial parts is 29.7m^3 .

The colluvial parts present some complications. Under saturation, 5.9 mm needed to reach a stable infiltration rate (Table 8.14). The pre-rain supplied one half of this amount, and even if the entire wetting rain is added, we are still 1.4 mm short. Therefore it is impossible to determine neither an infiltration rate nor an infiltration curve for the effective rain spell, because the range of the reasonable assumptions is too wide and may cause large errors .

This event is quite similar in character to the one described in the previous section (11 December 1978). Hence we assume also a similar response of the colluvium, and estimate that it yielded roughly one half, or slightly less, of the water yield of the rocky terrains, i.e. about $10\text{-}15\text{m}^3$.

Since the effective rain of this event fell only at one half of the intensity of the previous event (11 December 1978), it is possible that the water yield off the colluvium is even less. However, this effect may be compensated by some crusting on the small, inter-stone surfaces which had been preserved from the event which occurred four weeks earlier.

All these factors considered, we arrive at a total excess rainfall for watershed 05 of $50\text{-}55\text{m}^3$. Station 05 recorded 31m^3 , which leaves $20\text{-}25\text{m}^3$ for transmission losses.

The rainfall excess, including parts of the pre-rain and the post-rain, constitute 62-69% of the effective rainfall; the watershed runoff volume amounts to 39% thereof.

8.5.5 Rainfall event and indications of runoff threshold, 12 December 1977

During this event no flow reached gauging station 05, but the channel immediately upstream of the weir had low flow marks along a reach of approximately 50 meters. The rainfall data for the event, as evaluated from rain-gauges 26 and 33, were:

Type	Amount, mm	Duration, min	Mean int., mm/hr
Effective	2	2	60
Medium	1	4.5	15
Weak	0.5	7.5	4

Figures 8.13 and 8.14 relate the hyetograph to the mean infiltration curves of amphibolite and of other rocks, respectively. Note that the "medium" rain phase actually had a gradually decreasing intensity.

On colluvial surfaces no runoff was generated. Excess rainfall from amphibolite amounted to 4.9m^3 , and from other rocks - 6.2m^3 . Most of the total rain excess, which amounted to 10m^3 , was absorbed by the colluvium. Small residues were absorbed by several minute alluvial pockets in the channel, in conjunction with the very low flow mentioned above.

8.5.6 Rainfall event, 6 February 1978

On 6 February 1978 a rain event of eight hours' intermittent duration occurred in Nahal Yael. The total rainfall of 8 mm was insufficient to generate runoff, nor were low flow marks evident. Thus it was below the threshold of runoff.

The rainfall data for the early and relevant part of the event, based as usual on raingauges 26 and 33, were:

Time from start of event hrs:min	Type of rain	Amount mm	Duration min	Intensity mm/hr	Cumul. Amount mm
0:00					0
	wetting	2.6			
1:40					2.6
	intermission	0			
2:10					2.6
	intense	1.4	2	42	
2:12					4.0
	post-rain	0.3	5	3.6	
2:17					4.3

The wetting phase actually had quite variable intensities with some intervening rainless spells. The post-rain actually had a gradually declining intensity. The rainfall amount was also spatially fairly variable, with 4.3 mm being a mean value.

Assuming that the rain fell on a completely dry surface, the following figures result:

Amphibolite: Runoff initiated 65 seconds after onset of "strong" rain. Excess rainfall 0.12 mm or 2.1m^3 .

Other rocks: Runoff initiated 50 seconds after onset of "strong" rain. Excess rainfall 0.17 mm or 1.2m^3 .

Colluvium: No runoff.

Total excess rainfall: 3.3m^3 .

Some small amount must be added to this figure, to account for the possible contribution of the post-rain, facilitated, perhaps, by the cumulative effect of the long wetting phase. However, even the doubling of the above excess rainfall will not generate any channel flow.

8.5.7 Summary

Table 8.17 lists, for the Nahal Yael watershed 05, the volumes of excess rainfall for five events, as computed on the basis of the present study, and relates them to the measured runoff volume at the gauging station. For the three runoff events, the transmission losses amount to between 10 and 37m^3 per event. The recipients of this water are: I) storage in the few small patches of alluvium in the channel; II) filling of tiny rock pools in the main channel bed and in some tributaries; and III) infiltration into those parts of slope terrain characterized by excessive infiltration capacity (rill zones and negative dykes filled with coarse colluvium).

Theoretically, losses of types I) and II) should be constant, while those of type III) should relate in some consistent manner to the runoff which actually occurs on the slopes. From our data, the upper limit of losses is 37m^3 , and the lower limit, about 10m^3 . Further studies, including perhaps some additional measurements, are needed to verify the above reasoning and to elucidate its quantitative relationships.

As a summary estimate, the mean transmission losses for a one hour flood, volume $30\text{-}60\text{m}^3$, in watershed 05, generated by an effective rainfall duration of 5-10 minutes, are approximately 25m^3 .

8.5.8 The effect of the post-rain

The post-rain was, generally, disregarded in our computations of excess rainfall, because its intensity is lower than the terminal infiltration rate; hence it cannot contribute runoff. However, in a catchment of the size of Nahal Yael 05, the concentration time of excess rainfall from the slopes to the mouth amounts to several tens of minutes. Therefore, in certain rainstorm patterns, some post-rain may fall directly on the remnants of the water

Table 8.17: Watershed 05 - excess rainfall and runoff volume

Date	Duration of effective rainfall (min)	Computed rainfall excess (m ³)	Measured runoff volume (m ³)	Difference: transmission losses (m ³)
25.3.71	3	47 (62.5)	37.5	9.5 (25)
11.2.78	7	88	51	37
9.2.79	6	50 - 55*	31	19 - 24*
12.12.77	-	10	0**	10
6.2.78	-	5 - 10	0***	5 - 10
Mean value per runoff event				23

() incorporating the rainfall excess from colluvium terrains as determined by Klein (1972);

* low accuracy, inherent in method used;

** marks of a very low flow found in channel bed;

*** no marks of flow found.

"sheets" which flow down the slopes. In this situation these raindrops of the post-rain join the body of flowing water and thus are directly contributed to the runoff, in analogy to direct rain which falls on a flowing river. A quantitative estimate of this contribution is attempted below.

Figure 8.16 shows that the post-rain of the event of 11 December 1978 cannot affect the channel flow. The hyetographs reveal that the part of the post-rain contiguous with the effective rain had an intensity of 0.66 mm/hr. During this rain, a flow started at the 05 gauging station at a discharge of $0.038\text{m}^3/\text{sec}$; then it gradually receded. At 17 minutes after the beginning of flow at the station, the rainfall intensity rose to 4.3 mm/hr, but without any appreciable effect on the hydrograph, which continued its recession much like in the event of 25 March 1971 (the "unit hydrograph" event), until its extinction approximately one hour after its beginning.

In the event of 9 February 1979 the intensity of the post-rain was higher - 1.8 mm/hr over 15 minutes, later increasing to 3.5 mm/hr. Here too a possible effect on the hydrograph is not discernible (fig. 8.17).

A post-rain, mean intensity 1.8 mm/hr, followed also the effective spell of the storm of 25 March 1971. Its quantitative effect will be evaluated below.

Rainfall data, post-rain: amount - 0.5 mm; duration - 17 min; mean intensity - 1.8 mm/hr.

Assumptions: I) for the first 7 minutes - 5% of the catchment are covered by flowing water; II) for the subsequent 10 minutes - 3% of the catchment are covered by flowing water.

Result: The total volume contributed by the post-rain to these proportional areas is 1.7m^3 - a negligible amount.

Similary computed, the post-rain contribution to the event of 11 December 1978 was 1.0m^3 and to that of 9 February 1979 - approximately 1.5m^3 (over the first 15 minutes).

The addition of the potential excess rainfall from those small areas whose terminal infiltration rate is less than the relatively low intensities of the post-rain likewise adds only a negligible amount.

Therefore in calculating excess rainfalls for this study, the contribution of the post-rain was disregarded.

8.5.9 Sediment

The amount of sediment in the runoff collected at the outlet funnel of the plots during the infiltration tests described above defies simple analysis, because of its dependance on drop size and fall velocity through splash. It is possible, though, to meaningfully evaluate the variation in sediment concentration over time in a single plot during a simulated rainstorm. A preliminary evaluation of this kind is attempted on the basis of the data for plot 20, on which four successive storms had been rained over a time span of 24 hours (Table 8.18).

Within each of the sub-storms, produced by simulated rain lasting 10-15 minutes each, no systematic trend in sediment concentration is evident. The somewhat lower concentration values in the samples of the two last sub-storm in relation to the two first ones is probably caused by lessened availability of suitable particles due to a "cleaning" effect of the first flows.

Contrary to expectations, the concentration values for the first, high-intensity sub-storm are not significantly higher than those for the second, low-intensity storm. No explanation for this surprising phenomenon is offered at this stage. The sediment aspect of this study will be

Table 8.18: Sediment concentration - plot no. 20
in ppm = mg/l

Simulated storm no.	1	2	3	4
Time, in minutes after begin of simulated rain				
1			1521	
2			875	479
3	1648		916	626
4	573		512	573
5		1071	1312	
6	1213	1193	875	452
7	1120	451	620	521
8	1078	629	1040	
9		1150	740	
10		734		
11				
12				
13	876			

Note: For variation of concentration with time for each
sub-storm, read each column downward.

treated in detail and in a wider context in future.

R e f e r e n c e s

- Klein, M.Z., 1972, The effect of surface characteristics on slope runoff and erosion processes in three small experimental plots in an arid environment (Nahal Yael) (in Hebrew). M.Sc. thesis, Dept. of Geography, Hebrew University, Jerusalem (mimeogr.)
- Lavee, H., 1973, The association between debris mantle characteristics and runoff yield in an extremely arid environment. (in Hebrew). M.A. thesis, Dept. of Geography, Hebrew University, Jerusalem (mimeogr.)
- Moldenhauer, W.C., Burrows, W.C., and Swartzendruber, D., 1960, Influence of rainstorm characteristics on infiltration measurements. Proc. 7th Internat. Congress of Soil Science, Madison, Wis., I:426.
- Morin, J., Benyamini, Y., and A. Michaeli, 1976, The dynamics of soils - 5. Surface crusting and water movement in the profile as affected by raindrop impact. Preliminary Report, Israel Min. of Agric., 30 pp.
- Schick, A.P., and Sharon, D., 1974, Geomorphology and climatology of arid watersheds. Project Report DAJA-72-C-3874, U.S. Army European Research office. Department of Geography, Hebrew University, Jerusalem, Israel.

Shanan, L., 1975, Rainfall-runoff relationships in small catchments of the Avdat region in the central Negev mountains. Ph. D. thesis, Hebrew University, Jerusalem.

Shimron, A., 1974, Geology of Nahal Yael watershed. In Schick and Sharon, *ibid.*

Vaston, K.K., 1965, A statistical treatment of the factors affecting the infiltration capacity of a field soil. *J. Hydrol.*, 3:58.

Yair, A., and Lavee, H., 1976, Runoff-generative process and runoff yield from arid talus-mantled slopes. *Earth Surf. Proc.*, 1:235.

9. THE AREAL FRAMEWORK OF THE NAHAL Yael MODEL

by Gabriel Sharon and Asher P. Schick

9.1 Introduction

This chapter summarizes a preliminary effort to develop an areal framework for a distributed, geosystem-oriented model for a watershed, based on the example of Nahal Yael. In this paragraph the aim and general structure of the model are described, as well as the initial stages of its development. Subsequent sections deal with descriptive aspects of the model and explain how it is set to accept information (9.2.), and with a theoretical-mathematical description of the method adopted for the simulation of the terrain topography and of its drainage network on the basis of elevation data for grid points (9.3. and 9.4.). Section 9.5. discusses the solutions described in 9.3. and 9.4. as treated by computer programs.

For the sample input to these computer programs we have selected the uppermost part of the Nahal Yael watershed, with the incorporation of the entire watershed remaining to be done during a future stage of the work. The methods of computation and of data input into the computer programs as well as an analysis of the results are presented in section 9.5.

In addition, all along this chapter we have dwelt on general trends and evaluations as they gradually evolved during the development of the model framework. Clearly, this is only an initial step in the development of the

model. Therefore we have freely included ideas and suggestions, to be worked out in detail during the future stages of the project.

The objective of the model

The Nahal Yael model is designed as a distributed model, which should ultimately develop into a vehicle which will evaluate not only runoff but also erosion-sedimentation processes as well as effects thereon of short and long term pulses such as high-magnitude events, landuse changes, climatic shifts, and man-made intervention. The model is constructed in such a way as to accommodate the fact that variations both in time and in space of the input data substantially affect runoff and associated output data.

The areal framework chosen for the model is one of relatively small squares equal in area. It is assumed that within each grid element (= "square") the geophysical variables are homogeneous. The parameters vary from one square to the next. The dominant processes in the watershed occur in two phases: the diffuse slopeflow phase, regarded as taking places over the entire surface of the squares, and the concentrated channelflow phase, simulated by a trajectory composed of square sides.

The objective is to construct a general framework for the quantitative description of attributes and processes within a watershed in such a way, that it will be adaptable with little change and only minor preparatory effort to other watersheds and regions. Thus it is necessary to divide the area very mechanically into geometric elements (such as squares); a subjective areal division, such as one based on geomorphic or other terrain criteria, is totally unsuitable for the universality requirement.

It is very important to use in the model easily obtainable input data, of such kinds not requiring elaborate

measurements or special research. The information available is stored in relation to the individual grid elements. Likewise, the output - water depth and yield, sediment depth and yield - will be obtained discretely for each individual grid element or channel element and for every time unit, as required. Thus, the model we aim at is a distributed deterministic model.

Upon the completion of the model, it should be possible, in addition to the uses already mentioned, to follow in detail the evolution of landforms in diverse regions. The evaluation of the effects of changes which occur in one area within the watershed on another area in it will also be much simpler.

The numerous iterative, though mostly simple, computations which this model presupposes are possible only with the electronic computer. Such computations will be done separately for each grid element, and will be executed in addition to other computational stages common to models such as optimization of parameters.

This section describes only the first stage accomplished - the adoption of the grid network for the areal framework of the model and the construction thereon of the simulated topography and drainage system. To this framework it is possible to attach the input data.

9.2 The Rectangular Grid

As it is impossible to construct a model which will handle differently every single point within an area under study, we have to assume homogeneity of geophysical attributes within small areal elements. In particular, we assume homogeneity in the slope angle and slope orientation of each areal element, i.e. we are dealing with an assem-

blage of planar surfaces.

Because of the requisite of an arbitrary division into unit elements mentioned above, we need some perfect polygon for the unit area. We selected the square, with the grid predetermined by the map coordinate system, and the cardinal N-S and E-W coordinate lines coinciding with grid lines. This facilitated easy reading of data off the map for assigning to the squares. The parallel alignment of all the sides of all the squares constitutes a decided advantage in comparison with other perfect polygons such as the triangle or the hexagon; this is especially felt in the preparation of the data for the computer and in the ease of reading the evaluations off the map at grid intersections.

It might well be that the equilateral triangle and its analog, the equilateral hexagon, both constitute a more "natural" unit areal element, and perhaps they provide more directional flexibility in areal transfers of mass from one grid element to the next. But the inconvenience of handling and managing non-cartesian elements, coupled with the more involved mathematics necessary for simulating mass transfers, by far outweigh the advantages to be gained. In any case, if the unit area is small enough, and the transfer equations are handled properly, the exact form of the unit area is of no consequence, particularly if we recall that every element, however small, is only an approximation of the real-world terrain surface.

9.2.1 Considerations for the selection of the square size

In principle, the smaller the unit area, the larger will be the degree of homogeneity within each square. Therefore the tendency in distributed, deterministic modelling is to have unit areas as small as possible. However, there are a number of constraints: size of the area (watershed) under study, degree of detail of the information

(geophysical data), and computer capacity and time available.

For very large areas the degree of detail will be small, and the division into tiny units cannot be justified, because the rate of change of the geophysical parameters over adjoining unit areas will be very small. On the other hand, the square side will always have to be at least one order of magnitude smaller than Schumm's constant of channel maintenance (= the inverse of drainage density), in order to ensure that the mean slopeflow trajectory from divide to channel is covered by at least five unit elements.

In our sample area - described in more detail in section 9.5 below - we have elected to use unit elements of 12.5 meters square, delineated on a detailed, photogrammetry-based topographic map. The scale of the map is 1:1250 and the contour interval is one meter. At the present stage, the information input for each square consisted only of the elevation of each corner of each square (= every intersection for 80 grid lines per kilometer of N-S and E-W length). Thus, neither the density of geophysical information nor considerations of computer time and storage had any influence on the size selection. However, if both the size of the study area and the number of geophysical parameters increase substantially during future stages of the development of the model - the size selected for the unit area will have to be reconsidered.

Although we have divided the terrain continuum in the present work into equal-area elements, it is quite possible that in the course of further development the need for unit area flexibility will arise. This could be attained by starting with an equal-area basic grid, but certain squares or group of squares could be further subdivided on the basis of an objective criterion reflecting the

rate of change over adjacent squares of a given geophysical property. For example, let us look at topographic relief, i.e. rate of change of elevation over distance. We might wish to subdivide the standard square over areas of cliffs, canyons or badlands.

Assume h_1 , h_2 , h_3 and h_4 to be the elevations of the corners of a standard square, and h_m to be the elevation of the square center (fig. 9.1). Read from the map, or from the air photograph, those five values and compute

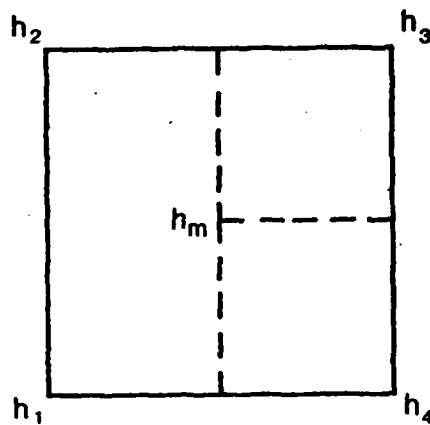
$$\alpha = \sum_{i=1}^4 (h_i - h_m)^2 \quad (9.2.1)$$

for all the standard squares. Squares with a large α will be those with a considerable inner relief, and those may be divided into four small squares each (fig. 9.1). In practice a threshold value \underline{a} - dependent on the frequency distribution of the computed α values - could be determined, and a further subdivision made wherever $a < \alpha$.

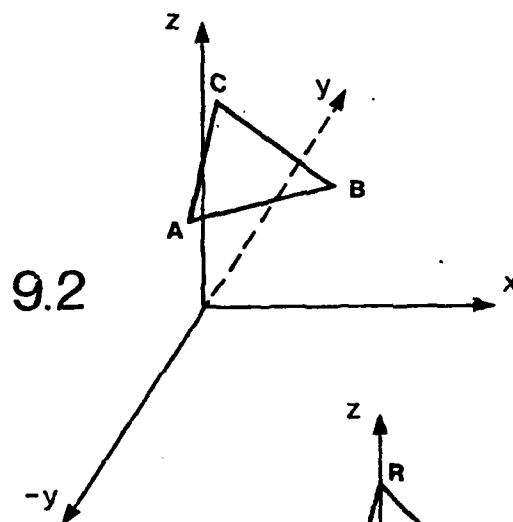
The application of a criterion of this type enables us to choose a relatively large standard square, and at the same time to augment the sensitivity of the model to changes in the geophysical input. However, the resulting complications in the mathematical representation of the mass transfer from square to square (not considered in the context of this chapter) may offset the advantages.

9.2.2 Mode of simulation with regard to the grid

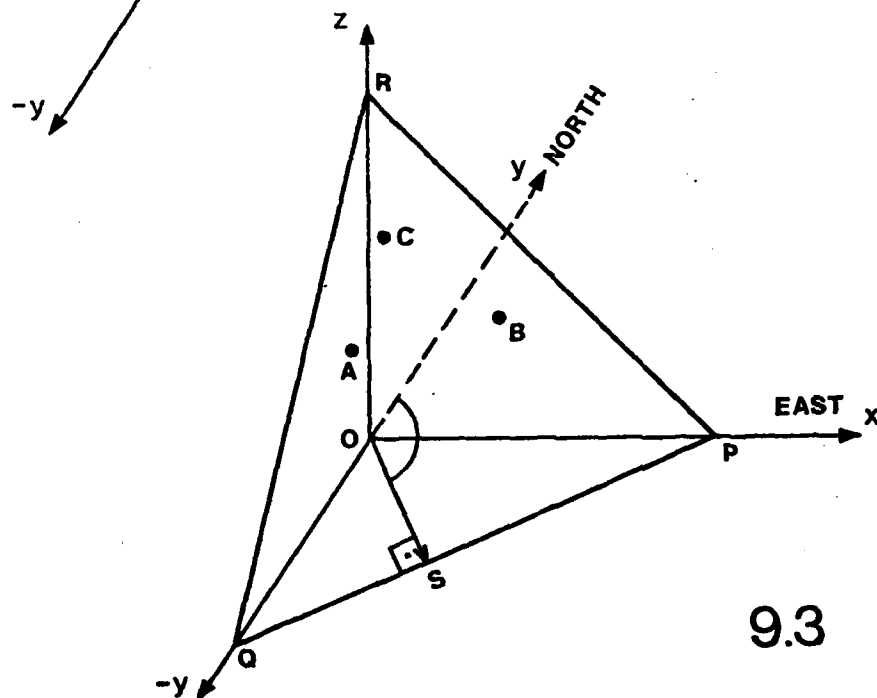
The simulation of process in the studied area will be tied to the grid as follows: the square areas will accommodate the assumedly unconcentrated slopeflow, and some of the square sides will carry along them the discontinuities of concentrated channel flow, as well as those of the divides.



9.1



9.2



9.3

All parameters, such as elevation, terrain composition, rainfall input, and others, will be referenced to the grid elements. For static parameters this will be constant for all time units, and for dynamic parameters they will change with time. The same will be done for those square sides which simulate channels.

Flow processes will occur diffusely from square to square, until they hit a channel side. From then on flow will proceed along the channel network simulated by a connective assemblage of square sides.

In this manner another constraint for the size of the square would be the actual width of the channel. It is undesirable in this model for a real-world channel to be wider than a square side.

9.3 The description of the topography by means of the grid data

From our basic premise according to which every square unit element approximates a plane surface, there follows immediately the first step of computing the orientation and slope angle of that surface on the basis of the elevation of its corners. The problem is analogous to the computation of dip and strike values for a geological stratum on the basis of four outcrops whose location in space is known.

The orientation, which will be also named below the azimuth, is the direction, in space, of the maximum slope of the plane surface. Every square can thus receive an azimuth value between 0° (northward) through 90° (eastward) and further clockwise all the way back to 360° (again northward, i.e. $= 0^{\circ}$). Clearly the azimuths are orthogonal to the terrain contours. The slope angle, subsequently also called the dip, is the rate of elevation loss of the plane surface with regard to the horizontal xy plane of

the grid.

Three points suffice to unilaterally define a plane surface in space. Since we have four points, the computation of both the azimuth and the slope angle was made separately for every combination of three out of these four points. The azimuth and dip values assigned to the square are the mean of these four combinations (details below).

Hence the computational procedure consists of two stages:

- I) Computation of the azimuth and the dip for three given points; and
- II) Estimation of the azimuth and the dip for the grid square.

9.3.1 Computation of azimuth and dip for three given points in space

The computation is based on considerations of analytical geometry in three dimensions as follows: there are given three different points in the XYZ space. XY is the map plane, with the x-axis directed east-west and the y-axis north-south; z is the axis of topographic elevation.

Let us assign the following coordinates to the three points:

$$A = (x_1, y_1, z_1)$$

$$B = (x_2, y_2, z_2)$$

$$C = (x_3, y_3, z_3)$$

(fig. 9.2)

The equation of the unilaterally defined plane which includes A, B and C is, in determinant notation

$$\begin{vmatrix} x & y & z & 1 \\ x_1 & y_1 & z_1 & 1 \\ x_2 & y_2 & z_2 & 1 \\ x_3 & y_3 & z_3 & 1 \end{vmatrix} = 0 \quad (9.3.1)$$

All the points (x,y,z) for which equation (9.3.1) holds are located on the plane defined by ABC. Evaluating the determinant after the first line:

$$x \cdot \begin{vmatrix} y_1 & z_1 & 1 \\ y_2 & z_2 & 1 \\ y_3 & z_3 & 1 \end{vmatrix} - y \cdot \begin{vmatrix} x_1 & z_1 & 1 \\ x_2 & z_2 & 1 \\ x_3 & z_3 & 1 \end{vmatrix} + z \cdot \begin{vmatrix} x_1 & y_1 & 1 \\ x_2 & y_2 & 1 \\ x_3 & y_3 & 1 \end{vmatrix} - \begin{vmatrix} x_1 & y_1 & z_1 \\ x_2 & y_2 & z_2 \\ x_3 & y_3 & z_3 \end{vmatrix} = 0 \quad (9.3.2)$$

For convenience let us substitute for the coefficients of equation (9.3.2) as follows:

$$\begin{aligned} a &= \begin{vmatrix} y_1 & z_1 & 1 \\ y_2 & z_2 & 1 \\ y_3 & z_3 & 1 \end{vmatrix} & b &= - \begin{vmatrix} x_1 & z_1 & 1 \\ x_2 & z_2 & 1 \\ x_3 & z_3 & 1 \end{vmatrix} \\ c &= \begin{vmatrix} x_1 & y_1 & 1 \\ x_2 & y_2 & 1 \\ x_3 & y_3 & 1 \end{vmatrix} & d &= - \begin{vmatrix} x_1 & y_1 & z_1 \\ x_2 & y_2 & z_2 \\ x_3 & y_3 & z_3 \end{vmatrix} \end{aligned}$$

the result is the equation of a plane surface:

$$ax + by + cz + d = 0 \quad (9.3.3)$$

with a,b,c and d derived directly from the above by using the usual determinant development of a 3x3 matrice as

follows:

$$\begin{array}{rcl} a & b & c \\ d & e & f \\ g & h & k \end{array} = a(e \cdot k - f \cdot h) - b(d \cdot k - f \cdot g) + c(e \cdot g - d \cdot h)$$

9.3.2 Computation of the azimuth

We are interested in the orientation downslope; hence we have to distinguish in the computation of the azimuth among several cases.

First assume:

$$a \neq 0, b \neq 0, c \neq 0, d \neq 0$$

This situation is shown in fig. 9.3, in which A, B, and C are the three given points; P, Q, and R are the intersection points of the plane with the axes; the origin $O = (0,0,0)$; and the vector \overrightarrow{OS} signifies the direction of the azimuth.

According to equation 9.3.3:

$$\begin{aligned} P &= (-d/a, 0, 0) \\ Q &= (0, -d/b, 0) \\ R &= (0, 0, -d/c) \end{aligned}$$

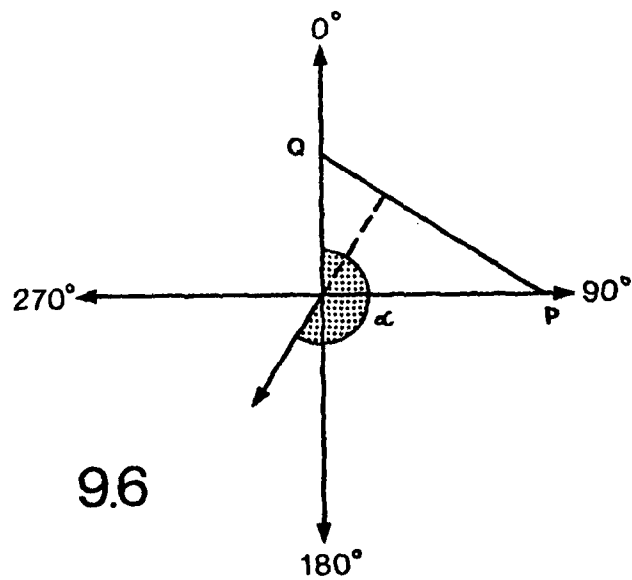
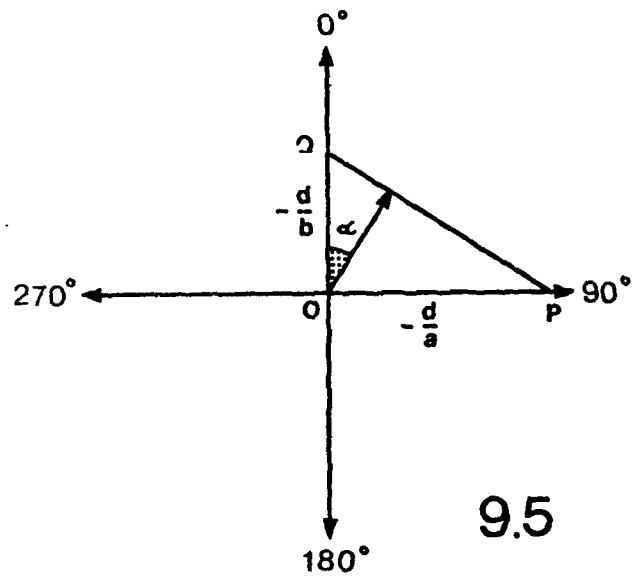
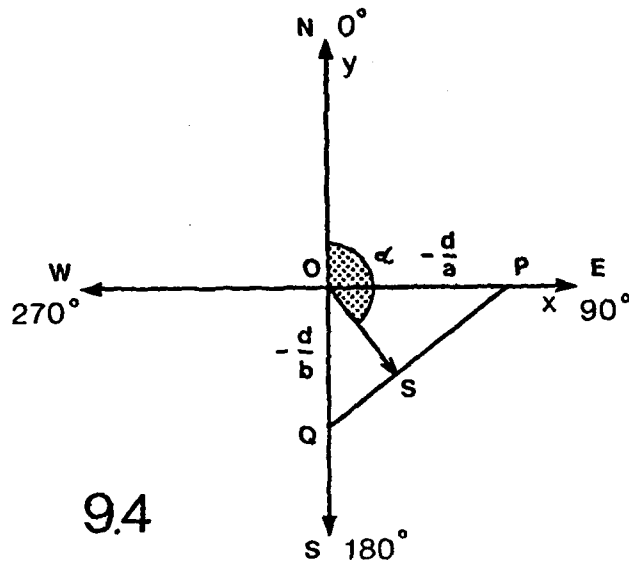
Now consider each case for triangle POQ in relation to the sign of $-d/a$, $-d/b$, and $-d/c$.

Case 1: As in figure 9.4:

Assume

$$\begin{aligned} -d/a &> 0 \\ -d/b &< 0 \\ -d/c &> 0 \end{aligned}$$

The projection on plane xy ($z \equiv 0$) is shown in fig. 9.4.
 α is the required azimuth.



The downslope direction of the plane is determined according to the sign of $-d/c$, because it signifies whether point R on the z-axis is above or below the origin.

In this case the solution is, considering the constraints mentioned above:

$$\tan \alpha = -a/b$$

$$90 < \alpha < 180$$

Case 2: Assume

$$-d/a > 0$$

$$-d/b > 0$$

$$-d/c > 0$$

The projection on the xy-plane is shown on fig. 9.5.

The solution:

$$\tan \alpha = a/b$$

$$0 < \alpha < 90$$

Case 3: Assume

$$-d/a > 0$$

$$-d/b > 0$$

$$-d/c < 0$$

It can be seen from the projection on the xy-plane (fig.9.6) that this resembles case 2, but the sign of $-d/c$ is reversed. Therefore the direction changes 180° .

The solution:

$$\tan \alpha = a/b$$

$$180 < \alpha < 270$$

It is possible to analyse in a similar way all the cases,

$2^3 = 8$ in total: four for $d/c < 0$ and four for $d/c > 0$.

Up to this point - for all cases discussed - a, b, c , or d were assumed never to be zero. Let us now analyse one special case, say:

$$\begin{aligned} a &= 0, & b &= 0 \\ c &\neq 0, & d &\neq 0 \end{aligned}$$

The planar equation reduces to

$$cz + d = 0$$

or
$$z = -d/c$$

This is a plane which parallels the xy -plane, that is to say that the elevation of all three points is identical. They are situated on a horizontal plane for which the azimuth is not defined, and the dip is 0.

Although c can be zero theoretically, it would mean that the plane defined by our three points parallels the z -axis and is perpendicular to the xy -plane. In practice this can only happen if the three points fall on a straight line, which never happens in our procedure. Hence always $c \neq 0$. Therefore also $a = b = d = 0$ is impossible, because then also c would be 0.

The solutions for the various applicable cases are summarized in Table 9.1. Parts A and B list conditions whose solutions are shown in part C, in the same column. For example, condition ($d = 0, c/a < 0, c/b < 0$) is found in part A, column 2. Hence the solution is $\tan \alpha = a/b$ and $180 < \alpha < 270$. Special cases are treated in Table 9.2.

9.3.3 Computation of the slope angle

Referring to fig. 9.3 we get the dip, or maximum slope angle, from triangle ROS as in the two-dimensional

Table 9.1: Solutions for the orientation in space of a plane defined by three points - general cases.

α is the required azimuth;

- means that the value of the expression in the left column is less than zero;

+ means that the value as above is positive.

		Conditions: $a \neq 0$ $b \neq 0$ $c \neq 0$ $d = 0$				A
and c/a		(-)	(-)	(+)	(+)	
and c/b		(+)	(-)	(-)	(+)	
		Conditions: $a \neq 0$ $b \neq 0$ $c \neq 0$ $d \neq 0$				B
and d/a		(+)or(-)	(+)or(-)	(-)or(+)	(-)or(+)	
and d/b		(-)or(+)	(+)or(-)	(+)or(-)	(-)or(+)	
and d/c		(-)or(+)	(-)or(+)	(-)or(+)	(-)or(+)	
Solution	$\tan \alpha =$	$-a/b$	a/b	$-a/b$	a/b	C
	Azimuth range	$270 < \alpha < 360$	$180 < \alpha < 270$	$90 < \alpha < 180$	$0 < \alpha < 90$	

Table 9.2: Solutions for the orientation in space of a plane defined by three points - special cases.

	Any d	
	$b \neq 0$	$c \neq 0 \quad a = 0$
b/c	(+)	(-)
Solution	$\alpha = 0$	$\alpha = 180$

	Any d	
	$a \neq 0$	$c \neq 0 \quad b = 0$
a/c	(+)	(-)
Solution	$\alpha = 90$	$\alpha = 270$

	$a = 0 \quad b = 0 \quad c \neq 0 \quad d \neq 0$
Solution	horizontal plane, azimuth undefined

figure 9.7, wherein the dip is denoted by ϕ .

From geometric considerations

$$\cos \phi = \frac{c}{(a^2 + b^2 + c^2)^{0.5}}$$

and therefore the dip is

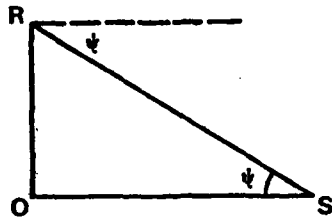
$$\phi = \arccos \left| \frac{c}{(a^2 + b^2 + c^2)^{0.5}} \right| \quad (9.3.4)$$

9.3.4 Evaluation of the slope angle and of its orientation for a square

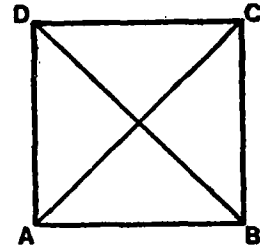
It has been shown above how it is possible to obtain the coefficients of an equation of a plane defined by three points in space, and how these coefficients enable us to establish the values of the azimuth and the slope angle. On the basis of this procedure, the problem of assigning slope angle and azimuth values to a grid square can be treated as follows.

In square ABCD, compute azimuth and slope angle as explained above for each of the triangles ABC, ABD, BCD, ACD (fig. 9.8). Now let us define the slope angle of the square as the mean of the four slope angles obtained for each of the above triangles. Similarly, the azimuth of the square will be defined as the mean of the four azimuths obtained for each of the triangles. Although we get in this way only an approximation of a segment of the actual surface by a plane, it may actually be more representative of the general trend of the surface, because it is not so dependent on a single elevation value as would have been the case with a triangle.

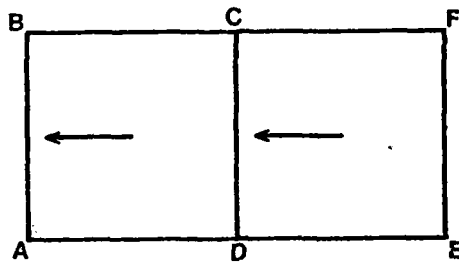
If all four points happen, by chance, to be exactly on



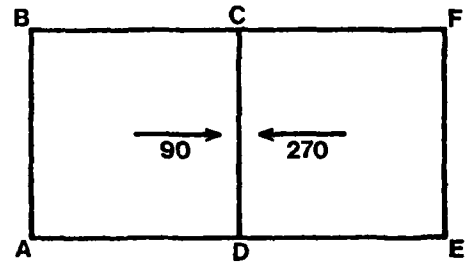
9.7



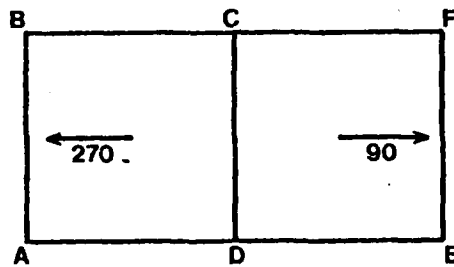
9.8



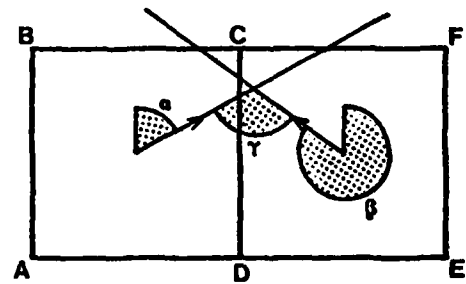
9.9



9.10



9.11



9.12

the plane, we would get the real values for the plane. But in the general case, the points will diverge from the plane fitted to them. The fit however, tends to be good. An application of the method to the Nahal Yael watershed has shown, in the majority of cases, a good reproduction of the slope directions as expected on the basis of the topographic map. In certain grid squares internal relief causes inaccuracies. For these the inherent assumption of a pseudo-planar surface is wrong, and the only available solution is a further subdivision of the unit area (section 9.2. above). Such a subdivision could be made to depend on an objective criterion, such as, for example, a standard deviation of the component triangle angles and azimuths above a given threshold value.

In summary, the above procedure yields a simulation of the terrain topography based on a square grid system. The next step in the development of the model - the simulation of the divides and drainage lines on the basis of the above plane assemblage - will be discussed in the next section.

9.4 Determination of divides and channels

The simulated divides and channels, to be generated from the square grid data, are designed to enable the dynamic functions of the model. The grid square network will merge into a stream channel network, and through these mass transfers (water and sediment) will take place.

In our model, the drainage network as well as the divides are represented by sides of grid squares. A square side which forms a segment of a stream channel is named a stream barrier, and a square side which forms a segment of a divide is called a divide barrier. Both types con-

stitute barriers in the sense that they do not transmit mass (water and sediment) through them. At most, in the case of stream barrier, mass is conveyed along the barrier.

The process of fluvial mass transfer in a watershed modelled along these lines is thus divided into two phases: I) the unconcentrated phase (i.e. slopeflow) occurs over the square surfaces; and II) the unconcentrated phase (i.e. channel flow) occurs along the square sides.

The criterion for determining whether a given square side constitutes a barrier depends on the directional trends (azimuths) of the two adjoining squares. Whenever those azimuths trend, generally, in opposing directions, a barrier is indicated. In cases where the azimuthal trends are, more or less, parallel, then the squares they represent are part of the same slope.

An extreme case of non-opposing directional trends occurs when the trends of two neighboring squares are identical (fig. 9.9). Here the azimuth of ABCD is, just like that of CDEF, 270° . CD cannot constitute a barrier because the flow within CDEF is totally toward CD, and within ABCD the flow is directed from CD toward AB. A continuous slopeflow over both squares is thus indicated.

If the trends are generally opposing, two cases are distinguished: I) convergence; and II) divergence.

In converging trends a stream barrier is formed, while for diverging trends we get a divide barrier. Extreme cases of converging and diverging trends are illustrated in figures 9.10 and 9.11, respectively. In both, CD is the barrier.

For the general case a threshold angle can be used to define the relationship between two adjacent opposing squares. If the angle between the azimuths of the two

squares is greater than the threshold - a barrier exists. For practical purposes, it is better to establish two different threshold values - one for channel barriers (called STBAR) and one for divide barriers (called DVDBAR).

The determination of the inter-azimuthal angle is shown in figure 9.12. The trend of ABCD is designated α . The trend of CDEF is β . The angle between the azimuths is designated ϕ .

According to the various directions of α , β we get by analytical substitution the following equation for the inter-azimuthal angle:

$$\phi = \begin{cases} |\alpha - \beta| & \text{for } |\alpha - \beta| \leq 180 \\ 360 - |\alpha - \beta| & \text{for } |\alpha - \beta| > 180 \end{cases} \quad (9.4.1)$$

The conditions for the existence of a barrier are:

Channel barrier - converging azimuths and $\phi > \text{STBAR}$

Divide barrier - diverging azimuths and $\phi > \text{DVDBAR}$.

For the threshold angles there exists the following theoretical constraint:

$$0 \leq \text{STBAR}, \text{DVDBAR} \leq 180$$

Clearly, the smaller the threshold angles, the larger the number of barrier sides. In the extreme cases of

$$\text{STBAR} = \text{DVDBAR} = 0$$

a channel barrier is simulated at any side toward which there is convergence, however slight, and a divide barrier will result at any side from which there is even a minute degree of divergence.

Alternately for

$$STBAR = DVDBAR = 180$$

no barriers are formed at all.

After finding the angle between two azimuths, it is necessary to ascertain whether it is converging or diverging, because the definition of ϕ (equation 9.4.1) does not enable the distinction, in itself, between a thalweg and a crest line. As an example, in figure 9.10 $\phi = 180$, and in figure 9.11 $\phi = 180$ as well; however, the first is diverging and the second is converging.

The distinction between a diverging and converging barrier can be made either by the method of segments or by comparing elevations.

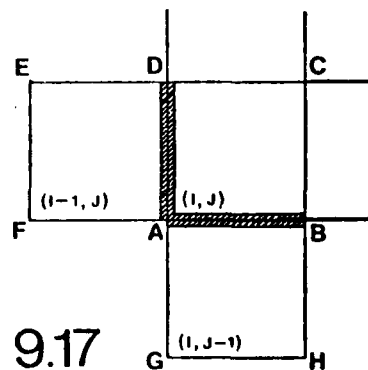
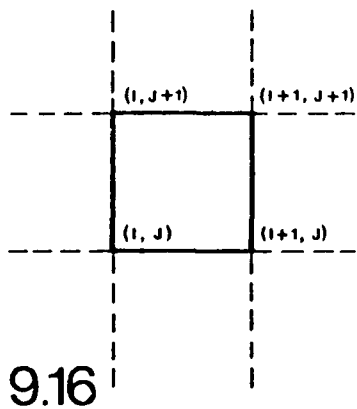
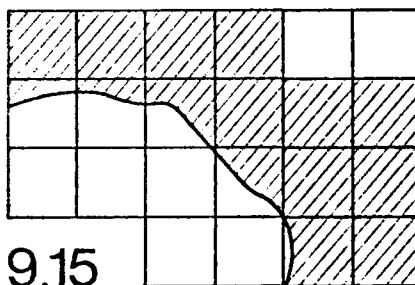
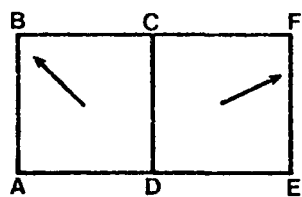
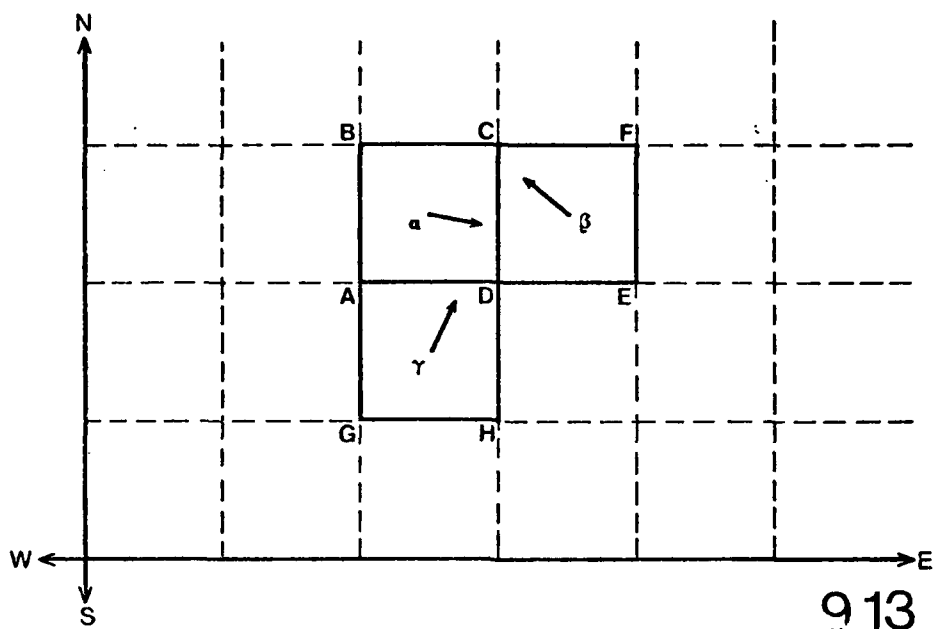
I) The "segment" method: Referring to figure 9.13, let us define

$$\begin{aligned} \text{azimuth } ABCD &= \alpha \\ \text{" } CDEF &= \beta \\ \text{" } ADGH &= \gamma \end{aligned}$$

Further, let us define side \overline{CD} , if indeed it qualifies as a barrier, a longitudinal barrier. Similarly let us define an east-west directed side, if it qualifies as a barrier, a latitudinal barrier, like \overline{AD} in fig. 9.13.

The divergence/convergence test is done separately for longitudinal and latitudinal barriers.

Longitudinal barriers: The azimuths of two east-west neighbor squares (such as ABCD and CDEF in fig. 9.13) converge if the azimuth of the eastern square (CDEF) is between 180^0 and 360^0 and the azimuth of the western square (ABCD) is between 0^0 and 180^0 . If both conditions are not met, there is no barrier. If both conditions are satisfied and ϕ (the inter-azimuthal angle) exceeds STBAR,



a longitudinal channel barrier is formed.

The azimuths diverge only when conditions opposite to convergence prevail, i.e.

azimuth ABCD is between 180° and 360° ;

azimuth CDEF is between 0° and 180° ;

If, in addition, the inter-azimuthal angle exceeds the threshold angle for divides, a longitudinal divide barrier is formed, such as along side \overline{CD} (fig. 9.13).

Latitudinal barriers: For a latitudinal barrier such as \overline{AD} in fig. 9.13, convergence or divergence are determined in an analogous manner:

Convergence exists if $90 \leq \alpha \leq 270$

and $\gamma \leq 90$ or $\gamma \geq 270$; and

Divergence exists if $\alpha \geq 270$ or $\alpha \leq 90$

and $90 \leq \gamma \leq 270$.

For any other set of azimuthal relationships no barriers between adjacent squares are formed and the flow over them is, accordingly, slopeflow only.

The application of the "segment" method is summarized in table 4.1.

The solutions in table 9.3 refer to the usual case of the simulation network paralleling the map coordinate network. If another direction is chosen for the grid of the simulation, the system must be rotated by an angle whose magnitude is the difference between the map north and the longitudinal axis of the model grid.

II) Comparing elevations: The second method usable for distinguishing between convergence and divergence relies on the data bank of topographic elevations as well as on the azimuth values.

Two adjacent squares converge toward the side common to both if the mean elevations of both pairs of outer corners are higher than the mean elevation of the two ends

Table 9.3: Conditions for the existence of barriers - the "segment" method.
See figure 9.13.

BARRIER	Description	C O N D I T I O N S			RESULT
LONGITU-DINAL	Refers to side \overline{CD} between squares ABCD and CDEF	Angle between α and β	Azimuth of ABCD, α	Azimuth of CDEF, β	\overline{CD} is a
		$\phi > \text{STBAR}$	$0 \leq \alpha \leq 180$	$180 \leq \beta \leq 360$	longitudi-nal channel barrier
		_____ and _____ and _____			
		$\phi > \text{DVDBAR}$	$180 \leq \alpha < 360$	$0 \leq \beta < 180$	longitudi-nal divide barrier
LATITU-DINAL	Refers to side \overline{AD} between squares ABCD and ADGH	Angle between α and γ	Azimuth of ABCD, α	Azimuth of ADGH, γ	\overline{AD} is a
		$\phi > \text{STBAR}$	$90 \leq \alpha \leq 270$	$\gamma \leq 90$ or $\gamma \geq 270$	latitudi-nal channel barrier
		_____ and _____ and _____			
		$\phi > \text{DVDBAR}$	$\alpha \leq 90$ or $\alpha \geq 270$	$90 \leq \gamma \leq 270$	latitudi-nal divide barrier

of the common side. Figure 9.14 shows two adjacent squares ABCD and CDEF, with \overline{CD} as their common side. Let H_A, H_B, \dots, H_F be the elevation of each corner. Convergence toward \overline{CD} prevails if

$$\frac{1}{2}(H_C + H_D) < \frac{1}{2}(H_A + H_B)$$

and

$$\frac{1}{2}(H_C + H_D) < \frac{1}{2}(H_E + H_F)$$

Actually, the factor $\frac{1}{2}$ may be omitted. Thus, divergence away from \overline{CD} will prevail if

$$H_C + H_D > H_A + H_B$$

and

$$H_C + H_D > H_E + H_F$$

If, in addition to the two convergence criteria detailed above, we have

$$\phi > \text{STBAR}$$

then \overline{CD} is a channel barrier.

Likewise, if, in addition to the two divergence criteria listed above, we have

$$\phi > \text{DVDBAR}$$

then \overline{CD} is a divide barrier.

Both, the segment method and the elevation method make sure by their structure that channel barriers and divide barriers are mutually exclusive: it is impossible for a given side to be both at one and the same time. The segment method has the advantage of not requiring another step of computation beyond the determination of the azimuths and their evaluation by segments. In handling a large network, this may result in some economizing of

computer time. Its main disadvantage is the fact that many borderline cases do not qualify, in this method, as barriers, when barriers actually do exist in nature. This point will be elaborated and illustrated in the next section.

The elevation method, though requiring another computational step, is less prone to border cases and, furthermore, is not dependent on network orientation. The determination if a given barrier as a channel or a divide is immediate. However, inaccuracies result from the use of an elevation average value as a criterion for comparison.

The threshold angles STBAR and DVDBAR

Throughout the discussion above we have taken for granted the applicability of the threshold ("critical") angles STBAR and DVDBAR, which were supposed to consistently determine whether a barrier between two adjacent squares exists solely by comparing their inter-azimuthal angle with these thresholds. This assumption will be discussed below.

From the evaluation of maps and of trial runs, it has been found that the angles which yield the best, optimal results for the Nahal Yael watershed are:

For STBAR $40^{\circ} - 45^{\circ}$;
for DVDBAR $50^{\circ} - 60^{\circ}$.

The procedure for the "manual" network involved the tracing of the drainage lines and the divides from a topographic map, and approximating them by the nearest grid link (= square side). By combining various values of STBAR with various values of DVDBAR, and making a link by link comparison of the resulting computer-simulated network with the manually approximated map-based network, the optimal values listed above have been determined.

Using the optimal threshold angles does not guarantee complete connectivity of the simulated network. Even for the combination of angles which produces the largest number of barriers, a certain number of links are not reproduced, while elsewhere unjustified links appear in the simulated network. An extreme example of the latter occurs for the theoretical case of

$$\text{STBAR} = \text{DVDBAR} = 0$$

As a means of "filling the holes" in the network, it is necessary in future to develop a technique which will connect disjointed links of the same type, i.e. stream barriers with stream barriers and divide barriers with divide barriers. Such a procedure might be based on the principle of searching out the nearest barrier of the same type and connecting to it without crossing another barrier.

Whenever the network as simulated by the optimal angles method has only few network discontinuities, it may be more practical, for a local project, to achieve complete connectivity manually.

Evaluation of the results obtained for various combinations of threshold angles revealed that very often a barrier is not generated at links which, in fact, are barriers, when the adjoining square(s) have a considerable internal relief. This means that, for those squares, the corner elevations do not adequately represent the terrain; therefore, the azimuth - a single parameter based solely on these elevations - is likewise not adequately representative, and a further subdivision is thus called for.

In summary, although fully connected networks of streamlines and divides are not generated even by the optimal STBAR - DVDBAR angle combination, a large part of the network is indeed produced. As a future development, the threshold angles could be made to vary over area as a

function of the slope angle relationships between adjacent squares, or even in conjunction with some non-geometric terrain characteristic.

9.5, Substitution of solutions in the computer

9.5.1 Introduction

Following the theoretical solutions arrived at for a single square (section 9.3) and for barriers between squares (section 9.4), a computer program in Fortran IV has been written for the application of these solutions to a field of squares. The main input of the program are the elevation data of the square corners as read from the topographic map. The main output of the program is:

- I) The mean elevation for each square;
- II) The azimuth of each square;
- III) The slope angle of each square;
- IV) The barrier network resulting from a given combination of inter-azimuthal threshold angles.

This output was also converted to a graphic display by means of a Gerber plotter.

In this section the computer programs are explained and evaluated, the methods of computation are detailed, and the results are discussed.

9.5.2 The study area and some technical remarks

The area whose map served as the base for trying the computer programs is located in the upper parts of the Nahal Yael Research Watershed, and comprises the whole of watershed 05 and a part of watershed 04. A square grid drawn on a map, scale 1:1,250, yielded about 1,000 squares 12.5 meters square. Each unit element had an orthogonally projected surface area of 156.25 m^2 .

The corner elevation of all squares was read manually off the map and punched on a data card. (Automatic reading devices might perform the same function either off a map or off an air photograph whenever the model is applied to large areas). The axes of the grid used run parallel to the map coordinate system. Point (250,800) is the southwestern corner of the source map and was designated (1,1) in the model. From this followed the model coordinates in such a way that the index of the easternmost corner was 41 and that of the northernmost corner was 26. Based on this grid, an individual square is identified by the coordinates of its southwestern corner. Numerical results for each square appear in the output in tabular form, with rows and columns parallel to the coordinate network.

Index I denotes the latitudinal (east-west) axis, with the highest value designated II.

Index J denotes the longitudinal (north-south) axis, with the highest value designated JJ.

The grid point network must clearly exceed the boundaries of the studied area, so that the entire divide zone is covered by full squares, as in figure 9.15. All corners of all shaded squares must be included in the data input, even though most of them are located outside the divide. In the area used here as an example, considerable areas, mainly in the SW part of the grid actually lie beyond the divide of the Nahal Yael watershed.

In the following pages the computer program and its tabular and graphic outputs are described in more detail. The program is available upon request.

9.5.3 Computer printout No. 1 (SJFCOAY)

This program includes the main inputs and outputs. It is based on the scanning by loops of the corners which belong to given squares in the main program. For every

square reached by the scanning process, the required output is arrived at by a suitable sub-program of a function or subroutine type. All the computations relating to an individual square (e.g. the slope angle) are performed within one major loop (from statement 13 to statement 65, inclusive). Another loop performs the interrelationships between two adjacent squares - the barrier decisions (from statement 66 to statement 72). After these two main parts there follow the printout statements: first for the graphic output (statement 73: CALL GERBRS) and then the numerical output which appears in the printout.

PROGRAM STAGES

I) Reading the data: The data - elevations of the square corners - are read into an $E(II, JJ)$ matrice (in our example $E(41, 26)$) and these data appear as the first table of the output. The reading is done line by line. The length of each line is II and the number of the lines is JJ . This rectangular field may include areas for which there are no data, as they are outside the watershed and its divide zones. For these points some impossible elevation value is punched; in our case, where all real elevations exceed 200m, we have punched 0 (zero). For the indices which refer to these points no computations were performed and all the variables computed for them were put as "blank". The computer cell which represents any one of these points does not contain any value. The check whether

$$E(I, J) = 0$$

is performed before the beginning of the computations (statement 15).

In the output, every location for which such a blank is indicated, there appears a character different from all others: N or -0.

II) Computing the mean elevation for each square: As

each square is identified by the coordinates of its lower left corner, the mean elevation of square (I,J) is (see figure 9.16):

$$0.25(E(I,J) + E(I+1,J) + E(I+1,J+1) + E(I,J+1))$$

The computation is performed by FUNCTION AVG which calculates the arithmetic mean of N arrayed values. The matrix of the mean elevations is designated AH. Its size is (II-1,JJ-1) or, in our example, AH(40,25). It appears as the second table of the output.

III) Calculating azimuth and slope angle for each square:

First a test is made for a special case, in which all corners of the given square are of equal elevation (statement 21). In such a case the azimuth is undefined, because we have a horizontal plane. The azimuth is then designated blank and the slope angle is zero. In our set of 1,000 squares there was no such case. Evidently it is unlikely in fluvially conditioned topography in general.

In all other cases it is necessary to calculate azimuth and slope angle separately for each combination of three out of the four corners (section 9.3 above). Each combination was designated M, (M = 1,2,3,4).

Assume we have a given M combination of 3 points. The values for the coefficients of the plane equation AT(M), BT(M), CT(M), DT(M) are obtainable through FUNCTION DET, which calculates the determinant of a matrix of the order 3x3 (see paragraph 9.3.1 above). The resulting coefficient values have a scale distortion, because the horizontal distance between adjacent corners is one unit (fig. 9.16), and the vertical difference between corner points is in meters; however, this distortion does not affect our procedure, because we are interested only in the relative values of the coefficients (except for one

case to be discussed below).

The four coefficients AT(M), BT(M), CT(M), DT(M) constitute the input to SUBROUTINE AZIDIP, which uses them to calculate azimuth and slope angle (see paragraph 9.3.2 above). In the process, the variables TAZT(M) - the "temporary" azimuth for the particular M combination and TDIP(M) - the "temporary" dip for same, are calculated. By repeating this four times, i.e. for each M combination, we get:

TAZT(1),....., TAZT(4)

and

TDIP(1),....., TDIP(4)

The final mean values are obtained through AVG, and the resulting azimuth and slope angle for square (I,J) are designated, respectively

AZIMUTH (I,J), DIP(I,J).

A special case occurs whenever a certain square has three corners of equal elevation. Then only the slope angle is calculated by AZIDIP, while the azimuth depends entirely on the fourth point, which will be either higher or lower than the three others (statements 42 to 56 inclusive). Such a case indeed occurred in our example, square (24, 14).

By comparing the results as computed by the model with the source map, a generally dependable reproduction of the terrain is indicated, both for orientation and for slope angle. Clearly, the more terrain homogeneity within a square (extreme homogeneity: parallel and equidistant contours), the higher the representativeness of the computed azimuth and dip.

In practice, the azimuth and dip values represent, for most squares, the characteristics of the topography. Internal relief within individual squares - such as caused by very densely dissected terrain, junction areas of

stream channels, or very localized cliffs - detracts from the representativity, since such varied squares require more than one set of two numbers to adequately portray their topographic composition.

The computer-generated topography is generally more moderate than the real-world prototype, i.e. its slope angles are somewhat lower. This is so because the randomly placed grid intersections often miss the very highest, as well as the very lowest, points in the terrain. Usually these special points cover only a small fraction of the terrain, but their role in landscape conditioning and evaluating is considerable. The upper part of the Nahal Yael watershed has a dissected and rapidly changing topography. It is possible that even better representativity would have been obtained for an example area with a more rounded and orderly fluvial topography.

In summary, we conclude that the simulated, computer-generated terrain is sufficiently representative of the actual topography and is thus suitable for the modelling of unconcentrated slope runoff. The terrain simulation would be further improved by the introduction of a square size which will vary as a function of the internal relief (see section 9.2 above).

SUBPROGRAM AZIDIP: The input to AZIDIP are the coefficients of the planar equation A,B,C,D and the output are the azimuth and the dip (= slope angle). The program is executed after Tables 9.1 and 9.2 and after paragraph 9.3.3 above. The sub-program consists essentially of comparing coefficients and evaluating their signs. The result is multiplied, for the azimuth as well as for the dip, by $180/\pi$, since the computer calculates angles in radians.

In calculating the dip, statements 28 and 29 read, respectively

$$A = A/12.5$$

$$B = B/12.5$$

These statements correct the scale distortion brought in during the calculation of A,B in the determinant, by multiplying first by 1/1250 (the map scale) and further by 100 (the number of centimeters in one meter). Remember the map distance between adjacent corners in 1 cm. For C this correction is unnecessary because it is calculated solely in units of cm, while D is not involved at all in the calculation of the dip. In evaluating the azimuth there is no scale distortion; it is calculated from coefficient relationships so that scale is irrelevant.

IV) Calculation of barriers: This program utilizes the method of segments (section 9.4). Its input are the azimuths of the squares (from paragraph 9.3.3). The main program scans all sides common to any two squares in a network. The decisions whether a given side is a barrier or not, and if it is - of which type, is done through the BAR function.

The scanning procedure verifies the barrier property, for square (I,J), by testing the inter-azimuthal angle in relation to the threshold angle(s) (section 9.4) immediately above (north) and immediately to the right (east) of point (I,J). Referring to figure 9.17, while scanning (I,J), i.e. point A, the BAR function determines, first, whether side AB is a latitudinal barrier and, if so, of what type. Then it determines whether side AD is a longitudinal barrier and, if so, of what type. The scanning process covers all points of the network. Thus, every side of the network is covered and the pattern of barriers is obtained.

In the numerical output, the numbers which appear in the barrier table indicate the various possible combinations

of barriers for the pair of sides tested for each grid point. In the main program the barriers were designated by BARRIER(I,J) according to Table 9.4.

From the way the barriers are listed, it follows that

$$\text{BARRIER}(1,1) = 0$$

This value is assigned a priori, because sq (1,1) has no barrier along the two sides which meet at point (1,1), which is the southwestern corner of the whole network.

In evaluating barriers for the first row ($J = 1$), only longitudinal barriers may result. Likewise, for the first column ($I = 1$), only latitudinal barriers are permitted.

The input for function BAR is as follows:

```
AZIMUTH (I,J) labelled AZIJ
AZIMUTH (I-1,J)    "    AZI1J
AZIMUTH (I,J-1)    "    AZIJ1
```

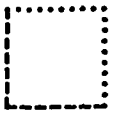
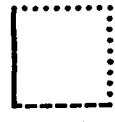

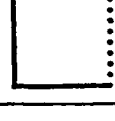





There is also an input parameter labelled IN. Whenever $IN = 11$, then $J = 1$, we are in the first row, and consequently latitudinal barriers are out. Likewise, whenever $IN = 1$ we are in the first column, and consequently longitudinal barriers cannot result. In normal cases $IN = 0$.

Further input are the values of the threshold angles STBAR, DVDBAR which result from the COMMON statement. The output of the BAR function is also named BAR, and the stages of calculation follow Table 9.4, as described below:

First, equation 9.4.1 is used to calculate the inter-azimuthal angle. DELV is the angle between AZIJ and AZI1J, and DELH is the angle between AZIJ and AZIJ1. We set $BAR = 0$ and test all the possible cases one by one. As a start, we ask: is there a longitudinal channel barrier? This question is analogous to:

- I) are the relevant azimuths converging? and
- II) is $DELV > STBAR$?

Table 9.4: The listing of barriers in the output

BARIER(I,J)	Meaning	Graphic
0	<u>No barrier</u> between sq(I,J) and either its western or its southern neighbour	
1	<u>Longitudinal channel barrier</u> between sq(I,J) and its western neighbour	
2	<u>Latitudinal channel barrier</u> between sq(I,J) and its southern neighbour	
3	<u>Channel barrier</u> of type 1 and 2 together	
-1	<u>Longitudinal divide barrier</u> between sq(I,J) and its western neighbour	
-2	<u>Latitudinal divide barrier</u> between sq(I,J) and its southern neighbour	
-3	<u>Divide barrier</u> of type -1 and -2 together	
4	<u>Longitudinal channel barrier</u> , type 1 and latitudinal divide barrier, type -2	
-4	<u>Latitudinal channel barrier</u> , type 2 and longitudinal divide barrier, type -1	

If both conditions exist, then

$$\text{BAR} = 1$$

Now we move on to the question: is there a latitudinal channel barrier? Again, first we check if there is convergence, and then if

$$\text{DELH} > \text{STBAR}$$

If the answer to both is positive, we deduce

$$\text{BAR} = \text{BAR} + 2$$

Now, if previously

$$\text{BAR} = 0$$

we get

$$\text{BAR} = 2$$

But if previously

$$\text{BAR} = 1$$

we get

$$\text{BAR} = 3$$

The procedure of testing for divide barriers is exactly analogous. After going through the entire procedure of testing for all possibilities, we finally determine BAR to be one of the nine values listed in Table 9.4.

For computer printout No.1 the following values were substituted for the threshold angles:

$$\text{STBAR} = 30$$

$$\text{DVDBAR} = 60$$

The best simulation of the drainage network is obtained somewhere in the vicinity of these values (see section 9.4), and the results are presented numerically in the last matrice of the output. This table, which describes the barriers numerically, will serve in future for the transfer of flow along the channel barriers. It also provides the basis for the graphic display.

V) Graphic output No.1: This is the last stage of the present program. It translates the numerical results into a graphic display, scale 1:1,250, code name SJFCOAY. The instrument used was a Gerber plotter, and all the read-in operations for the Gerber were carried out by a special sub-program named GRBER 8.

The input for GRBER 8 is the elevation of the grid points, the azimuth of the squares, the barriers, and the threshold angles STEAR and DVDBAR (in the present case, ST = 30 and DVD = 60). The graphic output is produced step by step, in the same scale as the source map, and consists of: the axes of the rectangular grid, its boundaries, and a designation of its cardinal directions; plots of arrows of a standard length from the center of each square in the direction of the azimuth; plotting the divide lines according to the divide barriers with a full black line; plots of stream lines according to the channel barriers with a full blue line, with an added blue arrow pointing towards the lower end of each barrier line.

As stated earlier, the result is not perfect. In addition to occasional lack of connectivity even for the "best" threshold angles, the channel segments composed of a number of grid links are not always unidirectional. Both inadequacies are caused, ultimately, by the fact that we use four points to represent the entire square. As long as we insist doing that, we have to, subsequently, go through a process of connection and redirection of links, be it by a subjective or an objective process.

Although the barrier calculation does not differentiate between large and small channels, the square size governs the sensitivity to the smaller channels. In our simulation some very small channels were obliterated because the contour indentation effect of their valleys was totally absorbed within a single square.

The graphic output shows some divide barriers touch a channel barrier, i.e. they have a common end point. These cases, represented by $BAR = 4$ and $BAR = -4$ (Table 9.4), are inconsistent with normal fluvially conditioned topography and a procedure must be devised to eliminate them. Figure 9.18 is a corrected and "smoothed" reproduction of this output.

9.5.4 Computer printout No.2 (SJFCOEK)

In its main aspects this program is similar to program No.1. The difference is that here no graphic output was produced, and the barriers were identified by comparing elevations. Using this method, the barriers were evaluated for any combination of angle values for STBAR and DVDBAR, with each being assigned successive values at 20° intervals (i.e. 0, 20, 40, 60, ..., 180).

The procedure employs the same notation and order of calculation for the two sides which meet at the grid point of square (I,J) as in program No.1. The barriers are evaluated via the BRR function, supplemented by the NC function. The barrier's notation is BRR.

The input ingredients for BRR are: the elevations of the intersections of the rectangular grid; the azimuths required for the barrier test $AZIMUTH(I,J)$, $AZIMUTH(I-1,J)$, $AZIMUTH(I,J-1)$; the parameter IN, which functions in the same way as in function BAR (computer printout 1); the index (I,J) of the given square; and the size of the elevation matrix E, i.e. $E(II,JJ)$.

First the inter-azimuthal angles DELV and DELH are defined, as in BAR. Now, after figure 9.17, the test whether AD is a barrier is performed in two steps. First, function NC is called to evaluate the elevations of the end points of EF and CB versus AD and to determine whether there is convergence ($NC = 10$), divergence ($NC = -10$),

or unconcentrated slopeflow. ($NC = 0$).

If $NC = 0$, the program passes on to test a possible latitudinal barrier at AB.

If $NC = -10$, i.e. there is divergence, the existence of a possible divide is tested, i.e. whether

$$DELV > DVDBAR$$

and BRR gets its value accordingly.

If $NC = 10$, i.e. there is convergence, and then, if also

$$DELV > STBAR$$

then

$$BRR = 1$$

and then the program moves on to test AB in a similar way for the possible existence of a latitudinal barrier.

Through NC the trend of either convergence, divergence, or slopeflow is determined, and the final value of BRR is assigned according to the relationships between each of the two threshold inter-azimuthal angles and DELH.

In the numerous barrier matrices we obtained, it is striking to observe the diminution in the number of barriers with the increase of the threshold angle values, until, at

$$STBAR = DVDBAR = 180$$

none remain - a necessary corollary of the principle used for the establishment of barriers. It is also possible to observe the tendency of STBAR to be smaller than DVDBAR; for higher angles an increase in the threshold values is especially felt in a drastic decrease in the number of channel barriers.

A rigorous objective criterion for the determination of optimal values for the inter-azimuthal threshold angles has not been developed at this stage.

SJFC09T 25/10/79

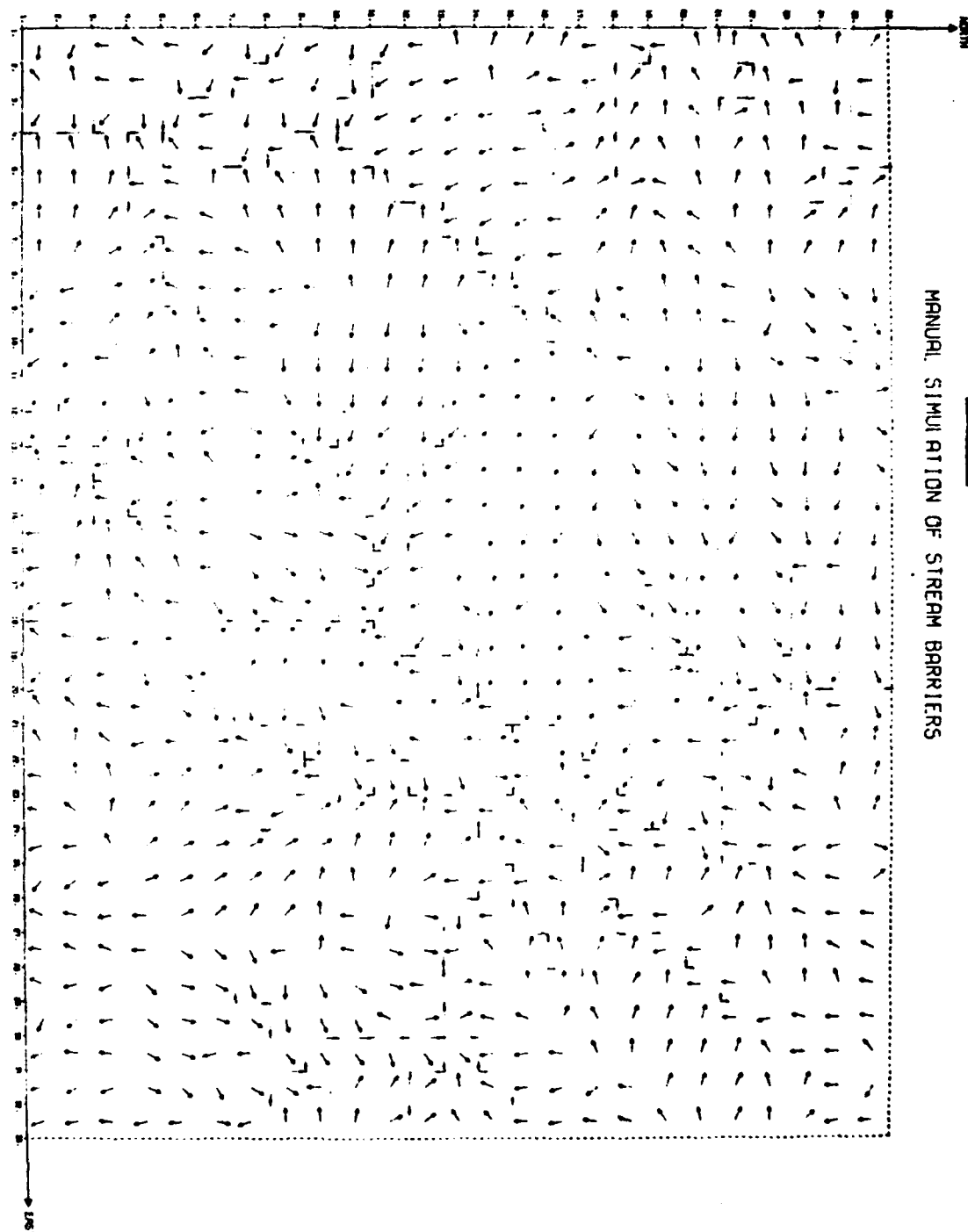


Fig. 9.18: Manually simulated drainage network, upper Nahal Yael watershed. Gerber output SJFC09T.

9.5.5 The graphic output for various angles

Graphic output No.1: This output has been obtained from the program of printout No.1. It determines barriers via the method of sectors for STBAR = 30, DVDBAR = 60, and displays them at the scale of 1:1,250 (this same scale is used for all graphic outputs).

Graphic output No.2 (SJFC09T): This is a manual simulation performed on a part of the example area by tracing the rectangular grid onto the source map and assigning barriers to square sides subjectively judged to be most closely representative of the generally irregular real-world "barrier" lines (fig. 9.4). Because of time constraints only the stream channel lines were simulated in this way. The channel barriers so determined were then transferred in the usual notation to the NREAL matrice.

Although the resulting barrier network faithfully reproduces the salient features of the real-world drainage network, here too some directional distortions do occur.

Graphic output No.3 (SJFC094): This is the barrier map for STBAR = 0, DVDBAR = 0, i.e. a barrier is indicated wherever the trends are opposing, however slightly. The result shows many closed depressions as well as numerous superfluous channel barriers and divide barriers. The barriers are of type BAR.

Graphic output No.4 (SJFCODY): This also shows the barriers for STBAR = 0, DVDBAR = 0, but the barriers are of type BRR. The output is similar to No.3. Also here we have many depressions which do not exist in nature as well as many superfluous barriers.

Graphic output No.5 (SJFCOAW): Shows barriers of type BAR for STBAR = DVDBAR = 150. It clearly emerges that this angle is too large: barriers are produced only when the inter-azimuthal angle for two adjoining squares exceeds 150° , i.e. nearly completely opposing trends (fig. 9.19).

SJFCOAW 25/10/79

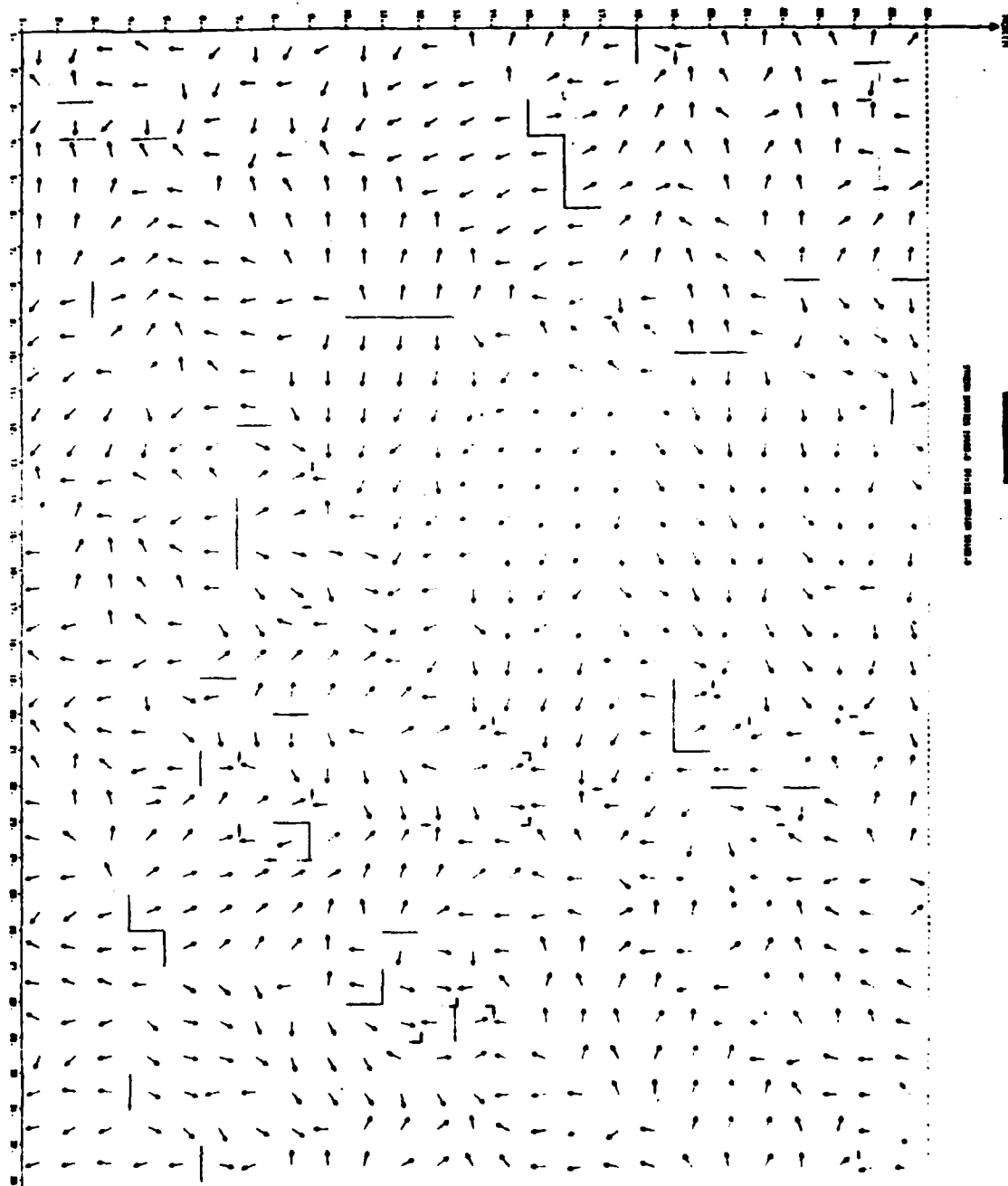


Fig. 9.19: Computer-simulated drainage network, upper Nahal Yael watershed. STBAR = 150°; DVDBAR = 150°. Gerber output SJFCOAW.

Function BRR yields, for the threshold angles, even less barriers.

Graphic output No.6 (SJFCOD5): Barrier computation based on STBAR = DVDBAR = 45, type BRR.

Graphic output No.7 (SJFCOD8): Barriers based on STBAR = 30 DVDBAR = 60 (fig. 9.20).

In summary, low values of threshold angles yield - for either barrier type (BAR and BRR) - numerous superfluous barriers. This is best evident from a comparison of graphic outputs No.3 and 4 with the manual simulation and with the source map. As we increase the values of the two threshold angles, the number of barriers, and especially of superfluous barriers, decreases. Very high threshold values, such as used for graphic output No.5, yield only a relatively small number of barriers, but all the barriers indicated do agree with real-world barriers. Conversely, however, in cases that produce many superfluous barriers, there still remain certain grid links which are barriers in the real-world, as represented by the numeral simulation, but are not indicated as such by the program. Therefore, the most significant set of threshold angles can be defined as the one generating the largest number of barriers which include the smallest number of superfluous barriers.

The probable effect of the sharp and dissected topography of the prototype area in relation to the square size has already been mentioned. To this might be added the fact that much of the prototype area is in reality a divide zone (see graphic output No.2). So further tests for other topographic regions will be needed if the model is adopted for more universal use.

Comparing barriers resulting from type BAR definitions with those resulting from type BRR definitions, it emerges that the comparative elevations method requires

SJFCOD8 25/10/79

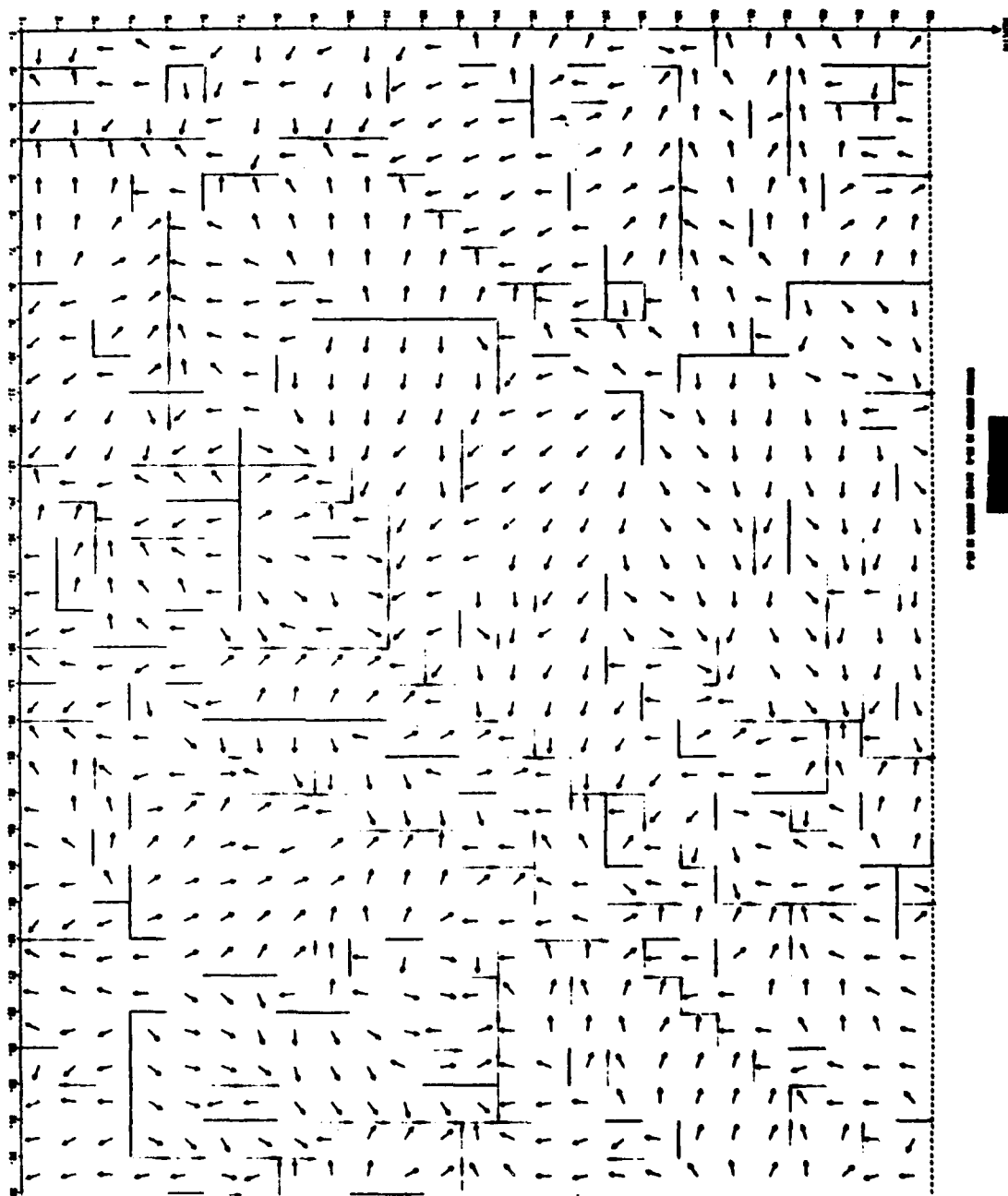


Fig. 9.20: Computer-simulated drainage network, upper Nahal Yael watershed. STBAR = 30° ; DVDBAR = 60° . Gerber output SJFCOD8.

"optimal" threshold angles which are lower in value than required for the sector method. Compare graphic outputs No.1 and No.7, where, for the same limiting angles, we get more barriers from the sector method than from the method using comparative elevations.

Whenever real-world barrier lines follow a north-south or an east-west direction, even approximately, the representativity by the BAR procedure (= the sector method) is good. Conversely, for reaches of streams (and divide lines) oriented roughly at 45° to one of the cardinal directions, barrier production is only partial. This effect is considerably increased whenever internal relief causes at least one of the two azimuths involved in a barrier determination to be unrepresentative.

In summary, similar networks are generated by the model for both methods for barrier determination (by sectors and comparing elevations), though the optimal threshold values are different for each method. In neither case complete connectivity of drainage lines or divide lines could be achieved.

9.5.6 Application of the program to other areas

One objective of our work on this simulation model was to enable its use in other areas with minimal changes, and the computer programs have been written with this in mind. We assume that, for other regions, the same input - elevations of grid points (rectangular) as well as the cardinal directions (N-S, E-W) will be used, so that no rotation will be necessary.

The following statements have to be changed when applying the program to another region (see printout No.1):

I) Statement 3:

DATA II,JJ/...../

which identifies the northernmost index of the grid JJ

and the easternmost index II (remember the southwestern grid point is indexed (1,1)).

II) Statements 1 and 2, which signify the dimensions of the variables for II, JJ should be, for the grid point matrice

E(II,JJ)

and for the other matrices

AH(II-1,JJ-1), DIP(II-1,JJ-1),
AZIMUTH(II-1,JJ-1), BARRIER(II-1,JJ-1)

III) Statements 7 and 8 should be changed according to the selected values for the threshold angles.

IV) In sub-program AZIDIP, statements 28 and 29 ($A = A/12.5$; $B = B/12.5$) should be changed according to the scale of the map and the units of grid point elevations used.

V) In subprogram GRBER 8 the statement FACTOR(0,394) (number 9) is also contingent upon the scale of the map used.

9.6 Summary and conclusions

The work reported here is only the first stage in the development of a comprehensive deterministic and distributed geo-system oriented model. Most of the work dealt with the "infrastructure" of such a model - the simulation of the topography and the construction of a rectangular reference system. Via this system the information input will be fed into the model, and through it also the output will be received.

The terrain simulation was accomplished by calculating azimuth and slope angle for each grid square. The drainage network and divide lines were simulated on the basis of assuming the existence of threshold inter-azimuthal angles for pairs of adjacent squares, which define

convergence to a channel or divergence from a divide. Optimal threshold angles ($30 - 45^{\circ}$ for channels, $45 - 60^{\circ}$ for divides) yield in general acceptable, though incomplete networks, but some inconsistencies still exist.

Two tasks left to be done concern the development of a criterion for the optimization of the threshold angles and the development of a "connectivity function" for the resulting drainage network and divide lines.

Subjective manual filling in of lines and occasional reversing of computer-indicated flow direction could substitute, for a specific area, for the "connectivity function", but it would detract from the generality of the procedure.

A considerable improvement of the final result - the drainage and divide network - can be expected with the introduction of a variable-size grid, to vary automatically with variation in relevant input data, especially of the relief.

10. RESULTS OF THE APPLICATION OF
A SIMPLIFIED VERSION OF THE STANFORD WATER -
SHED MODEL TO NAHAL Yael WATERSHED 05

by Harriet Feldman

As a background to the main thrust of the research in the direction of a fully distributed model, it was attempted to run a few of the Nahal Yael data through a simplified version of the Stanford Watershed Model. The basin selected was once again watershed 05.

The main results are listed in Tables 10.1, and 10.2. The rainfall data are listed in Table 10.3. Note that the printout lists erroneously the last nine months of a given water year as if they had the same year as the first three months (October - December), i.e. "year 68, month 12" should be followed by "year 69, month 1", etc.

It can be seen that the model functions fairly well on an annual basis (the error is 15%). However, if one breaks the results down into a monthly level, a different picture is obtained. During the 48 months long period considered, events occurred only during 5 months. Out of these:

Two months showed a computed flow of zero for actually recorded flow volumes (264 and 135 m³, respectively);
One month showed a computed flow of 366 m³ for an actual flow volume of zero;

Out of the remaining two months, one had a 48 per cent too high computed value (974 m³ computed versus 673 m³

recorded); and in only one month was the computed flow volume reasonably accurate (556 m³ computed versus 573 m³ recorded).

Tentatively, the conclusion is that the Stanford Watershed Model, and probably also similar models, are not suitable for successfully simulating the mechanics of runoff as needed for this (and similar) projects.

Table 10.1: Annual runoff in cubic meters, recorded and computed by a simplified Stanford Watershed Model procedure, Nahal Yael watershed 05, 1968/69 - 1971/72

ANNUAL RUNOFF IN CUBIC METERS

YEAR	RECORDED	COMPUTED
68/69	937	974
69/70	0	0
70/71	135	366
71/72	573	556
TOTAL	1645	1896

ERROR IS 15%

Table 10.2: Monthly runoff in cubic meters, recorded and computed by a simplified Stanford Watershed Model procedure, Nahal Yael watershed 05, 1968/69 - 1971/72

YEAR	MONTH	COMPUTED	RECORDED
68	11	0	264
68	01	974	673
70	01	366	0
70	03	0	135
71	12	556	573

Table 10.3: Recorded daily rainfall and computed runoff, Nahal Yael watershed 05, 1968/69 - 1971/72

YEAR	MONTH	DAY	RAINFALL (MM.)	RUNOFF (MM.)
68	11	20	0.9	
		24	6.2	
		25	7.2	
68	12	26	1.5	
68	1	21	19.4	18.4
		22	1.1	1.1
		28	0.2	
68	3	19	0.6	
		20	8.4	
		31	1.9	
68	4	11	0.3	
~~~~~				
69	10	19	0.6	
69	11	16	0.5	
69	1	20	0.1	
		21	0.1	
~~~~~				

YEAR MONTH DAY RAINFALL (MM.) RUNOFF (MM.)

70	1	9	1.4	
		10	3.0	
		20	0.2	
		24	0.5	
		25	7.7	7.3

70	3	25	5.0	
----	---	----	-----	--

70	4	3	0.1	
		12	0.3	
		14	0.5	
		15	6.3	
	9	19	0.7	

.....

71	11	5	1.3	
	12	18	0.1	
		22	11.7	11.1
		25	0.5	
		27	1.4	
		28	0.3	

71	4	20	0.1	
		21	0.1	

71	2	12	3.4	
----	---	----	-----	--

71	3	14	2.3	
		16	0.2	
		18	1.0	
		21	0.3	

.....

